SEISMIC PERFORMANCE EVALUATION OF REINFORCED CONCRETE FRAMES INFILLED WITH AUTOCLAVE AERATED CONCRETE MASONRY

A THESIS SUBMITTED TO
THE GRADUATE SCHOOL OF NATURAL AND APPLIED SCIENCES
OF
MIDDLE EAST TECHNICAL UNIVERSITY

BY

UMAIR AHMED SIDDIQUI

IN PARTIAL FULFILLMENT OF THE REQUIREMENTS
FOR
THE DEGREE OF MASTER OF SCIENCE
IN
EARTHQUAKE ENGINEERING AND ENGINEERING SEISMOLOGY

MARCH 2013

Approval of the thesis:

SEISMIC PERFORMANCE EVALUATION OF REINFORCED CONCRETE FRAMES INFILLED WITH AUTOCLAVE AERATED CONCRETE MASONRY

submitted by **UMAIR AHMED SIDDIQUI** in partial fulfilment of the requirements for the degree of **Master of Science in Earthquake Engineering and Engineering Seismology, Middle East Technical University** by,

Prof. Dr. Canan Özgen _____
Dean, Graduate School of **Natural and Applied Sciences**

Prof. Dr. Ahmet Cevdet Yalçıner _____
Head of Department, **Civil Engineering**

Prof. Dr. Haluk Sucuoğlu _____
Supervisor, **Civil Engineering Dept., METU**

Prof. Dr. Ahmet Yakut _____
Co-Supervisor, **Civil Engineering Dept., METU**

Examining Committee Members:

Prof. Dr. Barış Binici _____
Civil Engineering Dept., METU

Prof. Dr. Haluk Sucuoğlu _____
Civil Engineering Dept., METU

Assoc. Prof. Dr. Murat Altuğ Erberik _____
Civil Engineering Dept., METU

Assoc. Prof. Dr. Erdem Canbay _____
Civil Engineering Dept., METU

Asst. Prof. Dr. Tahsin Turgay _____
Architecture Dept., Abant İzzet Baysal University

Date: 15.03.2013

I hereby declare that all information in this document has been obtained and presented in accordance with academic rules and ethical conduct. I also declare that, as required by these rules and conduct, I have fully cited and referenced all material and results that are not original to this work.

Name, Last name: Umair Ahmed SIDDIQUI

Signature : _____

ABSTRACT

SEISMIC PERFORMANCE EVALUATION OF REINFORCED CONCRETE FRAMES INFILLED WITH AUTOCLAVE AERATED CONCRETE MASONRY

Siddiqui, Umair Ahmed
M.Sc., Earthquake Engineering and Engineering Seismology
Supervisor: Prof. Dr. Haluk Sucuoğlu
Co-Supervisor: Prof. Dr. Ahmet Yakut

March 2013, 119 pages

Seismic risk reduction requires detailed assessment and rehabilitation of vulnerable buildings to avoid significant property and life losses. Several reinforced concrete buildings are deficiently designed and constructed and also contain non-engineered unreinforced masonry infill panels which dominate the seismic response and impart excessive lateral forces for which they are not designed for. Therefore, seismic performance assessment procedures recommended in guidelines and codes needs detailed examination through rigorous experimental and analytical research to ensure the adequacy of suggested provisions and modelling parameters.

This study investigates the seismic behaviour of four reinforced concrete frames, constructed in the Structural Dynamics Laboratory at Middle East Technical University and tested by the pseudo-dynamic testing procedure. These four specimens are investigated in pairs of two: the "Non-conforming" with material and detailing deficiencies, and the "Code-conforming" compliant with Turkish Earthquake Code 2007. Each pair contains one bare frame while another frame infilled with autoclave aerated concrete (AAC) block masonry. The focus of this study is to experimentally investigate the influence of AAC masonry infill panels on the seismic response of RC frames in both configurations. Numerical modelling of frames is conducted on the OpenSees platform following guidelines of TEC-2007 and ASCE/SEI 41-06.Models, calibrated with experiments using time-history results, are used for assessment using pushover and time-history methods in accordance with the procedures of TEC-2007 and ASCE/SEI 41-06.

The presence of AAC infills is found to considerably influence deformation pattern, damage distribution and failure modes in deficient frames whereas in code-conforming frames the effect is not significant.

Calibrating the models of deficient frames by using reduced nominal strengths and modified joint-offsets in order to predict accurate seismic response and damage distribution, is not efficient. To capture the deformation pattern on local scale, joint flexibility and frame-infill interaction needs to be explicitly accounted.

The assessment of damage in members bounding the infill panels with ASCE/SEI 41-06 provisions gives accurate predictions of observed damages whereas TEC-2007 under estimates the damages for those members.

Keywords: Pseudo-dynamic Testing, Autoclave Aerated Concrete, Unreinforced Masonry Infill, Equivalent Strut, Performance Evaluation.

ÖZ

SEISMIC PERFORMANCE EVALUATION OF REINFORCED CONCRETE FRAMES INFILLED WITH AUTOCLAVE AERATED CONCRETE MASONRY

Siddiqui, Umair Ahmed
Yüksek Lisans, Deprem Mühendisliği ve Mühendislik Sismoloji
Tez Yöneticisi: Prof. Dr. Haluk Sucuoğlu
Ortak Tez Yöneticisi: Prof. Dr. Ahmet Yakut

Mart 2013, 119 sayfa

Sismik riskin azaltılması aynı zamanda can ve mal kaybını da önleyecek olan zayıf binalarının detaylı olarak incelenmesi ve güçlendirilmesini gerekli kılar. Bazı betonarme binalar, yapısal olmayan dolgu duvar panelleri ile yetersiz olarak tasarlanmakta ve inşa edilmektedir. Dolgu duvarlar bu tür yapıların davranışını önemli ölçüde etkilemekte olup, yapıya artan deprem yüklerinin etki etmesine yol açmaktadır. Dolayısıyla, şartname ve kılavuzlarda önerilen sismik performans değerlendirme yöntemlerinin deneysel ve analitik araştırmalarla ayrıntılı olarak irdelenerek yapılan önerilerin ve modelleme parametrelerinin yeterlilikleri konusunda değerlendirmeler yapılmalıdır.

Bu çalışmada, Orta Doğu Teknik Üniversitesi, Yapı Mekaniği Laboratuvarında inşa edilen ve dinamik benzeri yöntemle test edilen dört adet betonarme çerçevenin sismik davranışı incelenmiştir. Bu dört numune iki ayrı çift olarak incelenmiştir: malzeme ve detaylandıma açısından "Yönetmelik Uyumsuz", ve Deprem Bölgelerinde Yapılan Binalar Hakkında Yönetmelik (DBYBHY 2007) Uyan "Yönetmelik Uyumlu". Her çerçeve çifti bir adet yalın çerçeve ile aynı çerçevenin gaz beton (AAC) ile doldurulmuş numunesinden oluşmaktadır. Bu çalışmanın odak noktası her iki şekilde inşa edilmiş sistemde, AAC Kağir panellerin betonarme çerçevelerin sismik davranışı üzerindeki etkisini deneysel olarak irdelemektir. Çerçevelerin analitik modelleri DBYBHY 2007 ve ASCE/SEI 41-06 önerilerine uygun olarak OpenSees bilgisayar programı platformunda hazırlanmıştır. Deneysel sonuçlar ile kalibre edilen modellerin performans değerlendirmeleri itme analizi ve zaman tanım alanında yapılan analizler ile DBYBHY 2007 ve ASCE/SEI 41-06 yöntemlerine göre yapılmıştır.

AAC dolgu duvarlarının yetersiz çerçeveli sistemin deformasyon şekline, hasar dağılımına ve göçme moduna önemli etkisi olduğu ancak Yönetmelik Uyumlu çerçevelere etkisinin çok belirgin olmadığı görülmüştür.

Yetersiz çerçeve modellerinin daha iyi hasar dağılımı ve davranış elde etmek için nominal dayanım azaltılması ve birleşim bölgesi revize modeli ile kalibrasyonu etkin olmamıştır. Lokal düzeydeki deformasyon şeklinin elde edilebilmesi için birleşim esnekliği ve çerçeve-dolgu duvar etkileşiminin dikkate alınması gerekir.

Dolgu duvar çevresindeki elemanların hasarlarının tespiti için kullanılan kriterlerde ASCE/SEI 41-06'nın yeterli tahminler verdiği ancak DBYBHY 2007nin hasarları daha düşük verdiği görülmüştür.

Anahtar Kelimeler: Dinamik-Benzeri Deney, Gaz Beton Kağir, Donatısız Yığma Dolgu Duvar, Eşdeğer Çubuk, Performans Değerlendirmesi.

To my mother

Rashida SIDDIQUI

ACKNOWLEDGEMENTS

Writing this thesis would not have been possible without the keen involvement of many people in my life. First and foremost of all, I would like to thank my mother for her love and encouragement at every single step of my life; for her absolute devotion to children; for her priceless "Duas" for my success; and for her belief in me which lead my way through all difficult times. To my sisters, Alma and Sanila, for putting up with all the hard times without my presence.

This study would be meaningless without the sincere guidance of Prof. Dr. Haluk SUCUOĞLU as a supervisor. I express my sincere gratitude for his genuine advices, academic support and encouragement with due respect. My sincere thanks are extended to the co-supervisor of this study, Prof. Dr. Ahmet YAKUT for his guidance and useful discussions during the research work.

I am grateful to the Scientific and Technological Research Council of Turkey (TÜBİTAK) for providing necessary financial and technical support for this research project. My sincere gratitude is extended to ERASMUS MUNDUS, MEEES Masters Program and its entire teaching body for the award of scholarship and the opportunity to broaden my knowledge through this international masters program.

I express my sincere thanks to the following professors of NED University, Karachi who encourage me for higher education abroad: Prof. Dr. Asad-ur-Rehman Khan, Prof. Dr. Aftab Ahmad Farooqi and Prof. Dr. Sarosh Hashmat Lodi. In addition I am thankful to my teacher Mr. Zaman for bringing my academic intellect to light.

I am thankful to my friends in the simulation laboratory for their support during the entire time. I am in debt to my cousin Muhammad Ali for his support and encouragement. I also like to thank my "Yar", Wesley Wei-Chih Lin for the delightful memories during the entire master program which I will always remember with pleasure. My special thanks are due for Nermin GÜREL for her friendship, support and presence in all times.

Last, but certainly not the least; I am grateful to Allah for blessing me of all these beautiful people and opportunities and keeping me tied with Him in difficult times; though I will keep asking for more!

TABLE OF CONTENTS

LIST OF TABLES

TABLES

LIST OF FIGURES

FIGURES

CHAPTER 1

INTRODUCTION

1.1 General

Several reinforced concrete buildings around the world are inadequately designed and/or constructed according to the regulations of present seismic codes and best practices. In order to reduce the seismic risk posed by these vulnerable buildings, proper assessment and strengthening techniques are required. In the recent past, absence of sufficient knowledge and experience resulted in nonexistence of technical standards for risk reduction process.

The recent devastating earthquakes in Turkey as well as other seismically active countries in the World, which caused significant economic and human loss, have grown concerns about the performance evaluation of these deficient buildings. Preliminary seismic performance assessments funded by the government of Turkey has revealed that a significant number of reinforced concrete (RC) buildings have concerning deficiencies for the seismic zone they are situated in. Studies conducted by Sucuoğlu et al. (2007) have shown that commonly observed deficiencies are: plan irregularities, presence of heavy overhangs, low material strengths, inadequate member sizes, use of plain reinforcement, poor detailing in structural members and joint regions etc. Seismic performance of building is affected differently for each individual deficiency and therefore, should be separately studied.

In addition to these deficiencies, another important factor which affects the seismic performance evaluation, and is generally neglected, is the interaction of non-engineered masonry infill panels with the primary structural elements in resisting seismic loads. Sizeable analytical and experimental research has concluded that the stiffness and strength properties of the frame system are considerably altered by the integral action of frame-infill assemblage. Neglecting the interaction of infills can underestimate the amount of forces and result in brittle failures. It is of utmost importance to rehabilitate and retrofit the buildings at risk before a major earthquake strike since many populated cities in Turkey and generally in the World are located near active faults.

In the light of masonry infilled frame construction, the use of Autoclaved Aerated Concrete (AAC) masonry has gained familiarity due to its light weight and excellent fire resistant and thermal insulation capabilities which are ideal for seismic design and risk reduction. Because of these advantages, the utilization of AAC material for infill panels in areas of high seismicity have also gained popularity, for both new as well as rehabilitation of existing construction hence, signifying the need of sufficient experimental and analytical research to study the seismic response of AAC masonry infilled RC construction.

The current seismic building code in Turkey, the Turkish Earthquake Code (TEC), was released in 2007 and provides evaluation procedures and performance criteria for the design of building. For the first time in design code history, the Ministry of Construction and Resettlement in Turkey added a section regarding the assessment and strengthening of existing buildings to the TEC 2007 in order to address this issue. To address the reliability of these newly proposed additions experimental research is essential for validation, future revisions and improvements on the current code.

The Scientific and Technological Research Council of Turkey (TÜBİTAK) took this responsibility and approved funding for a comprehensive research project for the verification of these new additions in TEC 2007 through experimental testing on various concrete frames exhibiting existing construction

practises in Turkey. The title of this project is “Developing Performance-Based Evaluation Procedures and Strengthening Methods for the Turkish Seismic Code through Experimental and Analytical Research” with project number 108G034. The current thesis utilizes part of this overall experimental outcome to study the response of infilled frame systems under code-conforming and deficient construction.

1.2 Problem Statement

In Turkey, the general building stock is characterized by the presence of reinforced concrete (RC) frames infilled with non-structured unreinforced masonry wall panels which are, according to the current construction practices, completely in contact with the bounding frame (i.e. without separation joints) thereby interact considerably with the primary structural elements. These non-ductile infill panels can cause varying modifications in the seismic response of the building, both at the global as well as local scale, depending on their mechanical properties, geometric distribution and interaction with structural elements.

The Turkish Earthquake Code 2007 generally considers unreinforced masonry infill panels as non-structural component. The existing construction consists of non-engineered infill panels with no separation between the infill panel and the bounding frame. In addition, these panels lack either specific devices such as ties, belts, posts, shear connectors etc., as in the case of new construction, or retrofitting techniques such as bandaging in the case of existing structures, which are essential for integral interaction with the frame as well as prevention of expulsion or collapse. In TEC 2007 (section 7.5.2.4 and 7.6.4.6) effect of masonry infill panels is stated to be accounted in developing simulation models but limited to only those infill panels which are retrofitted with the techniques stated in Annex-7F of the code. However, other than strengthened masonry infill panels, there are no definite performance assessment provisions for the cases which reflect the existing construction. Further experimental and analytical research on the cases reflecting the existing construction is therefore necessary to adequately evaluate the performance of the composite assembly of frame-infill system.

The newly outlined procedures in the TEC 2007 for the assessment and strengthening of existing buildings are the first to be employed in engineering practice around the globe. Leading earthquake engineering countries such as the USA and Japan do not have legal documents regarding this matter rendering comparative analyses impossible. The procedures outlined in the code are loosely based off of ASCE/SEI 41-06 but differ slightly in defining the member acceptance criteria. Due to the urgent situation in Turkey regarding amount of rehabilitation needed, the validation of newly proposed additions in TEC 2007 through experiments and analyses is inherently necessary in order to ensure that modelling parameters are adequate and comprehensive enough for accurate seismic assessment and rehabilitation of existing structures.

1.3 Literature Review

1.3.1 Provisions for Seismic Assessment of Reinforced Concrete Frames

During a ground excitation, lateral loads imposed on a conventional reinforced concrete frame due to ground shaking are resisted by the gravity load-bearing columns of the structure. Thus, these columns need to be adequately designed in order to have the sufficient strength and ductility required from the force and displacement demands of an earthquake. Therefore, in designing of a reinforced concrete structure, the accurate estimation of column ductility is very vital because it is one of the main governing factors of its seismic performance and failure mechanisms.

In performance-based assessments, individual structural members are classified according to their failure modes based on their nonlinear deformation capacities. These classifications are then used to determine modelling parameters and deformation limits for a pre-defined performance level.

Released in 1997, FEMA 273 (Guidelines for the Seismic Rehabilitation of Buildings) was one of the leading global comprehensive documents which proposed various technical requirements for the seismic rehabilitations of existing buildings.

Soon after, in 2000, FEMA 356 (Pre-standard and Commentary for the Seismic Rehabilitation of Buildings) replaced FEMA 273 and became the new benchmark document. Methods outlined in FEMA 356 served as a basis for future developments and research topics of many codes and regulations around the globe. As this document was revised and improved over time, it was replaced by ASCE/SEI 41-06 in 2006. In 2007, a document titled ASCE/SEI-41 Supplement-1, based on research on the proposed effective stiffness models, modelling parameters and acceptance criteria, was released. This supplement to the original ASCE/SEI 41 contained provisions related to rehabilitation of existing reinforced concrete buildings. ASCE/SEI 41-13 is scheduled to be released in 2013, but there are virtually no changes for the reinforced concrete provisions outlined in the first supplement.

In ASCE/SEI 41-06, concrete provision for modelling parameters and numerical acceptance criteria are classified based on flexure failure, shear failure, flexure-shear failure, or inadequate lap splicing. However, it is stated in EERI/PEER (2006) that the original proposed acceptance criteria from ASCE/SEI 41-06 yield conservative results. Furthermore, studies conducted by Sezen and Moehle (2006) demonstrated the existence of limited plastic deformation capacities of columns due to flexural yielding prior to shear failure, commonly known as flexure-shear failure. Thus, a revision of ASCE/SEI 41-06's deformation limits was required in order to improve future estimations.

Classifications of columns for determining modelling parameters were revised and published in ASCE/SEI-41 Supplement-1, which included the flexure-shear failure mode. In this supplement, three conditions are defined and classification of columns is obtained through its shear capacity/demand ratio and the transverse reinforcements of critical sections. Once classified, modelling parameters and acceptance criteria can be obtained for each type of failure mode: flexure, flexure-shear, and shear.

In Chapter 7 (Seismic Assessment and Retrofit Design of Existing Buildings) of the TEC 2007, the failure of structural members is classified into either ductile or brittle failure, which respectively corresponds to flexure and shear failure as defined in FEMA 356. However, the TEC 2007 has yet to incorporate the flexure-shear mode in its classification procedures, which is essential in order to accurately estimate member modelling parameters and acceptance criteria.

The TEC 2007 provides a strain-based procedure for nonlinear performance assessment of existing buildings. Both pushover and time-history analysis methods are based on modelling with lumped plasticity elements. The nonlinear moment-rotation behaviour of members is modelled using rotational springs defined at the member ends.

Through this approach, deformation demands are calculated in terms of plastic rotations, whereas the classification procedures are defined in terms of strain limits, for both concrete and longitudinal reinforcement. These plastic rotation demands are then converted to their equivalent strain demands through individual member moment curvature analysis.

The strain values obtained are then used to determine the damage regions at member ends. This strain-based performance evaluation method yields more realistic results when compared to using the rotation demands. However, it is a tedious process which requires individual member cross-sectional analyses, an intermediate step which contains sensitive assumptions that may decrease the overall accuracy of the method.

It is essential in both linear and nonlinear modelling that joint strength and flexibility capacities are captured as accurately as possible. Earthquake-induced deformations in moment resisting frames cause moment reversals at joints of columns and beams which lead to high shear demands in these regions. If improperly modelled, frame stiffness reduction and/or premature strength loss will not be captured correctly.

Before the onset of plasticity, the elastic portion of a beam-column joint's behaviour can be modelled as rigid offsets of different lengths at element ends, representing the joint flexibility through the connecting beam-column elements.

In FEMA 356, the simple approach of setting rigid offsets equivalent to the joint dimensions of the beam and column is recommended. ASCE/SEI 41-06 improved on this, setting rigid offset lengths which are a function of the flexural strength proportions of connected beam-column joints. In the case of a strong column-weak beam system, rigid offsets are only required for columns, whereas in a strong beam-weak column system, rigid offsets are only recommended for beams. For intermediate cases, half the length of the joint dimension is modelled as the rigid offset length for columns and beams at the joint. The TEC 2007 (section 7.4.12) states to define infinitely rigid offsets for both columns and beams. In the current thesis, rigid joint offsets are defined in the model using ASCE/SEI 41-06 recommendations which are later modified as per experimental observations for the purpose of calibration.

In a recent study by Birely et al. (2012), recommended procedures from FEMA 356 and ASCE/SEI 41-06 for rigid offsets were evaluated through 45 models. The findings were that defining rigid offsets as per FEMA 356 resulted in overly stiff models and using ASCE/SEI 41-06 resulted in more realistic values. FEMA 356 predicts an overly stiff model which inaccurately predicts the initial yield displacements, while ASCE/SEI 41-06's predictions are generally good, except for in the case of joints which did not satisfy the requirements of ACI 318-08. Thus, it was recommended that an alternative definition of rigid offsets be set for joint compliance/non-compliance with ACI 318-08, in order to improve the estimation of initial yield displacements.

The behaviour of beam-column joints have been an extensively researched topic in the past, resulting in the general conclusion that joints experience high shear deformations prior to the yielding of longitudinal reinforcement. Once beam-column joints enter the plastic region, properly modelling their nonlinear behaviour becomes an important factor in accurate simulations.

1.3.2 Seismic Response of Unreinforced Masonry (URM) Infilled Frames

The behaviour of reinforced concrete frames infilled with masonry panels is a complex phenomenon and has been the topic of research since past several decades. Despite the differences in observations, hypotheses and methodologies claimed among the researchers and scientists, it is a well establish consensus that the stiffness, strength and energy dissipation characteristics are greatly altered by the integral action of the frame and the infill. The frame intends to transfer the lateral loads to the infill and the infills contribute to the overall stiffness depending on the manner the load is distributed to it and, in doing so, the lateral load response of the frame is greatly affected by the reaction of the infills.

The interactive behaviour of frame and infill is the governing factor for strength of the composite assemblage. Masonry infill material is non-ductile which fails in brittle fashion due to diagonal tension. However, once confined by the bounding frame, it is capable of resisting high compressive forces until a crushing failure is reached. This capability of resisting compressive forces depends on the properties of the confining frame as well as the infill itself.

The mechanism of load transfer between the frame and the infill during a seismic event is very important to be understood. When the lateral load is applied to the infilled frame, initially it is resisted solely by the frame until the motion is strong enough to mobilize the composite action of wall/frame system without any visible damage. This means that the induced displacements are sufficient enough to overcome the lack of fit between the wall and frame as well as the shrinkage of the masonry infill panel as demonstrated by Mosalam (1996). Once the composite action is mobilized, the tensile stresses starts to build up due to the distortions in the panel geometry causing the separation between the infill and the frame, except at the loaded corners, when the tensile strengths exceeds the bond strength of frame-infill interface. At this stage, the infilled frame exhibits a diagonally braced RC frame system. The similar behaviour is observed on both reversed and forward cyclic motion. With the increasing magnitude of lateral forces, the masonry panel cracks in a diagonal X-pattern when the tensile strength of the infill material is reached. Upon cracking of infill the stiffness of the composite system decreases. Further increase in the lateral forces causes further cracking parallel to the loaded diagonal. The composite assemblage can thus be represented with a frame system braced diagonally by means an '*equivalent compression strut'* with a degrading stiffness. The failure of the system is governed by the compression crushing of these struts or the brittle failure in the confining elements.

An enormous quantity of experimental and analytical research has been conducted to study the effects of masonry infills on the response of infilled frames. A good up-to-date review of the corresponding experimental research can be found in the PhD dissertation of Koutromanos I. (2011). Some of the research studies related to the current thesis are discussed here in brief.

Klingner and Bertero (1978) conducted a series of tests on 1/3-scaled single bay three and half storey masonry infilled RC frames to investigate the cyclic behaviour of engineered infilled frames under seismic action. The infills contained reinforcement and the frames were designed to show ductile response causing no shear failures. The bare frame was tested with strong column-weak beam configuration which was later infilled with masonry panels of hollow clay blocks and concrete block and test is carried out again. Initially, the cracks show the pattern consistent with deep beam stress orientation. After the frame infill separation occurred, the infill panels behaved like diagonal struts. In the end, crushing of infills led to the strength degradation and formation of soft-storey in every specimen tested. Important to note is that soft storey formed in the second storey for the specimen infilled with concrete blocks. They concluded that the performance of infilled frames was much better than bare frame with improvements in strength and stiffness of 2 and 6 times respectively which covers more than well the increased demand caused by period shortening. The energy dissipation capacity of frames was also better which was attributed to the distributed cracking of infills and prevention of deterioration of beam-column joints. The engineered panels achieved the desired performance preventing excessive permanent deformation reducing the secondary forces caused by P-delta effects.

Bertero and Brokken (1983) conducted the test in the similar type of specimens as Klingner and Bertero (1978) several types of masonry infills namely unreinforced hollow clay panels, reinforced concrete block panels, solid brick panels with welded-wire reinforcement and a stucco (mortar) cover, and lightweight concrete panels. The test results indicated that the strength of an infilled frame is not merely the sum of the strengths of the infill panel and the bounding frame, because the latter may not reach its capacity simultaneously with the infill. Depending on the type of the infill, the lateral stiffness was 5.3 to 11.7 times that of the bare frame. They also performed analytical studies using an equivalent strut model calibrated with their test results on the eleven storey prototype. They concluded that infills tends to fail in explosive (brittle) fashion and the strength, stiffness and deformational capacities of masonry infills are very sensitive to material and workmanship quality. They also indicated that majority of infilled specimen failed with soft-storey mechanism.

Kahn and Hanson (1979) investigated the importance of seismic detailing as well as infill to frame strength ratio on the structural response of infilled frames. They have found that the infill transfers shear stresses to the columns causing them to fail in brittle manner. They concluded that providing the separation between the bounding columns and infill panels and improving the transfer of shear from infill to the columns by providing adequate confinement reinforcement can prevent brittle failure of columns and hence enhance overall ductility.

Mehrabi et al. (1996) conducted the tests on fourteen 1/2 scaled frame specimens for monotonic and cyclic loads to investigate the strength increase as well as the impact of panel aspect ratio, strength of infill, magnitude of vertical stress and lateral load history on the structural performance of infilled frames. They found that the cyclic loads tend to cause reduction in peak strength as well as faster strength degradation of the frames as compared to monotonic loads. They also investigated that for the case of infill with solid units, the damage pattern was different for a non-conforming frame than for a code-conforming frame. For a weak frame the damage pattern included brittle shear failures in the columns, while for a strong frame, damage occurred in the form of crushing in the infill panel masonry in the diagonal compression strut and at the corners.

Another study conducted by Hobbs and Samai (1985) was aimed at investigating the effect of relative stiffness of infill with respect to the frame. They have also reached a conclusion that a weak infill give a smooth behaviour close to an ideal-elastic perfectly plastic while a stronger infill results in brittle response due to shear failure in the members.

The presence of openings is also an important factor causing an alteration in the response of infill panels. Mosalam et al. (1998) tested a 1/4-scale, two-story, two-bay, masonry-infilled steel frame with pseudo-dynamic test apparatus with a series of simulated ground motions. The second storey infills were provided with openings and thus the first cracks occurred at the second rather than the bottom story. However, the final damage was more extensive and concentrated at the bottom story based on the crack pattern obtained. In a similar study but with non-conforming concrete frames, Buonopane and White (1999) reported the similar behaviour as Mosalam et al. (1998).

Pujol and Fich (2010) tested a full-scale flat slab building consisted of two parallel planar three-story, two-bay frames. Six actuators were used to apply the lateral loads following a triangular distribution. The frame represents the non-conforming construction designed only for gravity loads. The infills were made of standard modular cored clay bricks. The bare frame was initially tested until punching shear cracks occurred at a column-slab connection on the third floor at a drift level of 3%. Later, one bay of each story for each frame was infilled and testing resumed. Considerable damage occurred in the infills in the form of diagonal-sliding cracks and corner crushing, with the latter even resulting in partial collapse of several infill panels. They found out that in general, the infills significantly increased the strength and stiffness of the structure, while the obtained drift capacity was deemed satisfactory. They concluded that infills would be able to improve the behaviour of non-conforming construction.

1.3.3 Autoclave Aerated Concrete Masonry Walls and Infill Panels

Autoclave aerated concrete (AAC) is a mortar mix of cement, lime, water and sand in which air voids are entrapped by adding suitable aerating agent, usually aluminium powder. The chemical reaction between aerating agent and concrete causes expansion as high as up to five times its initial volume. Masonry blocks formed using this cellular concrete material are later cured in pressurized chamber called autoclaves. A good review of structure and properties of aerated concrete is presented by Narayanan and Ramamurthy (2000).

The use of AAC blocks for both structural and non-structural purposes is increasing rapidly. The main advantage of using AAC masonry infill panels in RC framed structures is its lightness, which reduces the seismic inertial forces eventually economising the design of supporting structure and foundation as well as considerable savings in material due to porous nature. In addition, it has excellent thermal insulation and fire resistant properties which are crucial in risk reduction during a seismic event. These advantages validate the increasing interest for AAC masonry infills in areas of high seismicity and thus justify the need of analytical and experimental assessment.

The research already conducted for the seismic performance of AAC masonry is mainly concentrated on the evaluation of the performance of load bearing AAC masonry buildings. Costa et al. (2011) conducted the experimental and analytical research to test the seismic performance of AAC load-bearing masonry. They cyclically tested two unreinforced AAC masonry wall piers each of 1.5 meter length and 3 and 4.5 meters height to investigate the influence of vertical stress and slenderness ratio on the mechanical properties as well as the cyclic response of AAC masonry piers. Later this data is used to calibrate numerical model for the simulation of load bearing masonry building response. They concluded the maximum ultimate drift for AAC shear walls can safely be taken as 0.35% while 0.5% for walls failing in flexure. They also reported good correlation of experimental results with Euro code strength criteria for AAC load-bearing masonry walls.

The current study is unique in its sense that it provides useful data on the seismic performance of reinforced concrete frames that are infilled with AAC non-load bearing masonry by means of both the experimental and analytical research.

1.3.4 Analytical Modelling of Unreinforced Masonry Infill Panels

Several researchers have studied the effects of masonry infill panels on the RC frames over the past 50 years or more, proposing various approaches to incorporate and validate the contribution of infill panels to the local and global response of structures. These approaches can broadly be classified in to two classes. The first among them, described as *"micro-modelling approach"*, is a rigorous approach

in which the RC frame, the integrated masonry and their mutual connections are separately modelled by defining appropriate constitutive laws. The second approach includes *"macro-modelling approach"*, which is most widely used and involves the application of straightforward heuristic models in order to incorporate infill panels' contribution. By far, the most popular among these is the method of *"equivalent strut"*, which is based on the experimental and field observations that the load path within the infill panel follows a diagonal pattern through the compression region, so called the equivalent compression strut.

In the current study, the equivalent strut model with single compression strut is utilized to incorporate the response contribution of masonry infill panels because of its practicality and flexibility of use for nonlinear dynamic seismic analysis which is not the case in micro modelling approach. Polyakov (1960) was the first to propose the use of a diagonal strut to model the effect of an infill. Given the simplicity of use and application, equivalent strut model is sensitive to;

- the determination of mechanical properties of masonry infill panel and of the bounding frame;
- extent of contact of infill with the frame (e.g. completely or partially infilled);
- definition of the width of equivalent strut b_w;
- connection of equivalent strut with the frame (e.g. concentric or eccentric);
- presence and location of opening (e.g. door, window etc.) within a panel.

Literature provides a wide range of propositions for the choice of strut section. The thickness of strut is usually kept similar as that of panel while there are several proposals for the definition of width b_w. Among the earliest work for determination of b_w relates it to the diagonal length of the panel. Later, in order to account for the variability in determination of mechanical parameter for the infill, Smith and Carter (1969) introduced the stiffness parameter λ expressing the relation between stiffness of bounding frame and of panel. Klinger and Bertero (1976) also worked in the same direction with a different expression for b_w as function of λ. Durrani and Luo (1994) modified the formulation of stiffness parameter taking into account the effect of geometry of the frame. Kadir M.R.A. (1974) and Dawe and Seah (1989) accounts the influence of not only adjacent columns of frame, but also the top beam, and thence split stiffness parameter in to λ_P and $\lambda_T$for columns and beams respectively, although earlier it has been demonstrated by Stafford Smith (1967) that lateral stiffness is independent of beam stiffness.

The performance and calibration of equivalent strut model is largely dependent on factors such as width (b_w) of the strut, constitutive relationship of the panel, damage level attained by the panels and number of equivalent struts used; as demonstrated by G. Uva et.al (2012). Calibration of global and local responses is sensitive to the use of single or multiple struts respectively as demonstrated also by Fiore, A., Netti, A., and Monaco, P. (2012). Fundamental period is largely dependent on the definition employed to calculate the width of equivalent compression strut which affects the rigidity of the frame. Choice of a wider section of compression strut to model the infill panel tends to increase the strength but shows brittle behaviour whereas using thin section for equivalent strut exhibits ductile behaviour of the modelled structure. G. Uva et.al also demonstrated that constitutive relationship has a direct impact on the strength and stiffness of the panel but is indirectly dependant on the influence of failure mechanism affecting the panel. They added that damage to panel on the other hand, increases with growing magnitude of lateral force and renders the response of the system highly nonlinear and complex which these macro-models are unable to capture properly. A good review over the analytical modelling of masonry infill is presented by Crisafulli et al (2000)

1.4 Objective and Scope

In the light of aforementioned problem statement, The Scientific and Technological Research Council of Turkey (TÜBİTAK) has approved funding for verification and validation of the new additions in the TEC 2007 through analyzing and comparing various concrete frames using physical and simulation models. The project is entitled: "Developing Performance-Based Evaluation Procedures and Strengthening Methods for the Turkish Seismic Code through Experimental and Analytical Research" and is officially documented as "TÜBİTAK 1007" (Project # 108G034). The project has duration of 36 months and commenced on February 15, 2010.

The project frames of interest for the current thesis are as follows:

- Specimen #5 (hereinafter referred to as Specimen #1) Non code conforming deficient bare frame.

- Specimen #8 (hereinafter referred to as Specimen #2) Non code conforming deficient frame infilled with AAC blocks.

- Specimen #10 (hereinafter referred to as Specimen #3) Code conforming bare frame.

- Specimen #11 (hereinafter referred to as Specimen #4) Code conforming frame infilled with AAC blocks.

Each physical test frame constructed in the laboratory is essentially a ½ scale 3-storey and 3-bay frame of the project's prototype reinforced concrete frame, but varies with respect to code conformations and deficiencies. In addition, two out of four specimens are infilled with AAC masonry blocks in the entire middle bay of the frame. The ½ scaling is based on principles of equal stresses, leading to results that are half the displacements of the prototype frame but equal inter-storey drifts. The frames are subjected to pseudo-dynamic loads. The analytical modelling of the frames will be performed by the author on OpenSees software. Modelling of Unreinforced Masonry (URM) Infill walls is based on single equivalent strut methodology proposed by Smith and Carter (1969). Mechanical properties of AAC infill material are acquired by compression testing of masonry prisms.

The following objectives are set forth in this thesis:

- Processing the data from the Pseudo-Dynamic Testing of four reinforced-concrete frame specimens, including two bare frames and two frames infilled with AAC masonry panels;

- Acquisition of basic mechanical properties of AAC infill material by compression testing of masonry prisms;

- Investigating the effects of AAC infill panels on the response of code conforming and substandard reinforced concrete frames;

- Investigating the effect of additional shear imposed by the infill panel on the boundary columns;

- Development and calibration of numerical simulation models;

- Testing the accuracy of equivalent strut model for representing the AAC infill panels; and

- Evaluation of strain-based nonlinear performance assessment procedures as outlined in the TEC 2007 in light of experimental observations.

Chapter 2 briefly presents an overview of the experimental setup and their results. Experimental investigation of AAC masonry infill effects on RC frame response is presented in Chapter 3 by means of both, the damage observations as well as the time histories of global and local responses measured during the pseudo dynamic testing. Numerical simulations of bare and infilled specimens are presented in Chapter 4 in comparison with experimental results and observations. In addition to the examination of certain global responses, selected beams and columns will be examined in detail on a local scale. Chapter 5 includes performance assessment of test specimens using the experimental and analytical results as well as comparison with observed damages during the tests. Chapter 6 presents the main conclusions of this thesis with future recommendations.

CHAPTER 2

EXPERIMENTAL TESTING

2.1 General

In this chapter, discussion about the pseudo-dynamic testing procedure is presented along with the summary of experimental results and observations. Four reinforced concrete frame specimens were constructed and tested by the team of research assistants and PhD students of department of Civil Engineering at the Structural Mechanics Laboratory of METU as part of TÜBITAK1007 project on performance-based design and assessment of reinforced concrete buildings.

Two out of four specimens are deficient frames, hereinafter referred as "Non-Conforming" frames, as they are not compliant according to the standards of the Turkish Earthquake Code 2007 [TEC 2007]. Deficiencies include the use of low concrete strength, plain reinforcing steel, minimum flexure reinforcement, insufficient confinement, and insufficient shear strength. These frames are sufficient to resist gravity loads. Among the Non-conforming frames, the second specimen (hereinafter referred to as Specimen #2 or Infilled Frame) is essentially the same as the first specimen (hereinafter referred to as Specimen #1 or Bare Frame), but with the presence of Aerated Concrete Masonry infill walls in the entire middle bay of the frame.

The other two specimens (hereinafter referred to as Specimen #3 or Bare Frame and Specimen #4 or Infilled frame) have essentially the same configuration with the only difference is that they both are code-conforming as they are compliant with the provisions of TEC 2007 and TS 500 (2000). Their design is sufficient to resist both gravity and applied seismic loads.

Usually in designing of structures the presence of unreinforced masonry infills are neglected by considering them as non-structural components. Only their weights are accounted for in calculating the gravity loads. However their impact on the global seismic response of structure is now widely accepted. Therefore it is of utmost importance to study the effect of masonry infills on the overall performance of structure as well as individual components and to incorporate them in the analysis and design using simple and practically applicable procedures.

The strength and deformation response of a structure is highly affected by the presence and contribution of infill walls. Infill walls increase the lateral strength of the frame initially, until they sustain damage. Then this strength increase is removed suddenly as the strength of the infill is eventually lost with the accumulation of damage. This removal is usually quiet sudden since the response of unreinforced masonry infills is brittle.

Each test frame constructed in the laboratory is essentially a ½ scale 3-storey and 3-bay frame of the prototype reinforced concrete frame building which was designed according to the regulations of TEC 2007 for a residential building located in the first seismic zone on Z3 (highly weathered soft metamorphic rock, medium dense sand and gravel, stiff clay and silty clay) soil type.

The plan view of the prototype structure is presented in Figure 2.1. Detailed description of the specimens can be found in the following sections.

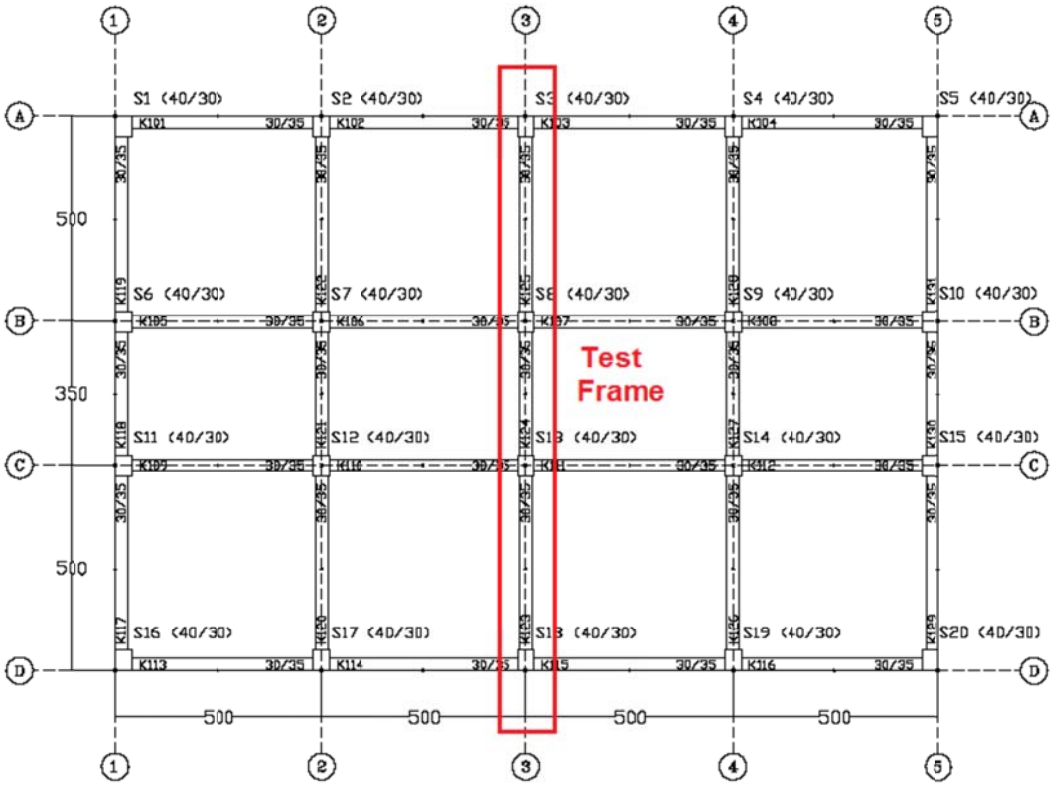

Figure 2.1: Plan of prototype building and selected test frame

Continuous pseudo-dynamic testing was carried out for all the specimens using synthetic ground motions compatible with the site-specific earthquake spectra developed for the city of Düzce, as a result of the 1999 earthquake.

Scaling of the test specimens and synthetic ground motion were analytically verified using preliminary pushover and time-history analyses. Using the similitude law, the original ground motion when compressed in the time domain by a factor of $\sqrt{2}$, produces the desired earthquake demands on the ½-scaled specimen.

2.2 Test Specimens

The construction of test specimens is based on the dimensions of prototype three-story building with the floor plan shown in Figure 2.1. The member sizes and longitudinal reinforcement details of the prototype frame were designed as per TEC 2007. The column dimensions were calculated to be 400 mm x 300 mm, with approximately 1.3% longitudinal reinforcement ratio. The beam dimensions were 300 mm x 350 mm, which remains uniform in all spans. The constructed test specimens would represent a typical interior bay frame shown in Figure 2.1. The dimensions of all the test frames and their member cross-sections were taken equal to ½ that of the prototype frame, as shown in Figure 2.2.

The mean uniaxial compressive strength of concrete determined from cylinder tests for the specimens are shown in Table 2.1. The reinforcement material strengths are shown in Table 2.2. The detailed section and joint drawings of Specimen #1 and #2 (Non-conforming) are presented in Figure 2.3(a) while those of Specimen #3 and #4 (code-conforming) are presented in Figure 2.3(b). The detailing was the same for all the elements in each story and each axis of a test frame.

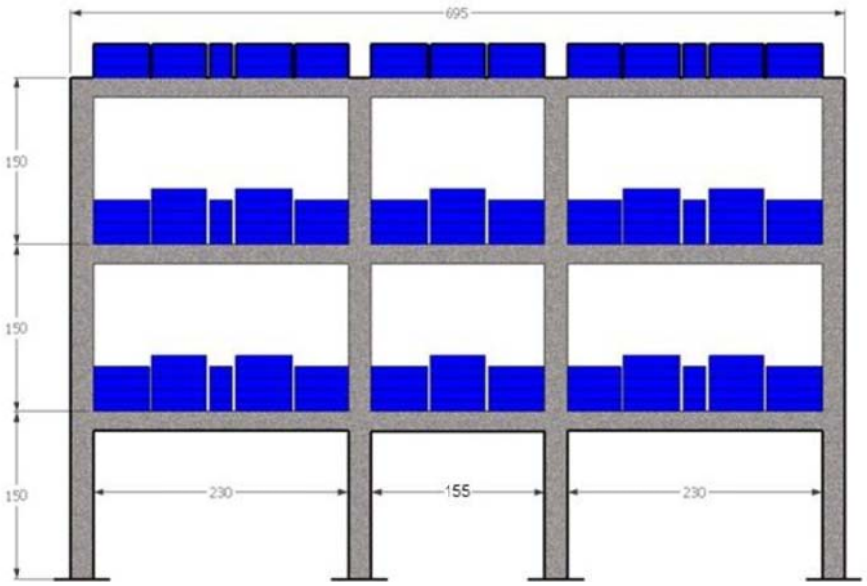

a) Elevation of Specimen #1 and #3 [Bare Frames]

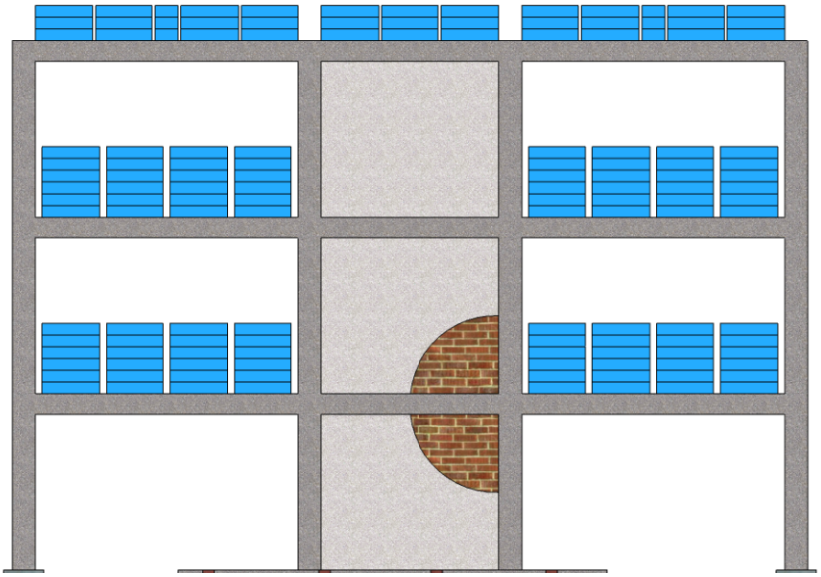

b) Elevation of Specimen #2 and #4 [Unreinforced AAC Masonry Infilled Frames]

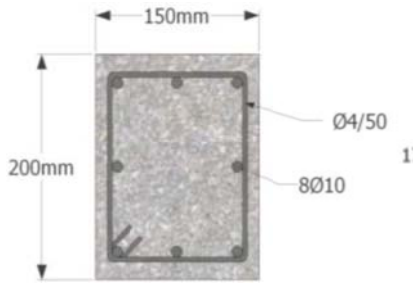

c) Typical Column Cross-Section

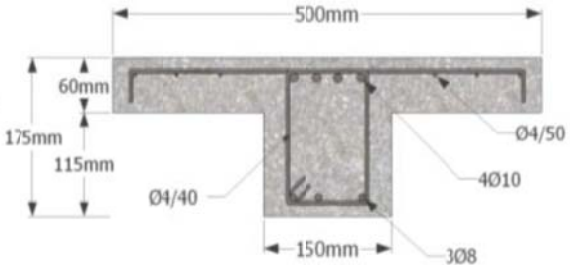

d) Typical Beam Cross Section

Figure 2.2: General views of the test specimens

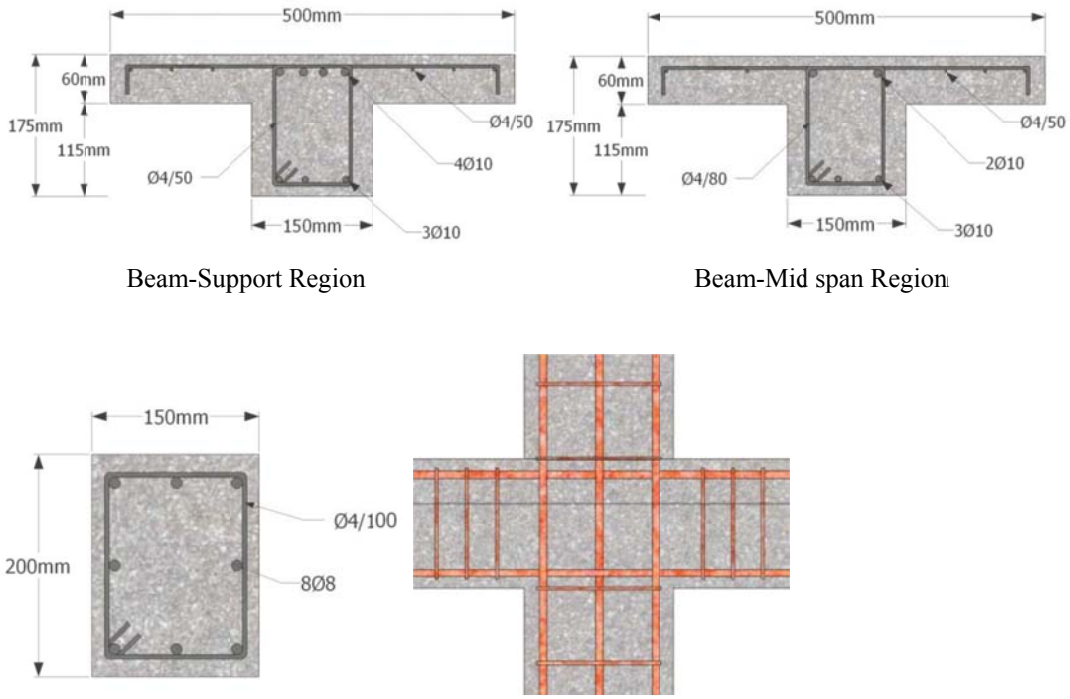

Figure 2.3(a): Specimen #1 and #2 (Non-conforming) column, beam and joint reinforcement details

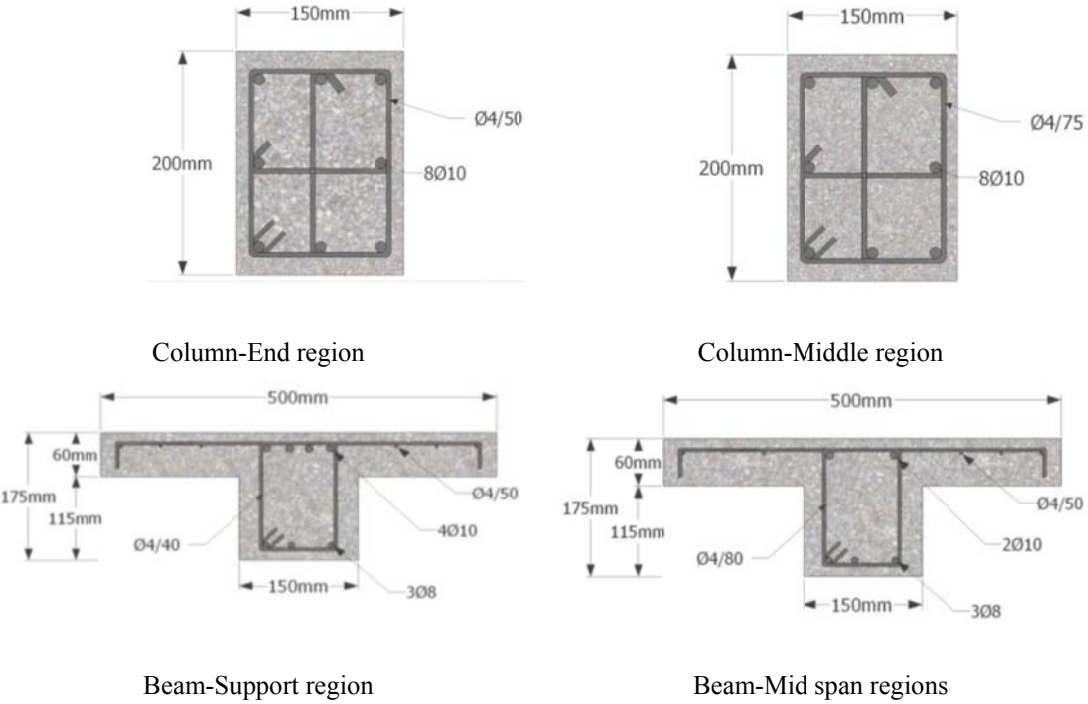

Figure 2.3(b): Specimen #3 and #4 (Code-conforming) column and beam reinforcement details

Table 2.1: Concrete compressive strengths of test specimens

Specimen	Mean cylinder compressive strength ($f_{c\ mean}$) [MPa]
# 1 [Non-conforming Bare Frame]	11.9
# 2 [Non-conforming Infilled Frame]	14.6
# 3 [Code conforming Bare Frame]	27.5
# 4 [Code conforming Infilled Frame]	27.5

Table 2.2: Reinforcement strength of test specimens

	Reinforcement Strength					
	Specimen #1 and #2 (Non-Conforming)			**Specimen #3 and #4 (Code-Conforming)**		
	Longitudinal		**Transverse**	**Longitudinal**		**Transverse**
	Columns	***Beams***		***Columns***	***Beams***	
Yield Strength (F_y) [MPa]	320	355	240	480	480	240
Ultimate Strength (F_u) [MPa]	460	555	-	750	750	-
Remarks	8 mm diameter plain bars	10 mm diameter plain bars	4 mm diameter plain bars for both columns and beams	10 mm diameter deformed bars	10 mm and 8 mm diameter deformed bars	4 mm diameter plain bars for both columns and beams

In addition to the above described material and geometric properties of the test frames, the non-conforming specimens (#1 and #2) were deliberately provided with deficiencies commonly observed in the buildings within Turkey. These include deficient material strengths, reinforcement amounts, reinforcement details and joint details in order to obtained insufficient capacities.

The properties of the non-conforming test specimens (Specimen #1 and #2) are as follows:

- The column longitudinal reinforcement was approximately 1.3%;
- Plain reinforcement bars with 8 mm and 10 mm diameters were used instead of deformed bars for both columns and beams, respectively;
- The yield strength of the 8 mm and 10 mm diameter bars were 320 MPa and 355 MPa, respectively;
- The ultimate strengths of these bars were 460 MPa and 555 MPa, respectively;
- The 4 mm plain reinforcement bars used as transverse reinforcement have the yield strength of 240 MPa;
- The mean value of uniaxial compressive strengths of concrete for both specimens were determined from standard cylinder tests and were well below the value required by the TEC 2007;

- The flexural and shear capacity of the beams and columns were designed to be sufficient for gravity loads;
- The conventional strong-column weak-beam requirement was violated in these specimens;
- The spacing of transverse reinforcement of the columns was kept constant throughout the column height, which resulted in unconfined zones at potential plastic hinge regions of the element; and
- Lateral reinforcements from the column members did not continue in-to the joints, reflecting joint shear deficiencies.

The properties of the code-conforming test specimens (Specimen #3 and #4) include:

- The column longitudinal reinforcement was approximately 2.1%;
- Deformed reinforcement bars were used with 10 mm diameter for columns and 8 mm and 10 mm diameter for beams at bottom and top respectively;
- The yield and ultimate strength of longitudinal bars were 460 MPa and 750 MPa respectively;
- The ultimate strengths of these bars were 460 MPa and 555 MPa, respectively;
- The 4 mm plain reinforcement bars used as transverse reinforcement have the yield strength of 240 MPa;
- The mean value of uniaxial compressive strengths of concrete for both specimens were determined from standard cylinder tests and were well above the minimum value required by the TEC 2007;
- The flexural and shear capacity of the beams and columns were designed to be sufficient for gravity and seismic loads;
- The conventional strong-column weak-beam requirement was satisfied in these specimens;
- The spacing of transverse reinforcement of the columns was reduced near the supports as per TEC 2007 provisions to provide proper confinement at the potential plastic hinge regions of the element;

The condition of insufficient shear capacity ($V_r<V_e$) corresponds to a flexure-shear failure mode as defined by ASCE/SEI 41-06. According to ASCE/SEI 41-06, the flexure-shear failure mode (referred as 'condition (ii)' is considered when member is expected to experience yielding in flexure prior to failing in shear. In the TEC, there is no intermediate failure mode between shear and flexure failure defined and as such, this condition would be classified as shear failure. In the TEC 2007, the shear force demand on a column ($V_e = (M_t+M_b)/l_n$) is determined by using the top and bottom moment values (M_t and M_b) of the columns, for a weak column-strong beam system. For the bottom ends of the base columns, the plastic moment capacities M_p were taken as the bottom end moments (M_b). A weak column-strong beam system is defined in the TEC 2007 (Section 3.3.5.1) when the plastic moments of the columns are less than 1.2 times the plastic moments of the beams connecting into a joint, which is the case for non-conforming frames (specimen #1 and #2) (see M_p values in Table 2.3 and Table 2.4). Most joints in the non-conforming specimens (#1 and #2) satisfy this condition for a weak column-strong beam joint, with the exception being the exterior joints at the 1st and 2nd storey. For code conforming specimens (#3 and #4), the condition of strong column-weak beam is satisfied for all the joints. Table 2.5 presents the shear capacities and capacity/demand ratios of the columns, calculated using the nominal strength values (without safety factors) for all the four frames according to TS-500 (2000). Note that label 'NC' corresponds to "**Non-conforming**" while 'CC' corresponds to "**Code-conforming**" specimens in the entire text.

Table 2.3: Reinforcement details and moment capacities of columns

Specimen	Column	Reinforcement Details			Moment Capacity [*kN-m*]	
		Longitudinal	Transverse (plain)		Yield	Plastic
			Middle	Ends	M_y	M_p
# 1 [Bare Frame – NC]	Outer	8Ø8(pl.)	2xØ4/100mm	2xØ4/100mm	13.0	14.1
	Inner				13.4	14.8
# 2 [Infilled Frame – NC]	Outer	8Ø8 (pl.)	2xØ4/100mm	2xØ4/100mm	13.2	14.8
	Inner				13.6	15.4
# 3 [Bare Frame – CC]	Outer	8Ø10 (def.)	3xØ4/75mm	3xØ4/50mm	23.8	27.3
	Inner				24.7	28.1
# 4 [Infilled Frame – CC]	Outer	8Ø10 (def.)	3xØ4/75mm	3xØ4/50mm	24.0	27.6
	Inner				24.4	28.0

Table 2.4: Reinforcement details and moment capacities of beams

Specimen	Reinforcement Details				Moment Capacity [*kN-m*]			
	Longitudinal		Transverse (plain)		Yield		Plastic	
	Span (a)	Support (b)	Span (a)	Support (b)	M_y^a	M_y^b	M_p^a	M_p^b
# 1 [Bare Frame – NC]	4Ø10+3Ø10	2Ø10+3Ø10	Ø4/80mm	Ø4/50mm	17.8	12.7	20.7	16.8
# 2 [Infilled Frame – NC]	4Ø10+3Ø10	2Ø10+3Ø10	Ø4/80mm	Ø4/50mm	18.0	12.9	21.0	17.0
# 3 [Bare Frame – CC]	4Ø10+3Ø8	2Ø10+3Ø8	Ø4/80mm	Ø4/50mm	23.3	10.2	26.6	15.3
# 4 [Infilled Frame – CC]	4Ø10+3Ø8	2Ø10+3Ø8	Ø4/80mm	Ø4/50mm	23.3	10.2	26.6	15.3

Table 2.5: Columns shear capacity and capacity/demand ratio

Specimen	Shear Capacity V_r [*kN*]	Shear Demand	Capacity/Demand ratio
		V_e [*kN*]	V_r/V_e
# 1 [Bare Frame – NC]	26.6	18.4	1.45
# 2 [Infilled Frame – NC]	28.4	18.6	1.53
# 3 [Bare Frame – CC]	55.7	37.73	1.48
# 4 [Infilled Frame – CC]	55.7	37.73	1.48

2.3 Pseudo-Dynamic Testing and Instrumentation

The dead and super-imposed live loads of prototype building were used to calculate the mass and gravity load acting on the test specimens. The floor mass and gravity loads were consistent throughout each Pseudo dynamic test. Solid steel blocks were used to replicate the calculated dead plus live loads on the test specimens as shown in Figure2.2. In case of infilled test frames (Specimen # 2 and #4), due to the presence of masonry infill walls, the load blocks were shifted to adjacent bays and top in a way that the total weight of blocks in all the test specimens remains the same. The blocks were arranged such that the ratio of axial load (N) to the axial load carrying capacity of the columns (N_o) is similar to the prototype frame. The axial load ratios of first storey columns under gravity loads are presented in Table 2.6.

Table 2.6: Concrete strength and axial load ratios of columns

Specimen	Concrete strength $f_{c\ mean}$ [MPa]	N/N_o (%) in first storey	
		Interior Column	Exterior Column
# 1 [Bare Frame – NC]	11.9	25.77	15.48
# 2 [Infilled Frame – NC]	14.6	18.96	15.36
# 3 [Bare Frame – CC]	27.5	11.15	6.70
# 4 [Infilled Frame – CC]	27.5	10.10	8.18

N = axial load due to steel blocks; N_o = Axial load carrying capacity of columns, $N_o = f_{c\ mean} \times A_c$

Pseudo-dynamic testing (also referred to as the online computer controlled testing) is a hybrid earthquake simulation technique which enables to numerically model part of the dynamic structural properties while rest of the structure is physically tested in parallel with computations, as often demonstrated (Mahin and Shing (1985), Nakashima (1985), Takanashi et. al. (1975)).

This testing method came out as an alternative to the more advanced testing method such as shake table testing and introduced greater accuracy providing the simplicity of conventional methods like quasi-static testing. It enables economical, convenient and realistic testing of large scale structures under seismic loading. Other attributes are the ability to observe general response and resulting damage formation in structure during the test because the seismic loading is applied in prolonged time or "pseudo-time" rather than in real time. The experiment can be hold at any pseudo time step to monitor the response closely and for necessary evaluations.

The main difference between pseudo-dynamic test and conventional dynamic tests is that at each pseudo time step, the computed structural displacements are actually applied to the structure and the resulting restoring forces are measured experimentally by the load cells. This removes the uncertainty linked with the analytical modelling of restoring forces of the structure. The measured restoring forces along with pre-defined ground motion and analytically computed inertia and damping characteristics would serve as an input for computing the displacement for the next time step. Servo-controlled hydraulic actuators are used to apply the computed displacement to the degrees of freedom of the test structure. The typical elevations for bare and infilled frames and schematic view of testing are shown in Figure 2.4 for the test specimens having three translational degrees of freedom.

Elevation view for bare frames

Elevation view for URM infilled frames

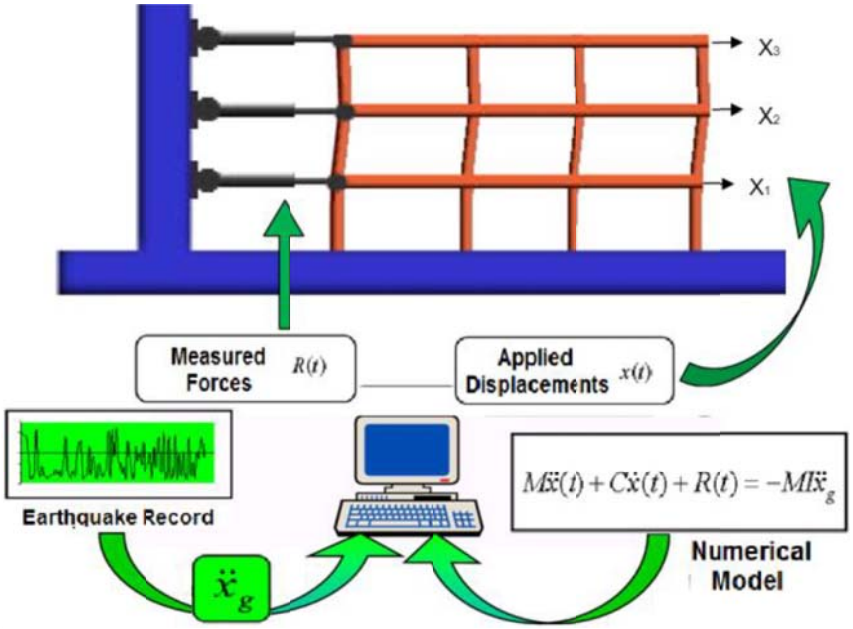

Figure 2.4: Test specimens and Pseudo-dynamic testing system scheme

Ground motions used for these pseudo-dynamic tests comprises of synthetic time-acceleration series of the 1999 Düzce earthquake which were generated in a separate work package of the overall research project. They were compatible with the site-specific earthquake design spectra for different exceedance probabilities on different soil types, as shown in Table 2.7. Three of the generated acceleration series (named D1, D2, and D3) were imposed on the test specimens sequentially.

Acceleration time series with the order of application and corresponding spectra of the ground motions are shown in Figure 2.5.

Table 2.7: Ground Motion Properties

Earthquake GM	Probability of Exceedance in 50 Years	Soil Class/Type	PGA [g]
D1	50%	Z1/Rock	0.254
D2	10%	Z1/Rock	0.545
D3	10%	Z3/Soft soil	0.604

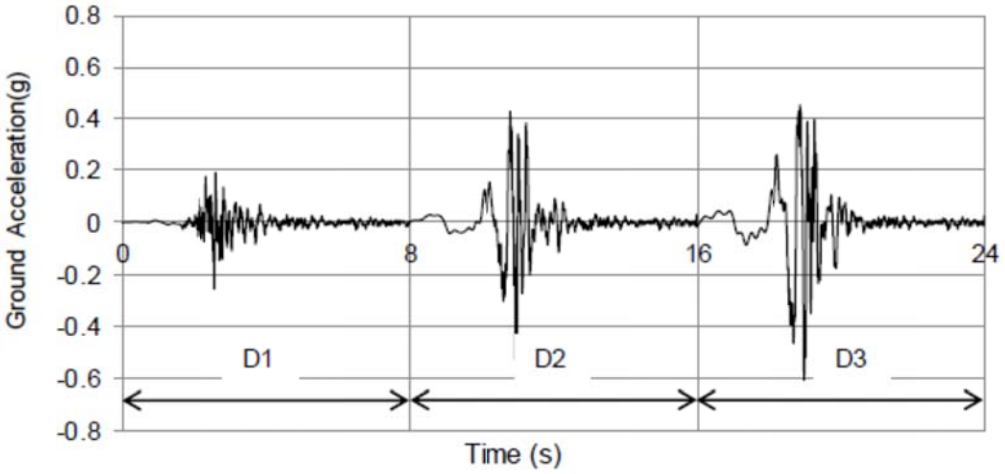

a) Acceleration-Time Series

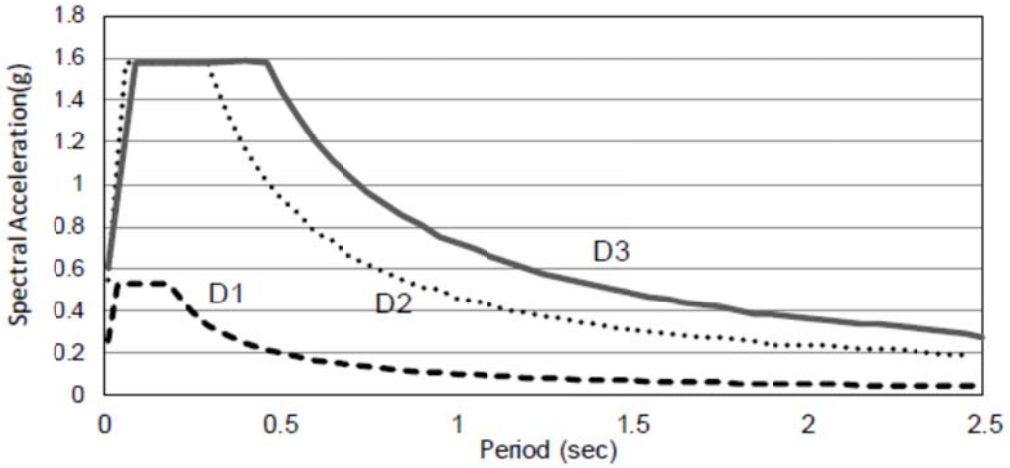

b) Design Spectra

Figure 2.5: Ground motions and acceleration spectra

Reaction forces applied on the specimen were measure by the pseudo-dynamic testing system and also by a separate data acquisition system by using load cells connected to the actuators at each storey of the test frames. For lateral displacements at each storey, LVDTs were used as measurement devices. LVDTs were also used to measure the curvatures and rotations at the bottom of the base columns and the extreme ends of all beams on the 1st and 2nd storeys as well as strains in the infill panels on all three storeys as shown in Figure 2.6a.

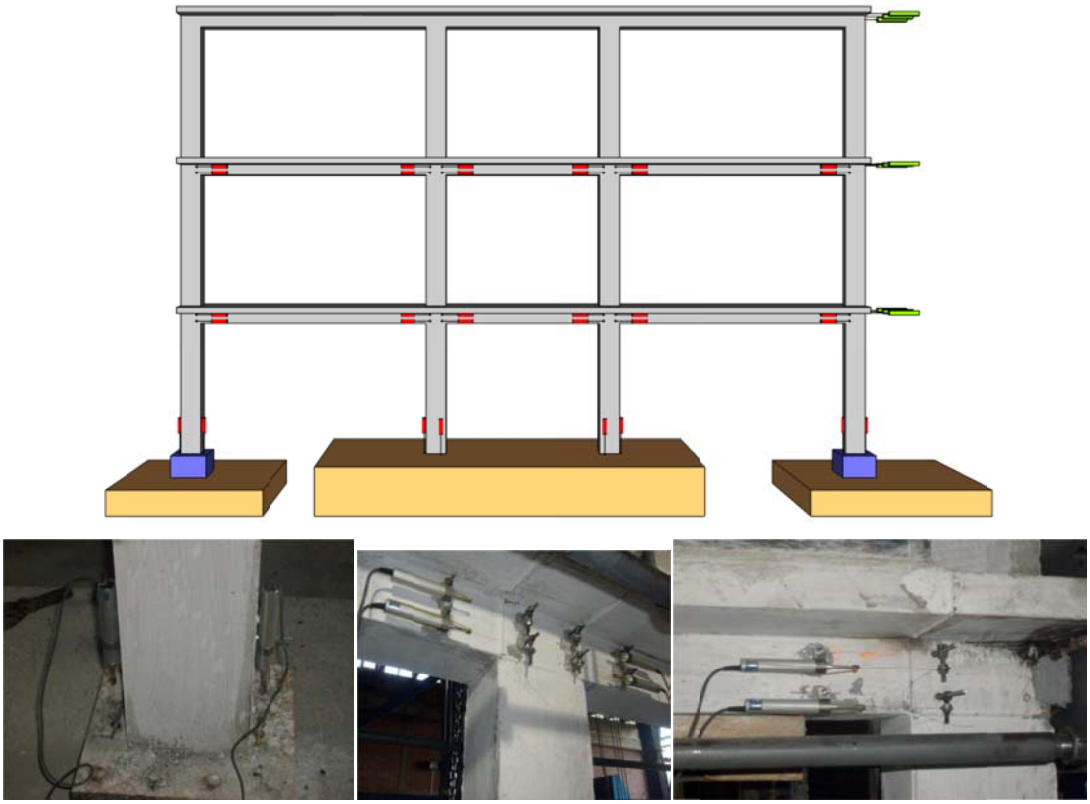

Figure 2.6(a): Measurement devices and their configurations

2.4 Test Results

This section comprises of test results from all the specimens. The main global response presented here includes storey displacement, inter-storey drift ratios and storey shear forces vs. storey drifts. Local demand parameters such as member end rotations are discussed in the next chapter along with the comparison of results between code conforming and non-conforming specimens. The members are labelled as shown in Figure 2.6 b in order to ease the member identification for presentation of results.

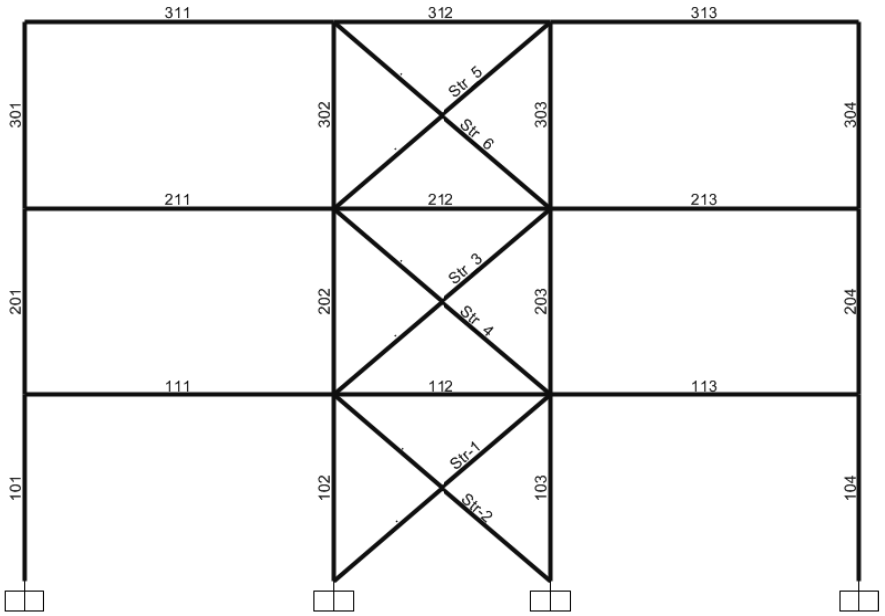

Figure 2.6(b): Member identification labels

2.4.1 Specimen #1 [Non-conforming Bare Frame]

The roof displacement response history from the experimental test is presented in Figure2.7, along with the pictures of damages observed at selected deformation peaks (Figure 2.8). The inter-storey drift ratio response history is presented in Figure 2.9. Under the first ground motion D1, no damage was observed on the test specimen. The inter-storey drift ratio limits to 0.26% for each storey and the maximum roof displacement was 9.1 mm. The frame response was nearly elastic with no residual displacement and a minimum damage state at the end of ground motion D1.

Under the second ground motion D2, the maximum inter-storey drift ratio recorded was 1.3% and the maximum roof displacement was 49 mm. Some of the major damages observed during D2 were the formation of flexural cracks in the first storey interior and exterior columns and initiation of visible cracking in first storey joint regions prior to the cracking in connecting beam and column ends. These damage formations are quiet expected and are directly associated with the lack of confinement in column ends and its absence in the joint regions. These observations imply that first storey experienced some inelastic deformations and the structure is in a moderate damage state.

Under the last ground motion D3, the visible flexural cracks at the bottom ends of base columns continued to spread and widen. Damages in the columns were followed by the spread of inclined crack in the joint regions and flexural crack formations at the beam ends. The first storey drift ratio increased to a maximum value of 4.1% and the roof displacement reached a maximum value of 206 mm. In the meantime, damages in the upper storeys spread in the form of shear cracks in the joint region and flexural cracks at the upper ends of second and third storey columns. Inter-storey drift ratios of the upper storeys were more than 5%, even higher than the first storey. These peak deformations resulted in large residual displacement at the end of pseudo-dynamic test which is also clear in both drift and roof displacement response histories. Large cracks at the top ends of the third storey columns indicated the longitudinal reinforcement pull-out phenomenon due to the unconfined joints. Severe damage state can be concluded after considering the observations on the specimen at the end of ground motion D3.

Shear force vs. inter-storey drift ratio for each storey and base shear vs. roof displacement plots are presented in Figure 2.10. The base shear vs. roof displacement plot shows severe strength degradation and a softening response, implying that the specimen lost its lateral load carrying capacity.

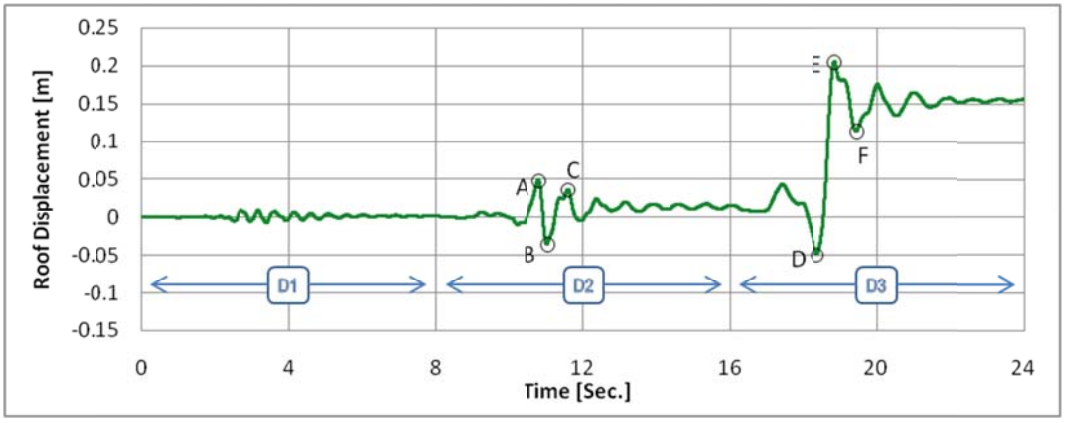

Figure 2.7: Roof displacement time-history

Figure 2.8(a): Roof displacement time-history and observed damages (SP#1)

Figure 2.8(b): Damages observed in the 3rd Storey columns at point-E (SP#1)

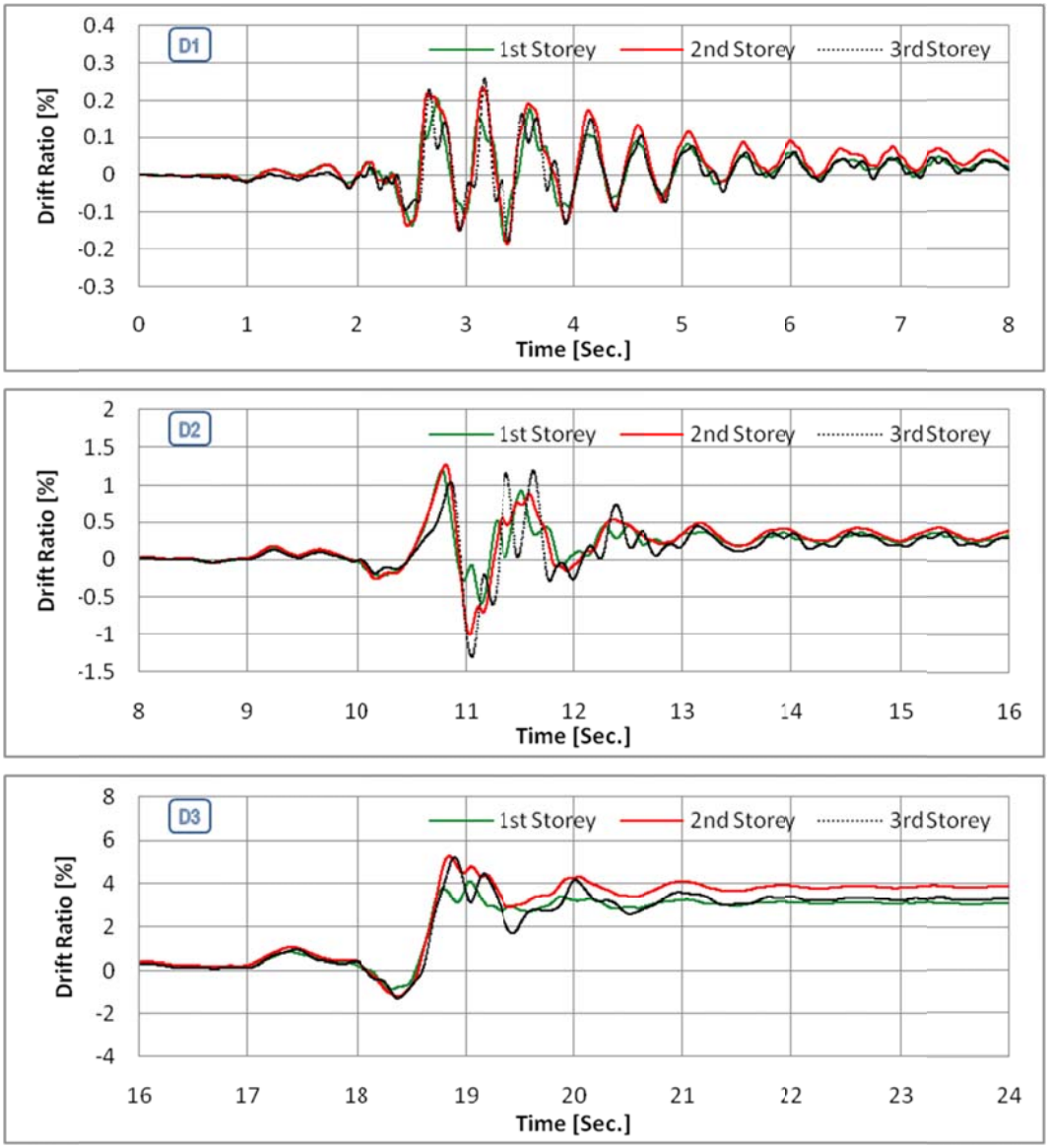

Figure 2.9: Inter-Storey Drift Ratio Time History for each Ground Motion (SP#1)

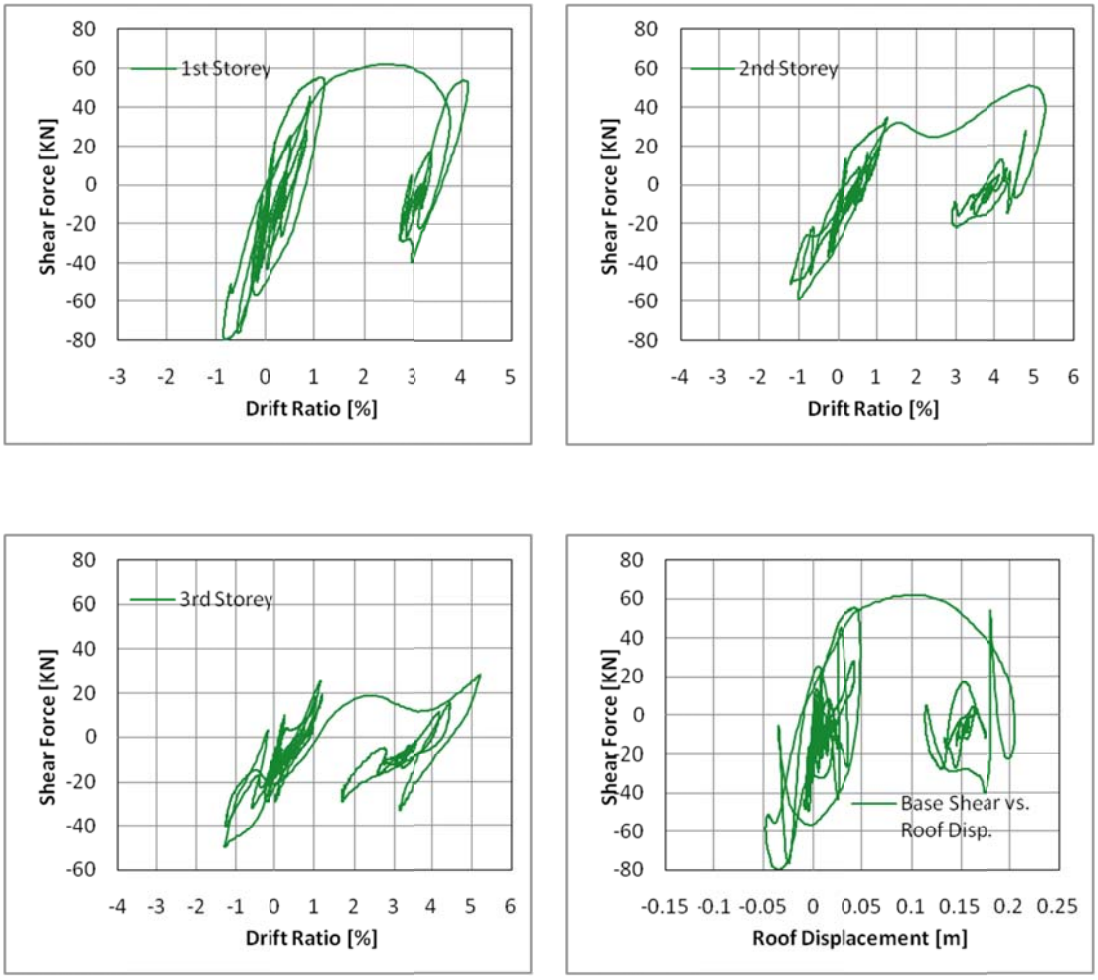

Figure 2.10: Story shear force vs. drift response (SP#1)

2.4.2 Specimen #2 [Non-conforming Unreinforced AAC Masonry Infilled Frame]

The roof displacement response history from the experimental test is presented in Figure 2.11, along with the pictures of damages observed at selected deformation peaks (Figure 2.12). The inter-storey drift ratio response history is presented in Figure2.13. Under the first ground motion D1, no considerable damage was observed on the test specimen. All the structural components as well as masonry infill panels remain intact; however masonry panels suffered tiny cracks along the diagonal. The inter-storey drift ratio limits to 0.18% for each storey and the maximum roof displacement was 6.9 mm. The frame response was nearly elastic with no residual displacement and a minimum damage state at the end of ground motion D1.

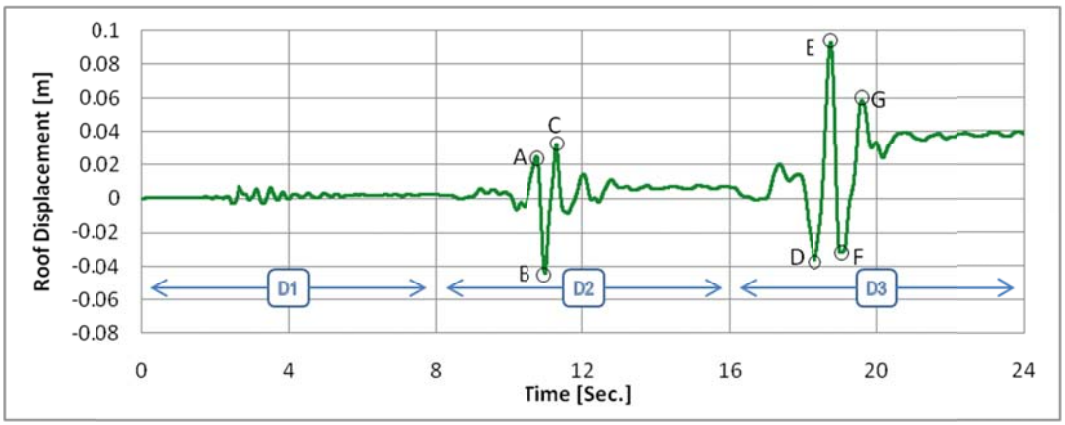

Figure 2.11: Roof displacement time-history (SP#2)

Under the second ground motion D2, the maximum inter-storey drift ratio recorded was 1.41% and the maximum roof displacement was 44.3 mm. Some of the major damages observed during D2 were initiated with the formation of flexural cracks in the first storey interior and exterior columns and initiation of visible cracking in first and second storey masonry infill walls. As the test continues the mortar joints of infill at first and second storey open and the diagonal cracks from the masonry spreads and widened. The diagonal masonry cracks penetrate into the first and second storey interior columns at the top end region in the form of diagonal cracks. Cracking of the exterior beams is observed at the face of support as well as flexural and shear cracks were observed in first storey exterior beams. These damage formations and cracking patterns indicate that most of the damage is concentrated within the middle bay containing the masonry infills and the interior columns are subjected to shear stresses in the plastic hinge region. The sources of these shear stresses are the transfer of shear to the column through the diagonal compression strut of infill panels. These observations imply that first and second storeys experienced some inelastic deformations and the structure is in a moderate damage state after D2.

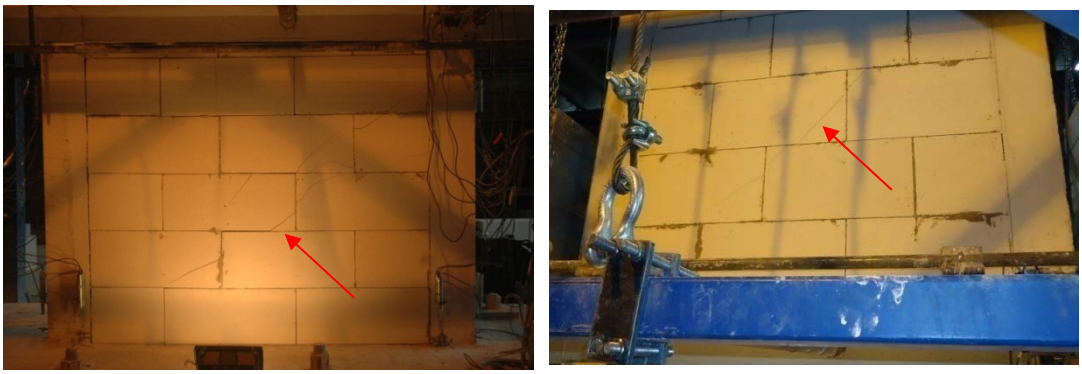

Point A – Initiation and propagation of diagonal cracks in masonry panels at 1st and 2nd storey

Point B –Diagonal cracks in masonry panels at 1st and 2nd storey in opposite direction

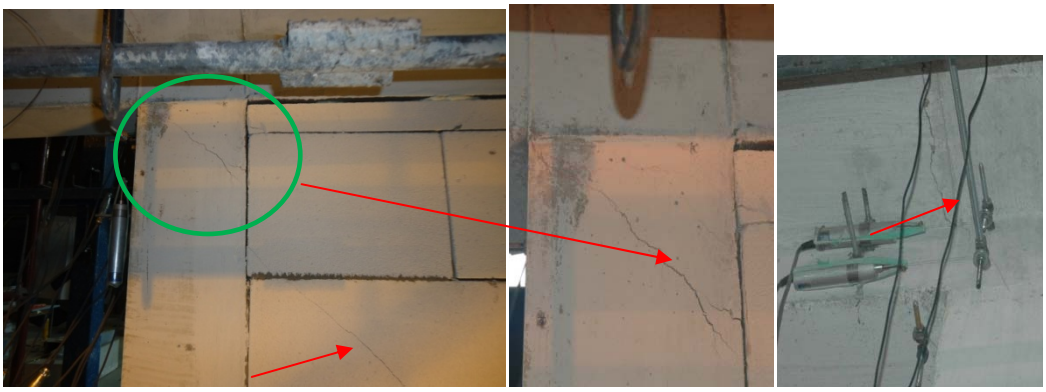

Point B –Diagonal cracks at the top of 1st storey column-102 of infilled bay and cracks in flanges of exterior beams at support

Figure 2.12: Roof displacement time-history and observed damages (SP#2)

Point C – Flexural cracks at the bottom of interior column

Point D – Flexural cracks at the bottom of exterior column

Point E –Diagonal cracks at the bottom of infilled bay column-102 and widening of flexural cracks at the bottom of column-103 while shear cracking at the top of the same column.

Point E –Formation of plastic hinge and permanent deformation of exterior column and overall damage to infill panels

Cont'd; Figure 2.12: Roof displacement time-history and observed damages (SP#2)

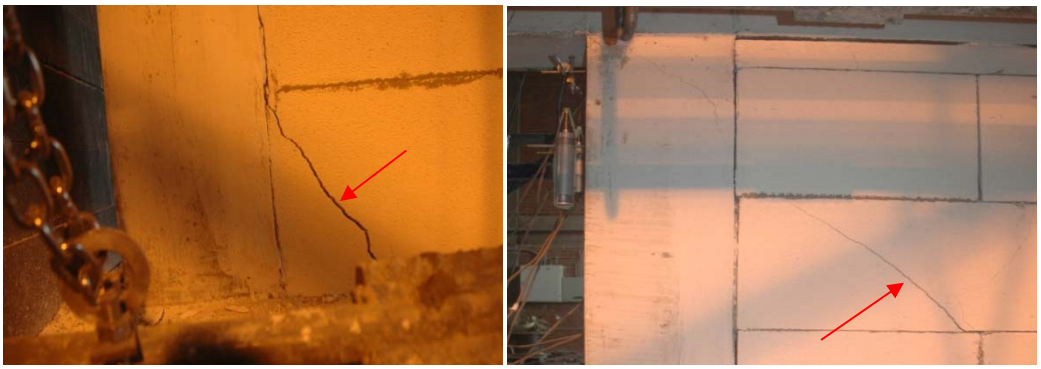

Point F –Corner crushing of masonry infill blocks and diagonal cracks in masonry

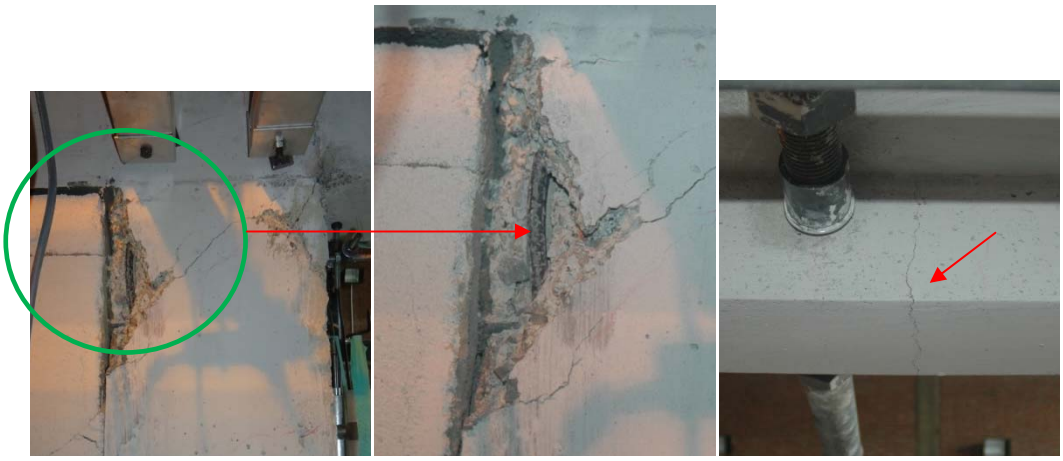

Point G – Spalling of concrete and reinforcement buckling in column 103 at top and widening of flexural cracks in beams 111 and 114

Cont'd; Figure 2.12: Roof displacement time-history and observed damages (SP#2)

Under the last ground motion D3, the visible flexural cracks at the bottom ends of base columns and flexure and shear cracks in the exterior beams of the first and second storey continued to spread and widen. Damages in the columns were followed by the spread of inclined crack in the first storey joint regions. Widening of cracks in the masonry infill of the first and second storey resulted in spalling of block's corners and at the same time diagonal cracks initiate in third storey masonry infill panel. Diagonal shear cracks are observed in exterior base column and shear cracks are observed in the interior beam of first and second storey beams. At the peak acceleration of ground motion, spalling of concrete and buckling of reinforcing steel is observed at the top end of first storey interior column after severe shear cracking. The first storey drift ratio increased to a maximum value of 3.2% and the roof displacement reached a maximum value of 93.0 mm. Inter-storey drift ratios of the second and third storeys were 1.9% and 1.14% respectively. The successively decreasing storey drift ratios from first to top storey is a result of damage pattern in infill panels where the most severe damage occurring in the bottom storey and moderate damage to the masonry in top storey restricting the drift to lower values. These peak deformations resulted in high damages and shear cracking in structural columns and fairly large residual displacement at the end of pseudo-dynamic test which is also clear in both drift and roof displacement response histories. Large shear cracks and spalling of concrete from the interior column's end region can be attributed to large shear stresses transferred through masonry infill, whereas the columns are unable to resist due to lack in confinements. In the same region, the buckling of reinforcing bar is also affiliated with deficient confinements. Considering these observations, Specimen # 2 is severely damaged at the end of ground motion D3.

Shear force vs. inter-storey drift ratio for each storey and base shear vs. roof displacement plots are presented in Figure 2.14. The base shear vs. roof displacement plot shows notable strength degradation and a softening response, implying that the specimen lost considerable lateral load carrying capacity.

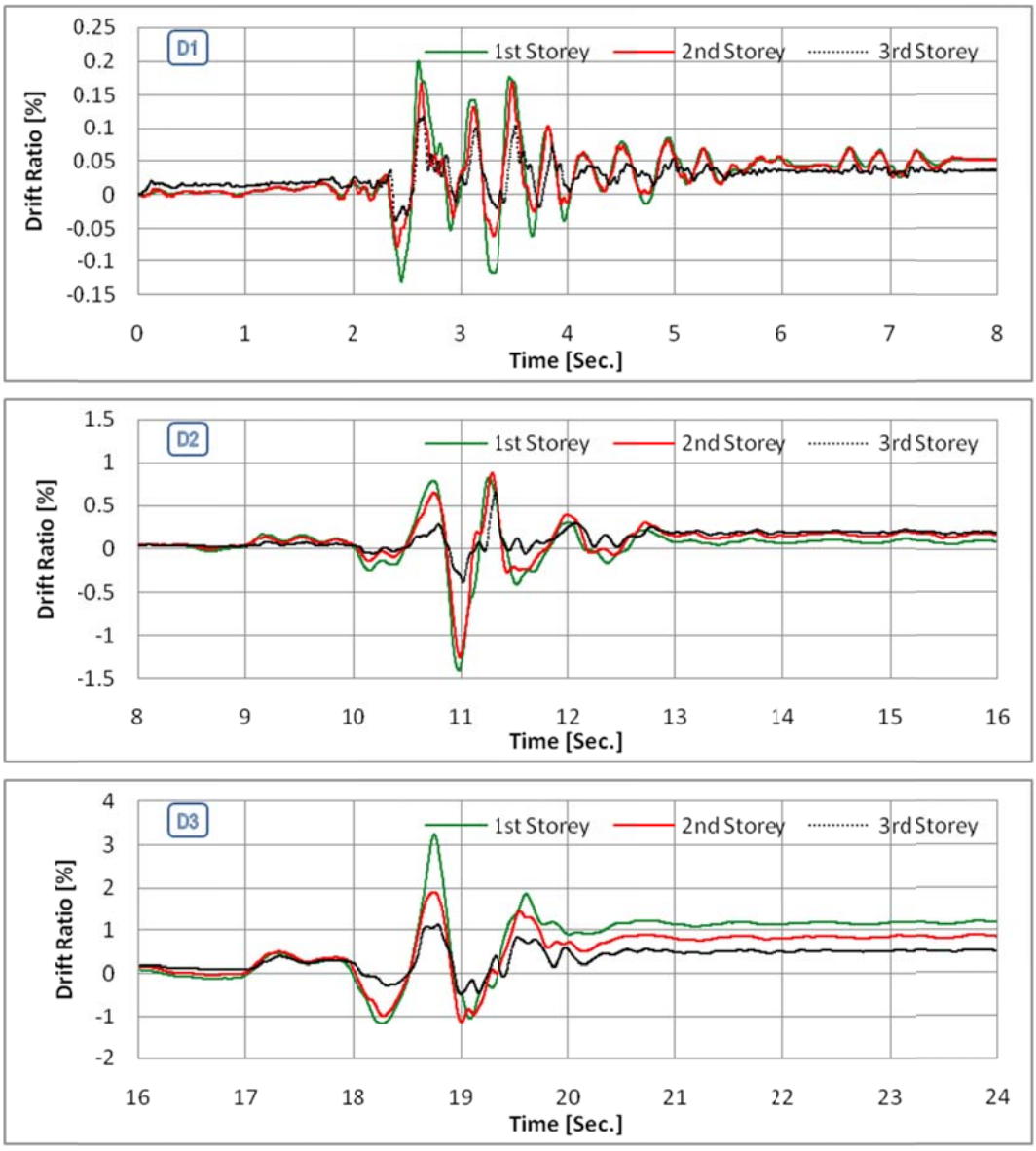

Figure 2.13: Inter-storey drift ratio time-history (SP#2)

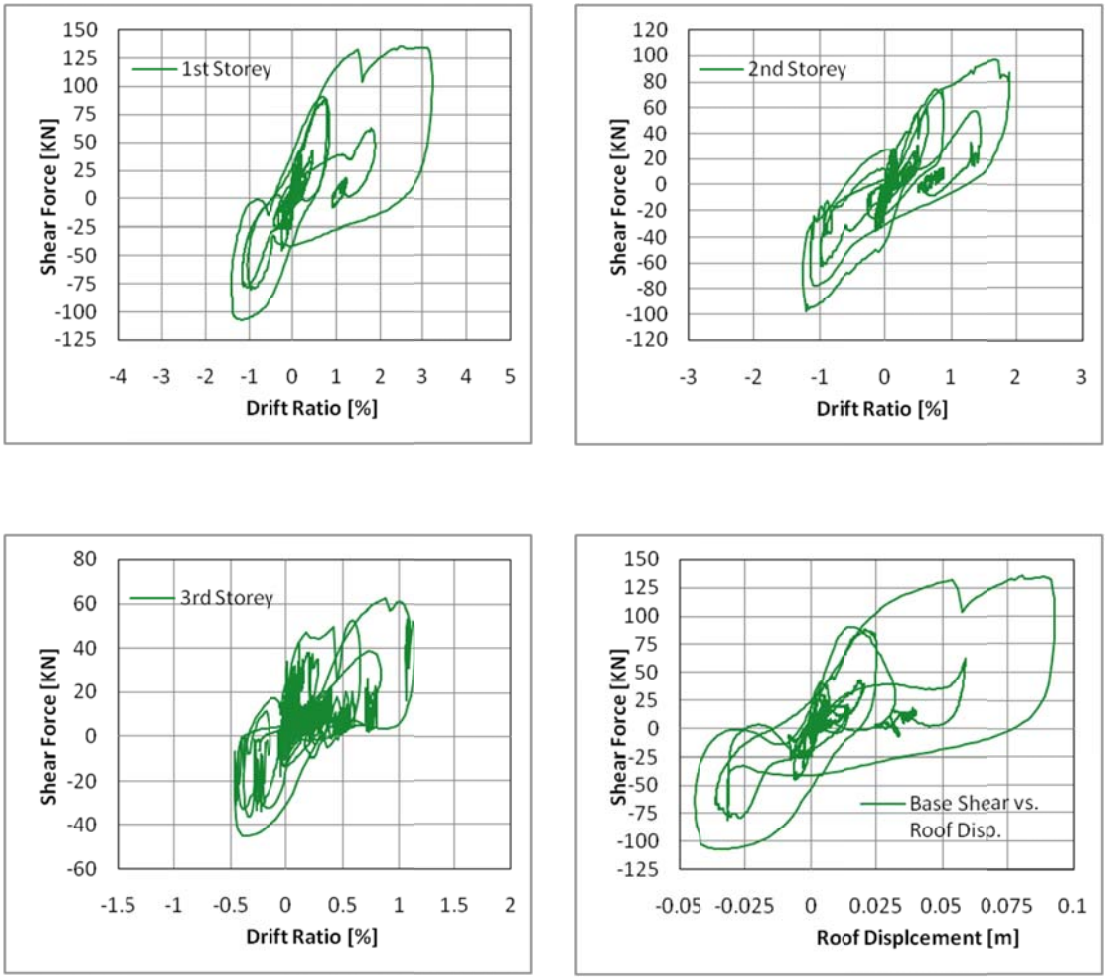

Figure 2.14: Story shear force vs. drift response (SP#2)

2.4.3 Specimen #3 [Code-Conforming Bare Frame]

The roof displacement response history from the experimental test is presented in Figure 2.15, along with the pictures of damages observed at selected deformation peaks presented in Figure 2.16. The inter-storey drift ratio response history is presented in Figure 2.17. Under the first ground motion D1, no noticeable damage was observed on the test specimen. The inter-storey drift ratio limits to 0.27% for each storey and the maximum roof displacement was 9.4 mm. The frame response was elastic with no residual displacement and no damage at the end of ground motion D1.

Under the second ground motion D2, the maximum inter-storey drift ratio recorded was 1.36% and the maximum roof displacement was 49.9 mm. The damages observed during D2 include initiation of diagonal cracks in the joints and flexural cracks at the beam ends of the 1stand 2ndstoreys. In addition, tiny flexural cracks also appear at the bottom of the 1ststorey exterior columns. These observations imply that first and second storeys experienced minor inelastic deformations and the structure is in a light damage state after D2.

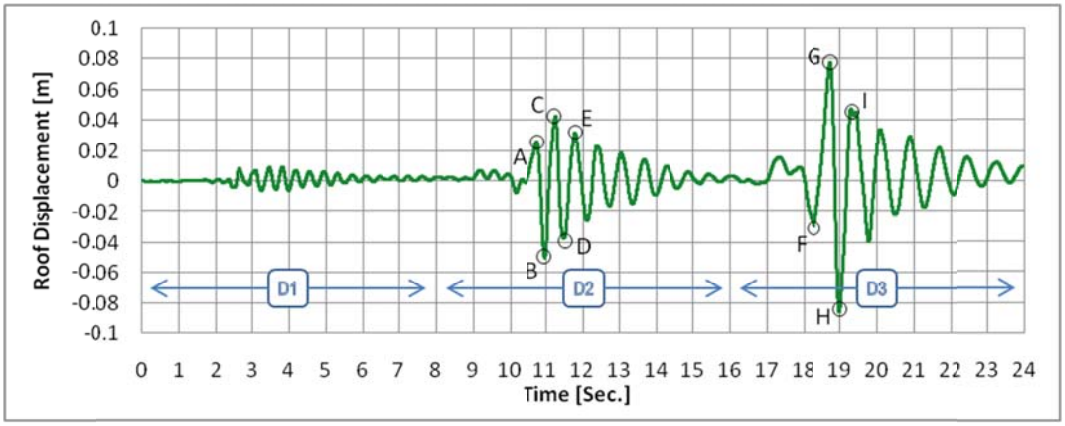

Figure 2.15: Roof displacement time-history (SP#3)

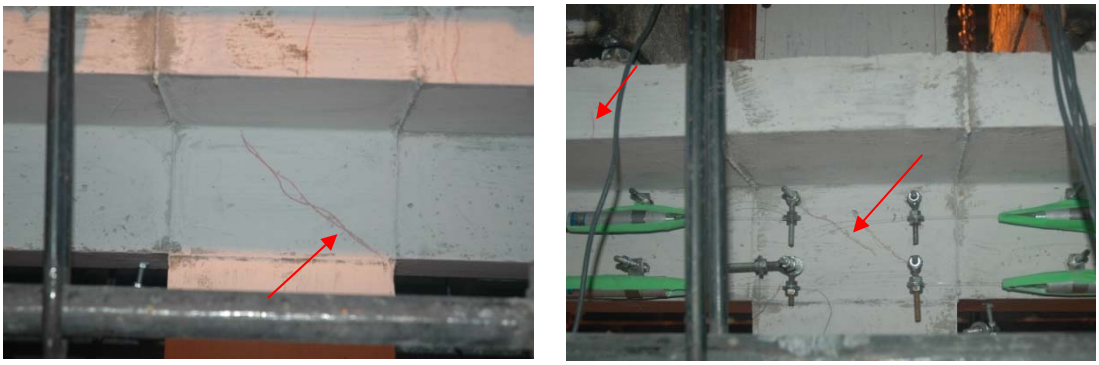

Point A & B – Initiation of diagonal cracks in joints of 1st and 2nd storey interior columns and propagation of cracks in flanges of beams

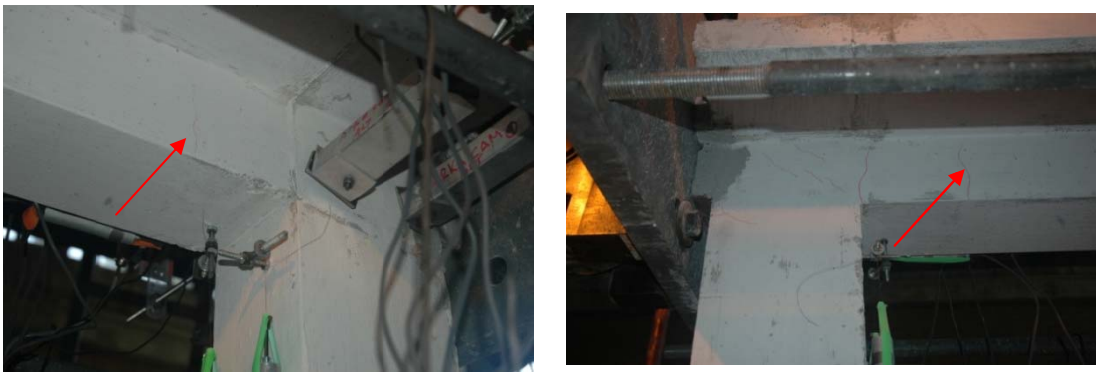

Point C –Initiation of diagonal cracks in 1st and 2nd storey columns 101, 104, 201 and 204 and flexure cracks in the 1st storey beams 111 and 113

Figure 2.16: Roof displacement time-history and observed damages (SP#3)

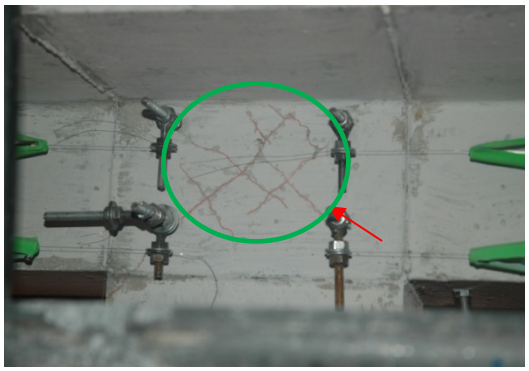

Point D – Joint diagonal cracking

Point E – Flexure cracks at bottom of column 101 and 104

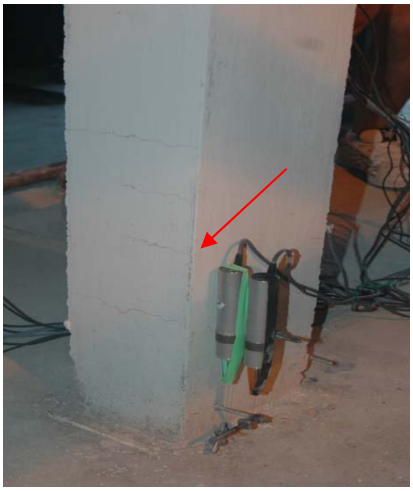

Point F –Flexural cracks at the bottom of column 102 and 103

Point G – Widening of interior joint cracks. Distribution of flexural cracks in 1st and 2nd storey exterior columns.

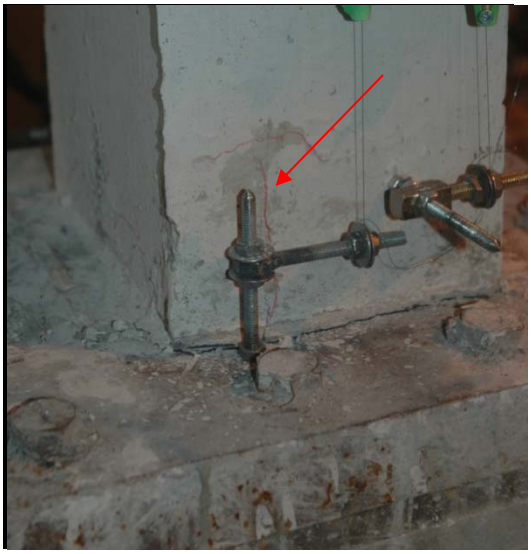

Point H – Bond slip cracks in column 104

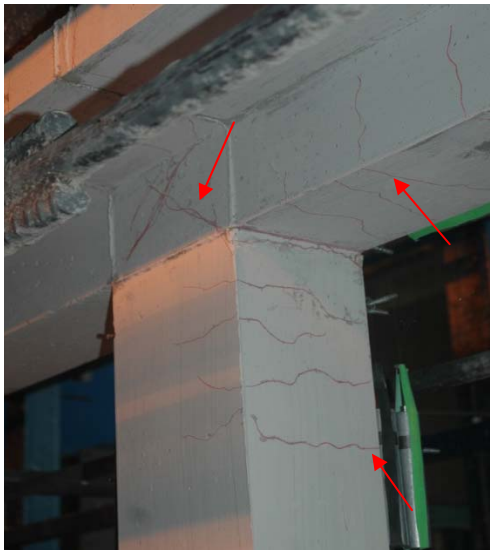

Point I – Overall damage in interior joint region

Cont'd; Figure 2.16: Roof displacement time-history and observed damages (SP#3)

During the last ground motion D3, the visible flexural cracks at the bottom ends of base columns and flexure and shear cracks in the exterior beams of the first and second storey continued to spread and widen. The joint diagonal cracks also increases at first and second storeys. During the peak deformation, small bond slip crack appear at the bottom of exterior base column.

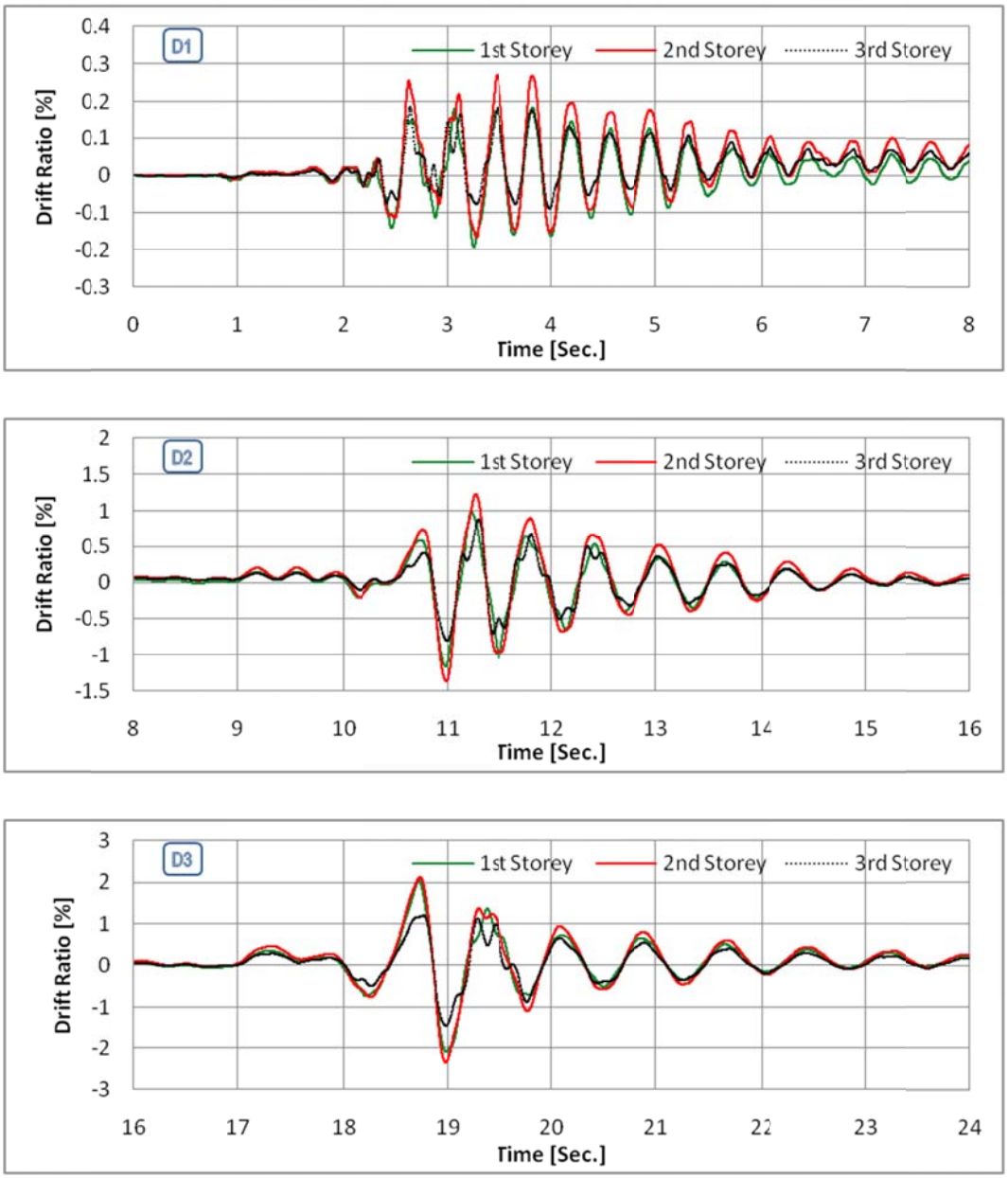

Figure 2.17: Inter-storey drift ratio time-history (SP#3)

The first storey drift ratio increased to a maximum value of 2.1% and the roof displacement reached a maximum value of 85.6 mm. Inter-storey drift ratios of the second and third storeys were 2.3% and 1.4% respectively. Overall damage at the 1stand 2ndstorey joints consisted of hairline flexure and flexure-shear cracks in columns and beams respectively and diagonal cracks in joints. Considering these observations, Specimen # 3 is at a moderate damage state at the end of ground motion D3.

Shear force vs. inter-storey drift ratio for each storey and base shear vs. roof displacement plots are presented in Figure 2.18. The base shear vs. roof displacement plot shows no notable strength degradation indicating that specimen has not reached failure.

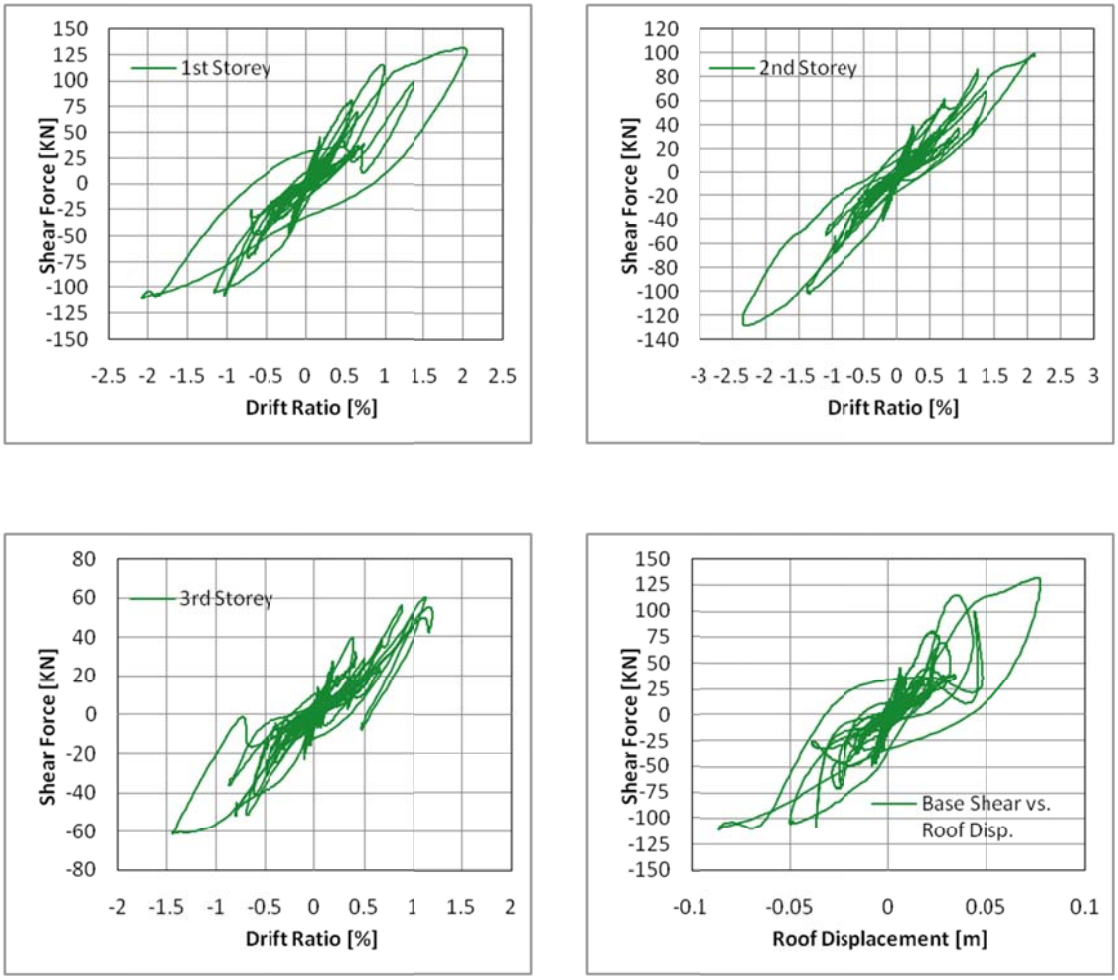

Figure 2.18: Story shear force vs. drift response (SP#3)

2.4.4 Specimen #4 [Code-conforming URM Infilled Frame]

The roof displacement response history from the experimental test is presented in Figure 2.19, along with the pictures of damages observed at selected deformation peaks (Figure 2.20). The inter-storey drift ratio response history is presented in Figure 2.21. Under the first ground motion D1, no considerable damage was observed on the test specimen. All the structural components as well as masonry infill panels remain intact; however masonry panels suffered very tiny cracks along the diagonal. The inter-storey drift ratio limits to 0.18% for each storey and the maximum roof displacement was 5.1 mm. The frame response was elastic with no residual displacement and no damage at the end of ground motion D1.

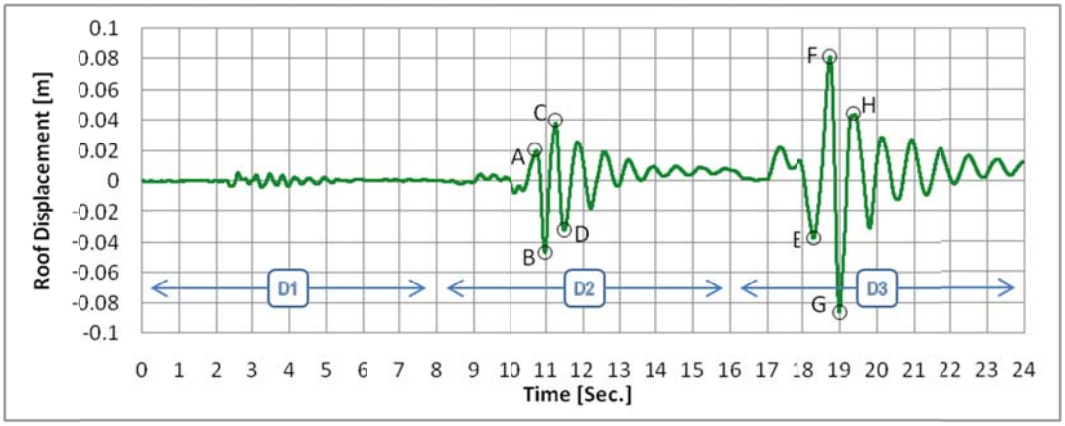

Figure 2.19: Roof displacement time-history (SP#4)

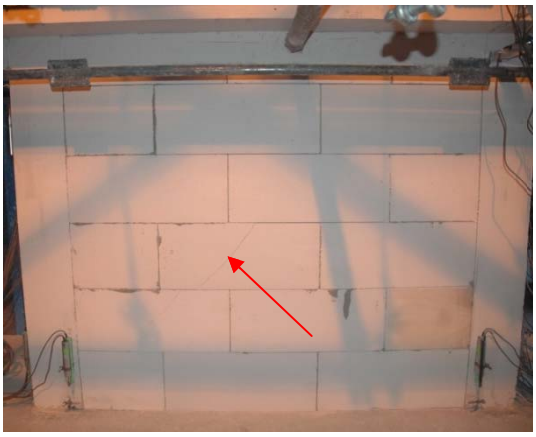

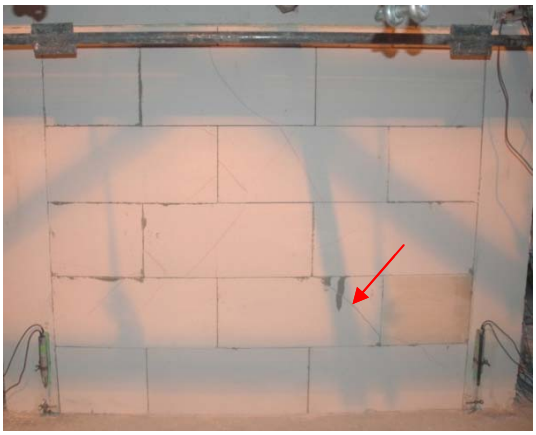

Point A & B – Initiation of diagonal cracks in infill panels

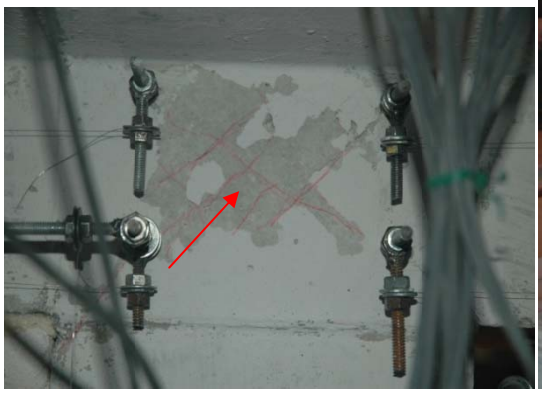

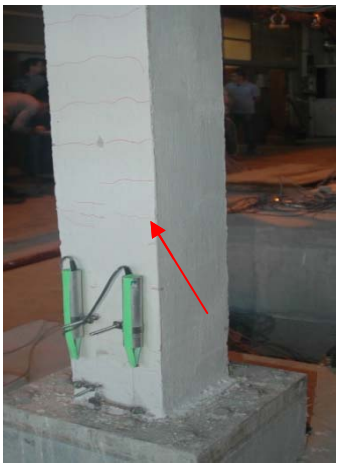

Point C –Initiation of diagonal cracks in 1st and 2nd storey interior joints and flexural cracks in exterior columns

Figure 2.20: Roof displacement time-history and observed damages (SP#4)

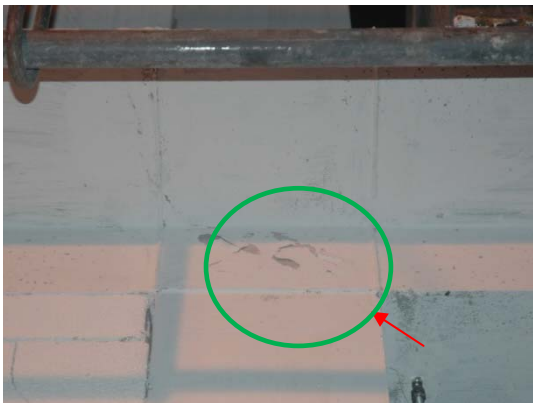

Point D – Diagonal cracking at 2nd storey interior joints

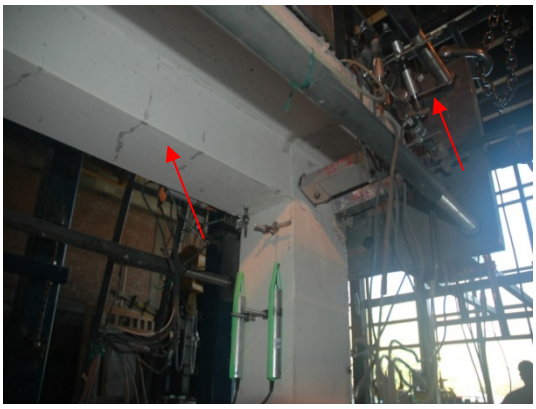

Point D – Flexure cracks at 1st storey exterior beams

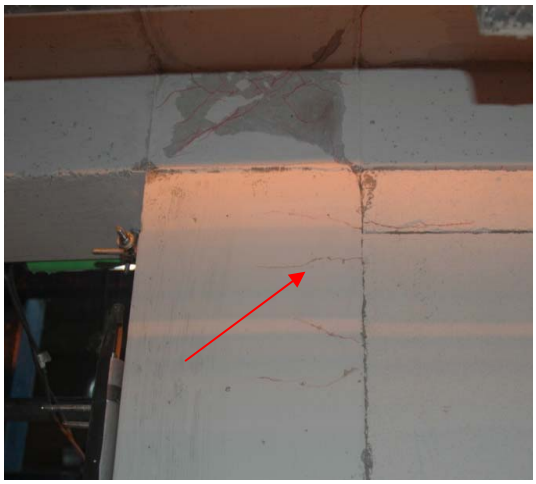

Point E – Cracking at top of 1st storey interior columns

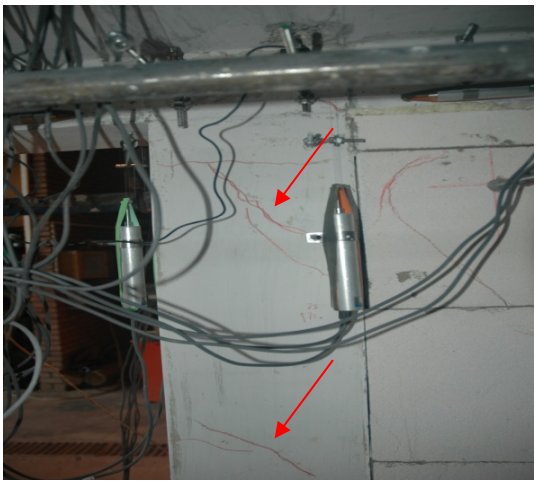

Point F – Shear cracks in 1st and 2nd storey interior columns

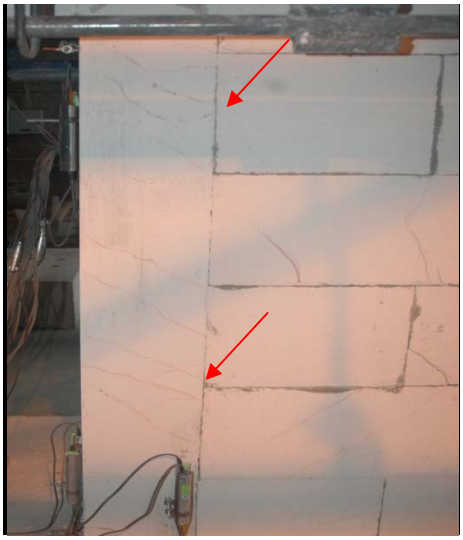

Point G – Distribution of diagonal cracks in 1st storey interior columns

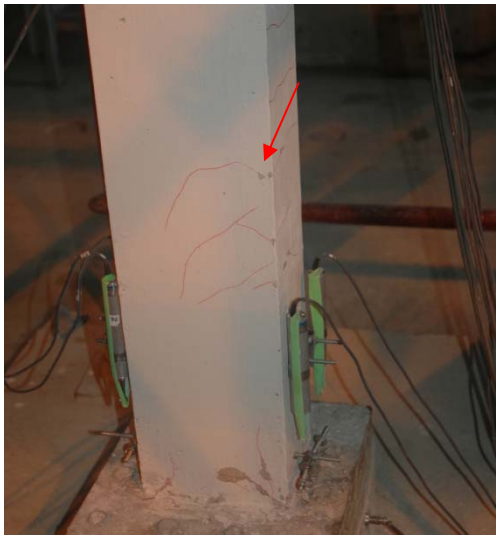

Point G – Flexure shear cracks at bottom of 1st storey columns

Cont'd; Figure 2.20: Roof displacement time-history and observed damages (SP#4)

Point H – Overall damage to infill panel and diagonal cracks in 1st and 2nd storey joints.

Cont'd; Figure 2.20: Roof displacement time-history and observed damages (SP#4)

Under the second ground motion D2, the maximum inter-storey drift ratio recorded was 1.13% and the maximum roof displacement was 44.3 mm. The visible damage during D2 was first started with diagonal cracks in the infill panels of first and second storey. Other notable damages include initiation of diagonal cracks in the joints and flexural cracks at the beam ends of first and second storeys and flexural cracks at the bottom of first storey exterior columns. These observations imply that first and second storeys experienced minor inelastic deformations and the structure suffers slight damage after D2.

During the last ground motion D3, the visible diagonal cracks at the first and second storey infill panels continue to grow along with opening of mortar joints. Flexural cracks in the beams and flexure shear cracks in the exterior columns of first and second storey spread and widens while flexure cracking at the bottom of interior columns initiates. Shear cracks in the interior columns of first and second storey initiates and distributed along the entire length. The source of these cracks is the shear stresses transmitted through the compression strut of masonry infill panels as observed in specimen #2. The first storey drift ratio increased to a maximum value of 2.0% and the roof displacement reached a maximum value of 82.0 mm. Inter-storey drift ratios of the second and third storeys were 2.2% and 0.87% respectively. The above mentioned observed damages imply that the specimen #4 is in the moderate damage state at the end of ground motion D3.

Shear force vs. inter-storey drift ratio for each storey and base shear vs. roof displacement plots are presented in Figure2.22. The base shear vs. roof displacement plot shows no notable strength degradation indicating that specimen has not reached failure.

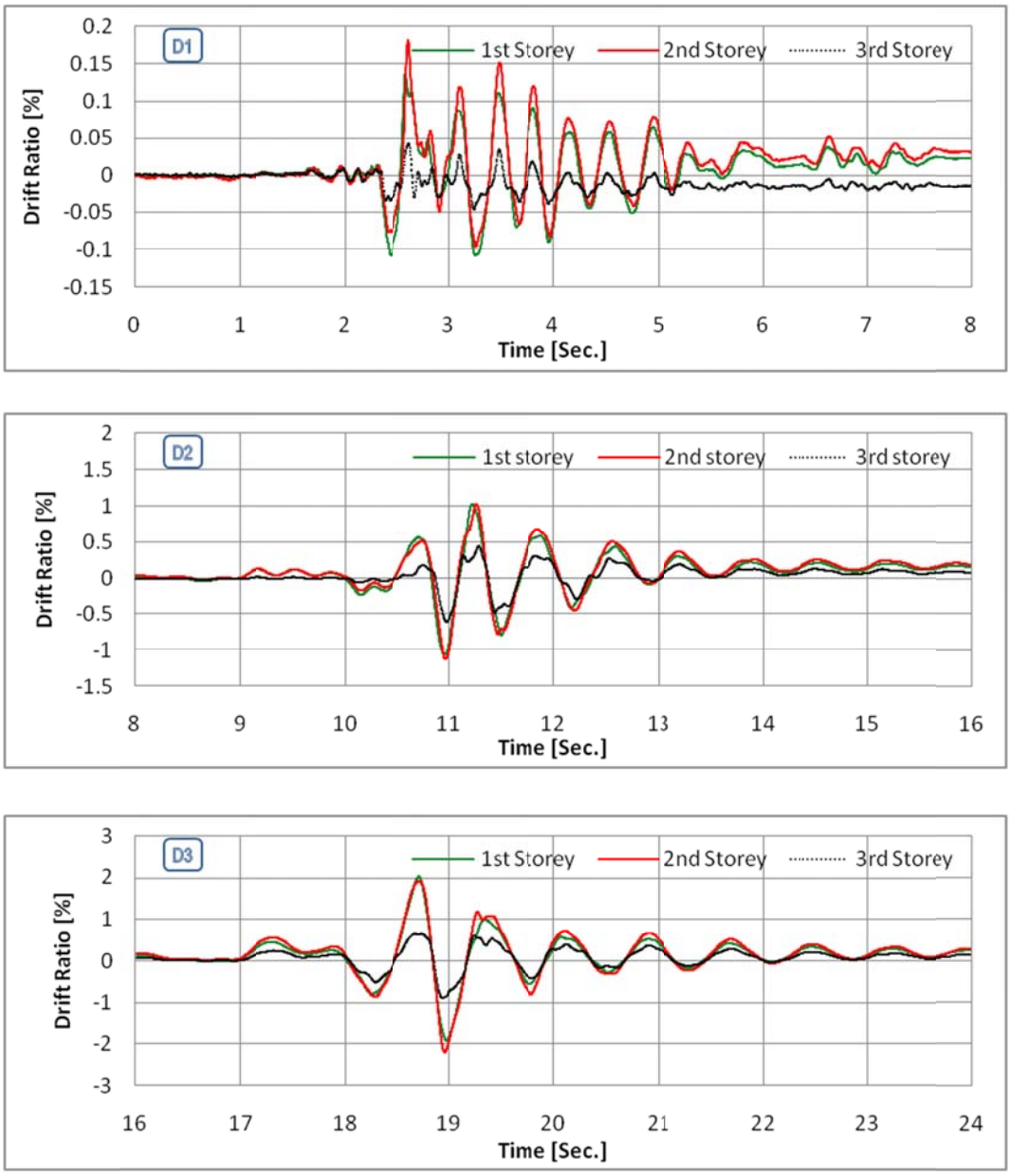

Figure 2.21: Inter-storey drift ratio time-history (SP#4)

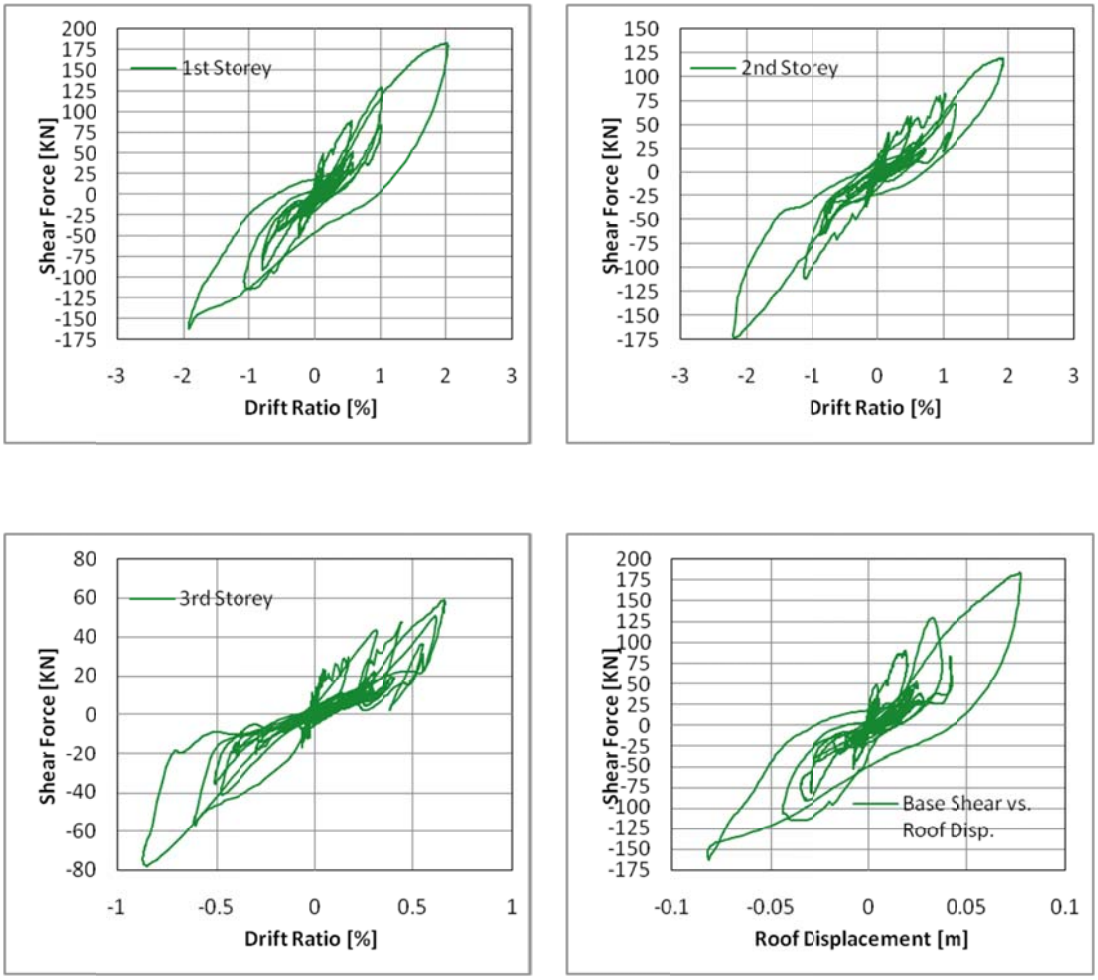

Figure 2.22: Story shear force vs. drift response (SP#4)

2.5 AAC Masonry Prism Compression Test

The compression tests on three masonry prisms were conducted to investigate the stress-strain response of the AAC masonry. The size of all the specimens was kept same, except the width, as shown in Figure 2.23. The width of the masonry prism is selected based on the approximate width of diagonal compression strut observed during the pseudo dynamic test of infilled frame specimens as shown in Figure 2.24.

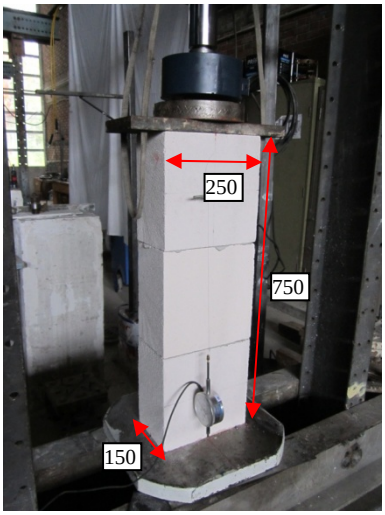

Figure 2.23: AAC masonry test prism

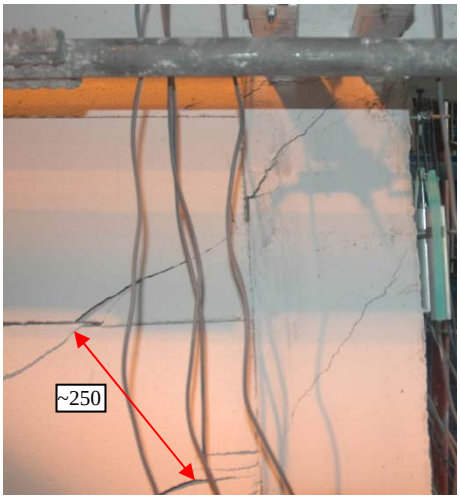

Specimen #2

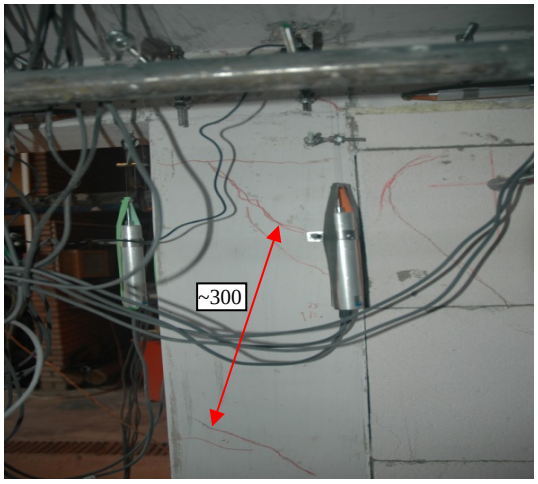

Specimen #4

Figure 2.24: Width of diagonal compression strut observed during the test

The ultimate compressive stress and strain results of prisms are tabulated in Table 2.8 and the stress-strain curves are plotted in Figure 2.25.

Table 2.8: Masonry prism compression test results

Maximum compressive stress [MPa]	Strain at maximum stress	Initial modulus of elasticity [MPa]	Secant modulus of elasticity [MPa]
2.66	0.00220	1430	1209

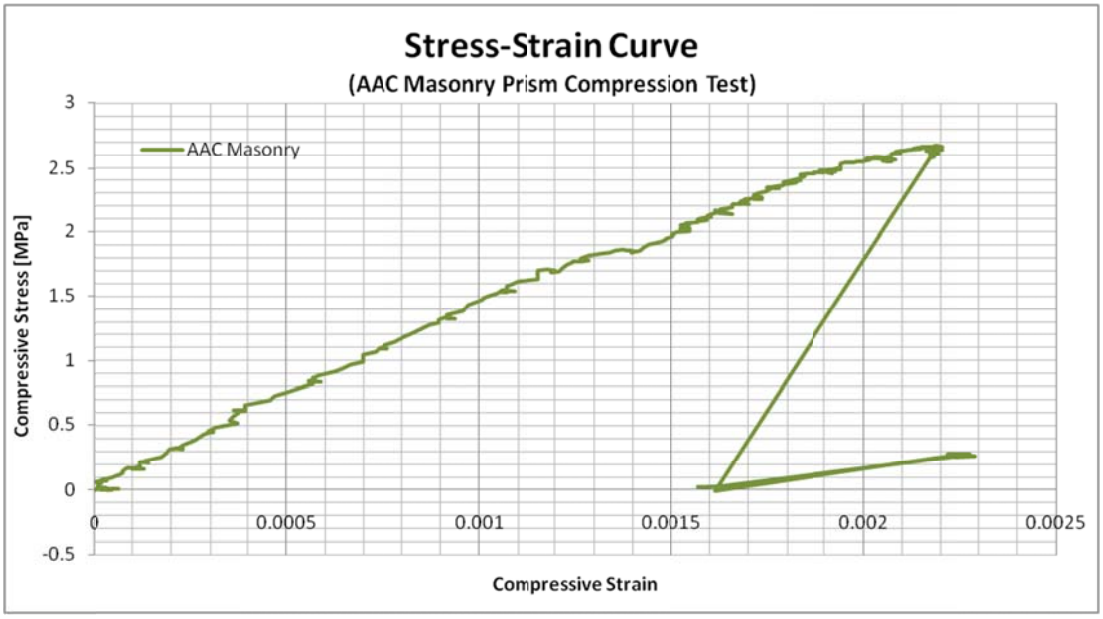

Figure 2.25: AAC masonry material stress-strain curve

CHAPTER 3

THE EFFECT OF AAC INFILLS ON THE RESPONSE OF RC FRAMES: EXPERIMENTAL COMPARISONS

3.1 General

This chapter focuses on the effect of AAC masonry infill on the seismic performance of reinforced concrete frames, based on comparative evaluation. The results from pseudo dynamic testing of all four specimens are compared in terms of global responses, such as roof displacement, inter-storey drifts, storey shears and time variation of fundamental period (T_1). In addition to the global responses, local response, such as end rotations are also compared for the first and second storey beams and columns. The fundamental periods were determined by the procedures as demonstrated by Molina et. al [1999], where the experimental displacements $u^T(n)$, velocities $v^T(n)$, and restoring forces' $r^T(n)$ during the pseudo-dynamic testing, are related to each other using the relation:

$$[u^T(n) \quad v^T(n) \quad 1] \cdot \begin{bmatrix} K^T \\ C^T \\ o^T \end{bmatrix} = r^T(n) \tag{3.1}$$

where K and C are the secant stiffness and viscous equivalent damping matrices, respectively. o is a constant force offset term. The equation contains "2.ndof^2 + ndof" unknowns and the number of available equations is "N.ndof", for N time intervals. By satisfying the condition that N>2.ndof+1 and estimating K and C by a least mean squares algorithm, the complex Eigen-frequencies and mode shapes can be determined by solving the generalized Eigen value equation:

$$s\begin{bmatrix} C & M \\ M & 0 \end{bmatrix} w + \begin{bmatrix} K & 0 \\ 0 & -M \end{bmatrix} w = 0 \tag{3.2}$$

where$M$ is the theoretical mass matrix, w contains the eigenvectors, and s is the conjugate couples of Eigen values.

The investigation for the response of AAC masonry infilled frames with respect to bare frames is carried out separately for two different set of specimens, i.e. non-conforming frames (Specimen #1 vs. Specimen #2) and code-conforming frames (Specimen #3 vs. Specimen#4). Initially the performance is evaluated on the basis of observed damages during the test and the failure mode or primary source of plastic deformation in the specimen. Peak global and local responses are then compared during each ground motion and the differences are tabulated in percentage. Some of the peak global response parameters are also presented graphically. The chapter ends with the comments based on these observations.

It is important to note here that the main difference between the two specimens of each set is the presence of unreinforced AAC masonry infill panels in the entire middle bay which are provided after the test on bare frame has been conducted, except for the case of Specimen #1 which was very severely damaged and abandoned and therefore Specimen #2 is created from another non-conforming specimen which was already tested having moderate damage. However, the responses of the specimens are also affected to the second degree by various inherent factors such as construction methods and material strengths etc. Therefore, the discussions presented here focus on the main differences and the results are interpreted accordingly without going into a detailed comparison considering these inherent factors.

3.2 Comparative Evaluation of the Performances of AAC Infilled and Bare Non-conforming RC Frames
(Specimen #1 vs. Specimen #2)

This section consist of the comparison of pseudo-dynamic test results between two non-conforming R.C. frames i.e. Specimen #1 and Specimen #2 in order to evaluate the effect of AAC infill on the response of RC frames. Figure 3.1 and Figure 3.2 presents the pictorial presentation of the major damages in Specimen #1 and Specimen #2 respectively, which are observed in the structural members during three successive ground motions. Table 3.1 summarizes the observed damages with reference to the pictures. The global response time histories including, inter-storey drift, storey shears and fundamental period variation are presented in Figures 3.3 to 3.5. Figures 3.6 and 3.7 contain the member end rotation time histories for columns and beams respectively.

3.2.1 Performance Evaluation through Damage Observation and Failure Mode

3.2.1.1 Specimen #1 [Bare Frame – NC]

Specimen #1 is non-conforming and not designed to resist seismic loads and hence depict older deficient construction. The observation of damage pattern at several instants of peaks during the test is presented in section 2.4.1 along with damage pictures in Figure 2.8 of Chapter 2. During the ground motion D1 with return period of 72 years (50% probability of exceedance in 50 years) the behaviour of the frame is nearly elastic with no visible damage to the structural elements. During ground motion D2 with return period of 475 years on rock strata (10% probability of exceedance in 50 years), the beams and columns suffered visible flexural cracking. In addition, the diagonal cracks in joints appeared before the flexural cracking in connecting beams and columns. Overall the specimen was in moderate damage state after the ground motion D2 with no apparent failure in any structural member. During D3 ground motion with return period of 475 years on soft soil profile (10% probability of exceedance in 50 years), wide flexural cracks in the bottom and top storey columns at potential plastic hinge regions results in permanent deformations. Flexure and shear-flexure cracks in beams grow wider and excessive diagonal cracking occurs in the joint region. The beams fail in flexure with the flexural cracks observed at the bottom prior to the cracks at the top as expected since the amount of reinforcement at the bottom is less as compared to the top reinforcement. The absence of confinement reinforcement in the joints could be the cause of joint shear cracking. Permanent deformation of the frame, especially first storey columns is observed.

3.2.1.2 Specimen #2 [Infilled Frame – NC]

Specimen #2 comprises of non-conforming deficient RC frame infilled with AAC block masonry in the entire middle bay. The observation of the damage pattern at several instants of peaks during the test is presented in section 2.4.2 along with damage pictures in Figure 2.13 of Chapter 2. During the first ground motion D1, no apparent damage was noted in any of the structural members of the specimen. In addition none of the masonry panels suffered visible damage except minor separation cracks along the boundary of the panel and boundary frame at first storey. The specimen was at the minor damage state at the end of ground motion D1. During D2, flexural cracking in the beams occurs with the diagonal cracks in the joints. Diagonal cracks in the masonry panels of first and second storey occur indicating the limit of cracking of the panels. As the test progresses, further diagonal cracks appeared parallel to the loaded diagonal which verified the equivalent diagonal strut action being representative of the infill response. The masonry diagonal stresses caused the diagonal cracks from the masonry to penetrate into the 1st storey bounding columns resulting in shear cracking at the top. At the bottom of these columns flexural cracking occurs and spread along the potential plastic hinge region. Exterior columns show flexural cracks at the bottom. Damage was mostly concentrated in the 1st storey. Overall the specimen receives inelastic deformations and is at a moderate damage state after D2.

During the last ground motion, severe damage occurs to the bounding columns in the form of diagonal crack in the top and bottom resulting in their brittle shear failure. The wide flexural cracking in exterior columns also caused them to fail in a brittle manner. Cracks in joints and beam ends grow wider. The masonry panels reached failure due to extensive diagonal cracking with cracks wide

enough to see through. The brittle failure of columns resulted in the apparent permanent deformation of the entire frame. The specimen suffered severe damage with the failure of first storey columns.

Legends:

a & c	Flexural cracks at 1st storey columns bottom end – D2	**b**	Diagonal cracks at 1st storey interior joints – D2
d	Shear cracks at 1st storey exterior beams ends – D2	**e**	Diagonal cracks at 3rd storey exterior joints – D3
f	Shear cracks at 3rd storey exterior beams ends – D3	**g**	Diagonal cracks at 1st storey interior joints – D3
h	Flexural cracks at 3rd storey columns top end – D3	**i**	Flexural cracks at 1st storey columns bottom end – D3

Figure 3.1: Major damages observed during D2 and D3 (SP#1)

3.2.1.3 Failure Mode

From the observations above, it is apparent that both of the specimens suffered severe damage at the end of ground motion D3. These damages resulted in large plastic deformations in both specimens. However, the dominant cause of plastic deformations for both specimens differs greatly from each other.

Specimen #1 failed because of the flexure failure at the bottom ends of first storey column and top ends of 2nd and 3rd storey columns but the failure was abrupt with sudden increase of inter-storey drifts. Although some ductility was present but the ample warning usually associated with the flexural failure was absent in this specimen. However, it was as expected because the frame elements were not designed and detailed to resist seismic loads.

The failure of Specimen # 2 was also governed by the failure of first storey columns however the failure mode of columns differs from each other. The exterior columns depicts flexure failure at the bottom but the failure was abrupt with sudden increase of inter-storey drifts which is similar to the one observed in bare frame (Specimen #1). On the other hand, the failure of interior columns surrounding the infill panel was brittle caused by excessive diagonal shear cracking at the column tops. The cracking thereby resulted in spalling of concrete and buckling of reinforcement. The primary mode of failure of the first and second storey infill panels is diagonal cracking. The ratio of mean compressive strength of frame to the infill is as high as 4.5 indicating the strong frame-weak infill system and given that, the masonry panel behaved as expected, however the excessive diagonal cracking and shear failure in the bounding columns is unusual for this system. The main cause of such failure is the transfer of shear stress from the loaded diagonal of the infill panel and the absence of adequate confinement reinforcement to resist these stresses signifying the impact of poor seismic detailing.

Legends:

- **a** Diagonal crack at 1st and 2nd storey infill Panel – D2
- **b** Diagonal cracks at 1st storey bounding column top – D2
- **c** Flexure cracks at 1st storey exterior beams end – D2
- **d** Flexure cracks at 1st storey bounding column bottom – D2
- **e** Diagonal cracks in 1st storey exterior joints – D2
- **f** Flexure cracks at 1st storey bounding column bottom – D3
- **g** Diagonal cracks at 1st storey bounding column top – D3
- **h** Diagonal cracks at 1st storey bounding column bottom– D2
- **i** Overall Failure of 1st and 2nd storey infill Panel – D3
- **j** Flexure cracks at 1st storey exterior column bottom –D3
- **k** Reinforcement buckling at 1st storey bounding column D3

Figure 3.2: Major damages observed during D2 and D3 (SP#2)

Table 3.1: Summary of observed performance of non-conforming specimens

Ground Motion	Observation
Specimen #1 – Non-conforming Bare Frame	
D1	• No visible damage
D2	• Flexure cracks at columns (Figure 3.1 a & c) • Shear and shear-flexure cracks in beams (Figure 3.1 d) • Diagonal cracking of 1st storey joints (Figure 3.1 b)
D3	• Abrupt flexure failure of columns (Figure 3.1 h &i) • Wide shear-flexure cracks in beams (Figure 3.1 f) • Extensive diagonal cracks in joints (Figure 3.1 e& g)
Specimen #2 – Non-conforming Infilled Frame	
D1	• No apparent damage
D2	• Shear and flexure cracks at bounding columns top and bottom respectively (Figure 3.2 b and d) • Flexure cracks in exterior columns • Flexure cracks in beams (Figure 3.2 c) • Diagonal cracks in joints (Figure 3.2 e) • Multiple diagonal cracks at 1st and 2nd storey AAC masonry panel (Figure 3.2 a)
D3	• Brittle shear failure of bounding columns at 1st storey (Figure 3.2 g, h and k) • Abrupt flexure failure of exterior columns of 1st storey (Figure 3.2 j) • Extensive flexure cracking in bounding columns (Figure 3.2 f) • Extensive flexure cracking in beams and diagonal cracks in joints • Failure of 1st and 2nd storey masonry panel due to wide diagonal tension cracks (Figure 3.2 i)

3.2.2 Global Responses

This section evaluates the performance of frames on the basis of time histories of global responses obtained after pseudo-dynamic testing as well as from the comparison of peak responses during each ground motion given in Table 3.2. The inter-storey drift responses (Figure 3.3) for infilled and bare frames during D1 indicates that AAC infills does not reduce the peak drift response of the 1st storey significantly while the drifts of the 2nd and 3rd storeys were contained very successfully without any visible damage to the masonry panel or structure. This is attributed to the fact that Specimen #2 was already cracked when tested with most of the cracking already present and concentrated in the first storey and the ground motion was not strong enough to overcome the initial cracking and to cause infill to contribute fully.

Table 3.2: Comparison of peak global responses between Bare and Infilled frames (NC)

Response Parameter *"N"*	Ground Motion	SPECIMEN		Difference [%] *
		#1 Bare - NC	#2 Infilled - NC	$\frac{(N_{SP\#2} - N_{SP\#1})}{N_{SP\#1}}$
Roof Displacement [m]	D1	0.0091	0.0069	-24.46
	D2	0.0484	0.0443	-8.36
	D3	0.2056	0.0929	-54.81
1st storey/Base shear [*kN*]	D1	36.3	41.4	14.02
	D2	68.6	107.1	56.01
	D3	75.2	130.4	73.36
2nd storey shear [*kN*]	D1	24.5	30.9	26.34
	D2	48.0	95.5	99.07
	D3	62.0	97.9	57.89
3rd storey shear [*kN*]	D1	21.0	27.7	32.25
	D2	39.7	45.7	15.04
	D3	38.1	58.6	53.57
1st storey drift ratio [%]	D1	0.20	0.18	-10.67
	D2	1.20	1.41	17.81
	D3	4.13	3.22	-21.96
2nd storey drift ratio [%]	D1	0.23	0.17	-27.52
	D2	1.28	1.26	-1.57
	D3	5.29	1.90	-64.08
3rd storey drift ratio [%]	D1	0.26	0.12	-54.20
	D2	1.30	0.65	-50.04
	D3	5.23	1.14	-78.19
Base shear ratio (V/W)	D1	0.12	0.14	
	D2	0.23	0.36	
	D3	0.25	0.44	

NC = Non-conforming;
*: Positive values indicate **increase** while negative values indicate **decrease.**
W = Total seismic weight of the specimens = 298 *kN*; V = Peak base shear

The storey shear response histories of both specimens are also presented in Figure 3.4. During several peaks of D1, as compared to the bare frame, the increase in the 1st storey shear of infilled frame as compared to bare frame is the least due to strength contributed by the AAC infills while this increase is higher in the2nd and 3rd storeys (Table 3.2). This observation also provides an overall confidence on the hypothesis of drift responses during D1 that infills at the 1st storey are not fully mobilized in the infill-frame composite response.

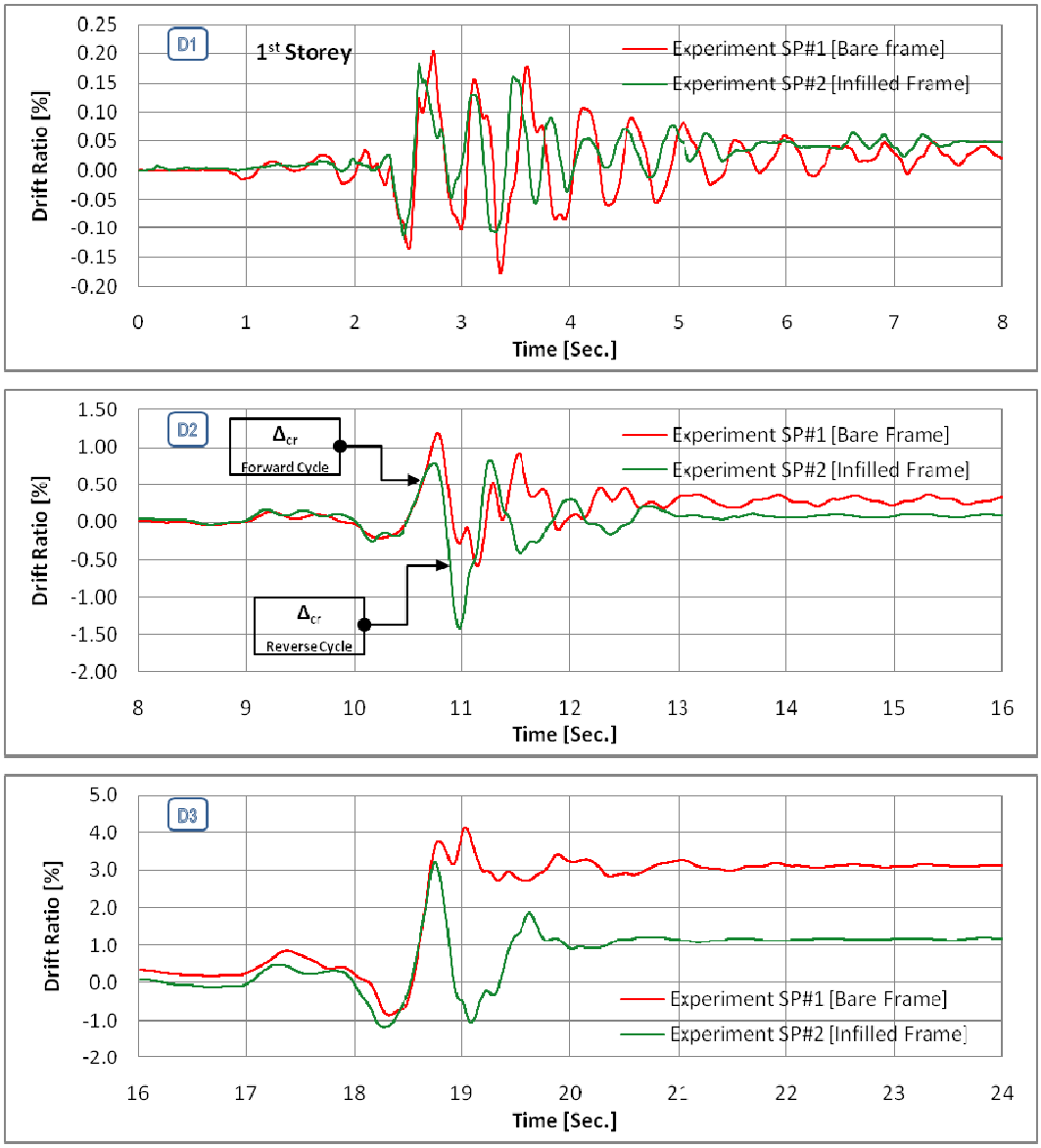

Figure 3.3(a): First storey drift ratio time-history (NC specimens)

The storey drifts plot during ground motion D2 are also plotted in Figure 3.3 with the cracking drift Δ_{cr} that is, the drift at which first visible diagonal crack appears and noted in the masonry panels, in both forward and reverse cyclic motion, at the 1st and 2nd storey (the diagonal compression struts str_1, str_3 and str_2, str_4), is marked ((Point-A and B in Figures 2.11 and 2.12).

It can be noted that at the peak of cracking drift, the AAC infills contained the drift very effectively as compared to bare frame, however immediately after the cracking point during the reverse cyclic motion; the drift of infilled frame reaches larger value than the bare frame in both the 1st and 2nd storeys. The reason for this behaviour may be that since the infill material is brittle and its abrupt yielding causes a sudden drop in the stiffness of the infilled frame soon after the infill cracking thereby causing large deformations at the peak accelerations.

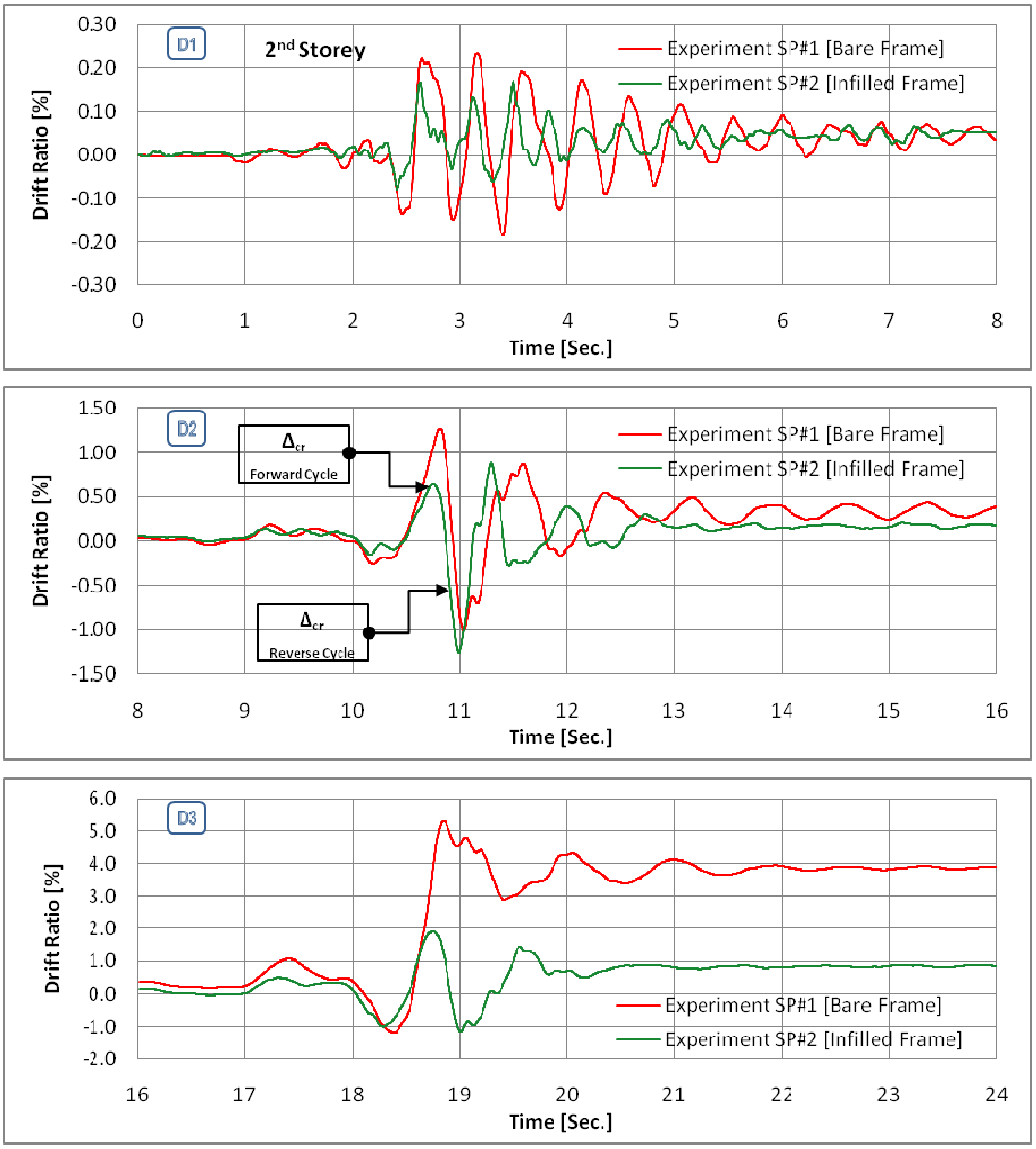

Figure 3.3(b): Second storey drift ratio time-history (NC specimens)

Another probable cause of these large drifts is the occurrence of shear failure in the bounding columns at the same instant (Point-B in Figures 2.11 and 2.12). The failure indicates the exceedance of shear capacity of column i.e. 28.4 *kN* (refer Table 2.5). At this instant of column shear crack and panel cracking, the maximum base-shear of infilled and bare frames are 107 *kN* and 44 *kN* (Figure 3.4a) respectively. If the difference of these i.e. 107 - 44 = 63 *kN* is assumed to be resisted by the panel until it cracked, then this shear transfer to the column is more than enough to exceed the shear capacity of column. In fact, if only half the shear from the panel goes to the column, assuming the rest half is redistributed in beam or respective beam-column joint, it is still greater than the shear capacity of column. Just before the first diagonal cracking of the infill, the storey drift of infilled frame at the 1st, 2nd and 3rd storeys are 1.52, 1.95 and 3.6 times lesser than that of bare frame. Table 3.3 shows the observed limiting drifts of AAC infill panel.

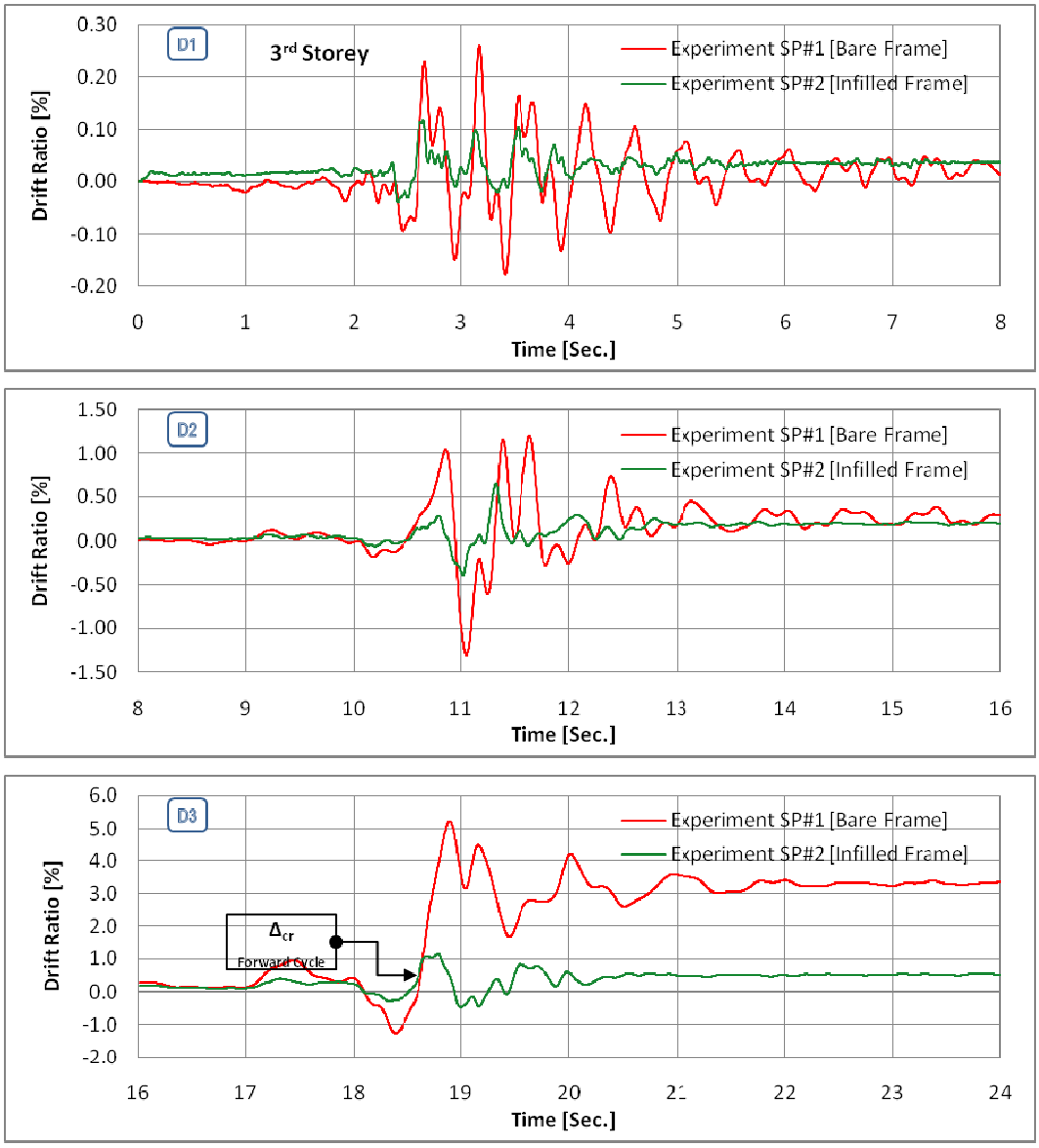

Figure 3.3(c): Third storey drift ratio time-history (NC specimens)

The storey shears of infilled frame increases considerably as compared to bare frame during the peak drifts during D2. The increase in peak storey shears is shown in Table 3.2 as well, indicating the integral behaviour of frame and infills in all three stories of Specimen #2 and verifying the contribution of AAC infill panels in overall strength.

During the ground motion D3, the peak roof drifts occur at approximately 18.79 seconds as can be seen in Figures 3.3 (a) to (c) (3rd graph). Due to severe damage to the masonry infill at the 1st storey of Specimen #2 (Figure 2.12 Point-E), the 1st storey drift response of both frames is essentially the same until the peak drift. However, the drift of 2nd storey at peak instant in infilled frame is more than 2.5 times smaller as compared to the bare frame. At the 3rd storey the drift in infilled specimen during all three ground motions is considerably smaller compared to bare frame because the infills do not show any visible damage and are fully intact until the cracking. The 3rd storey infill reaches cracking limit during D3 and peak drift is more than 4.5 times lesser than that of bare frame.

Table 3.3: AAC panel observed limiting drifts (SP#2)

Storey	Cracking Limit		Failure/Severe damage Limit	
	Drift ratio [%]	Ground motion	Drift ratio [%]	Ground motion
1st storey	0.526	D2	1.42	D3
2nd storey	0.531	D2	1.47	D3
3rd storey	0.524	D3	-	-

The AAC infill however contributes notably in reducing the residual inter-storey drift. The residual inter-storey drift in all the stories of infilled frame are as low as 3 times to that of bare frame at the end of D3. The first storey of both frames receives severe damage due to brittle failure of the elements (Figures 3.1 and 3.2) causing permanent deformations in both specimens which is also evident from the drift response (Figure3.3).

The storey shear responses in Figure-3.4 indicate that the shears in infilled frame during all the peaks during D3 are considerably greater than that of bare frame. The maximum storey shears in the 1st, 2nd and 3rd storeys of infilled frame are 1.73, 1.58 and 1.54 times greater than that of bare frame as shown in Table 3.2. This indicates that AAC infill panels take over and attract greater shears once the deficient frame suffers severe damage.

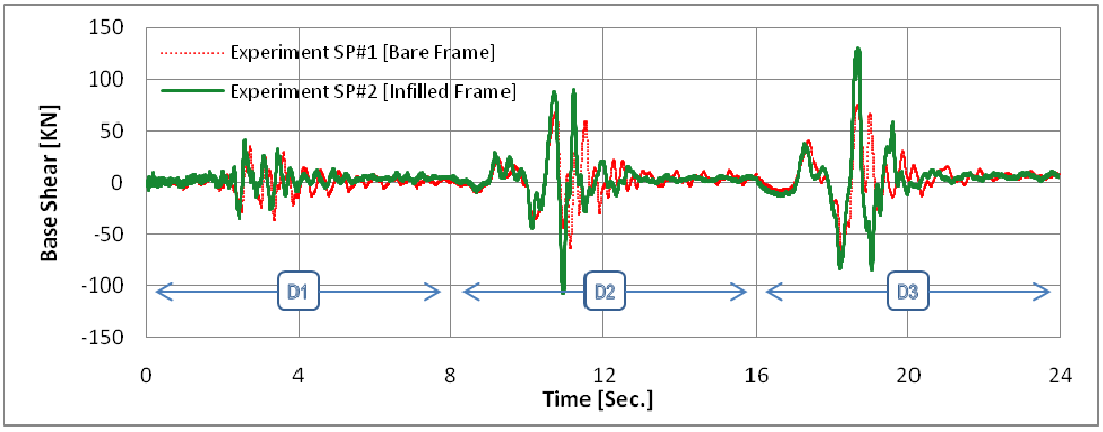

Figure 3.4(a): First-storey shear/base-shear time-history (NC specimens)

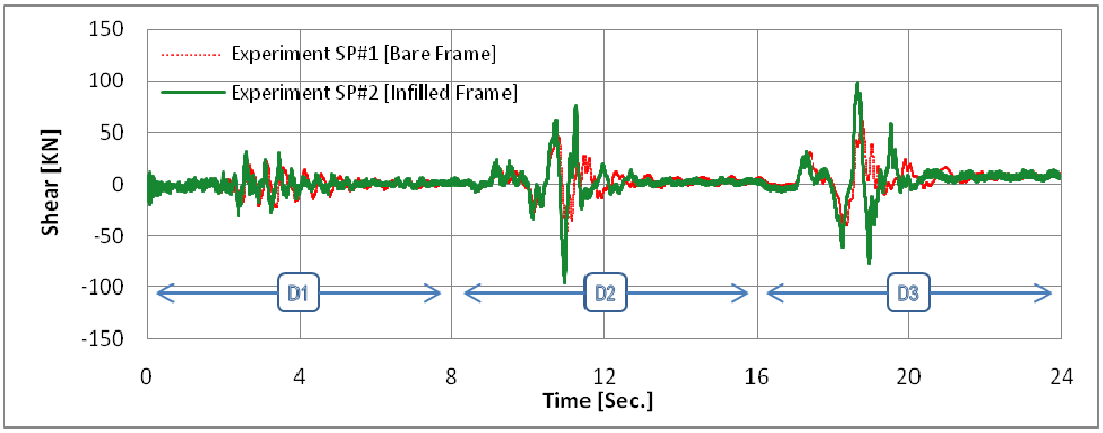

Figure 3.4(b): Second storey shear time-history (NC specimens)

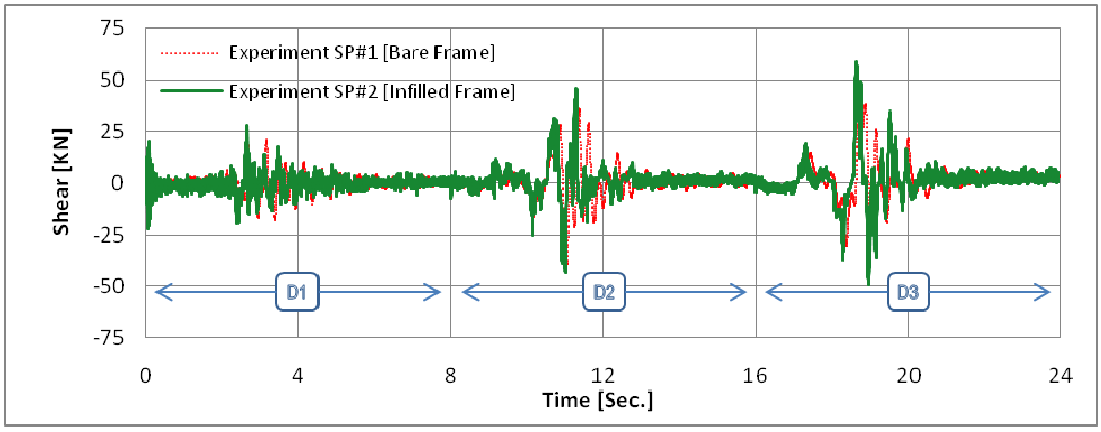

Figure 3.4(c): Third storey shear time-history (NC specimens)

Fundamental period time histories of the two specimens are shown in Figure 3.5. The mean initial time period of Specimen #1 is 0.345 sec. while that of Specimen #2 is 0.275 sec., lesser than the bare frame. Since the total weight of both frames is the same, the reduced initial period of infilled frame can be attributed to the stiffness added by the infill panels. The period of both specimens increases as the ground motions become stronger, attributed to the degradation in strength as a result of damages and inelastic deformations. It is worth noticing that the period of infilled frame is very close to that of bare frame at the peak drift of D3 after the excessive cracking of infills in the 1st and 2nd storey indicating that the frame behaves essentially like a bare frame after the failure of infill panels. The period of infilled frame is however a little lesser compared to bare frame after the peak drifts during D3 possibly due to the fact that the infills at the 3rd storey are still contributing to stiffness.

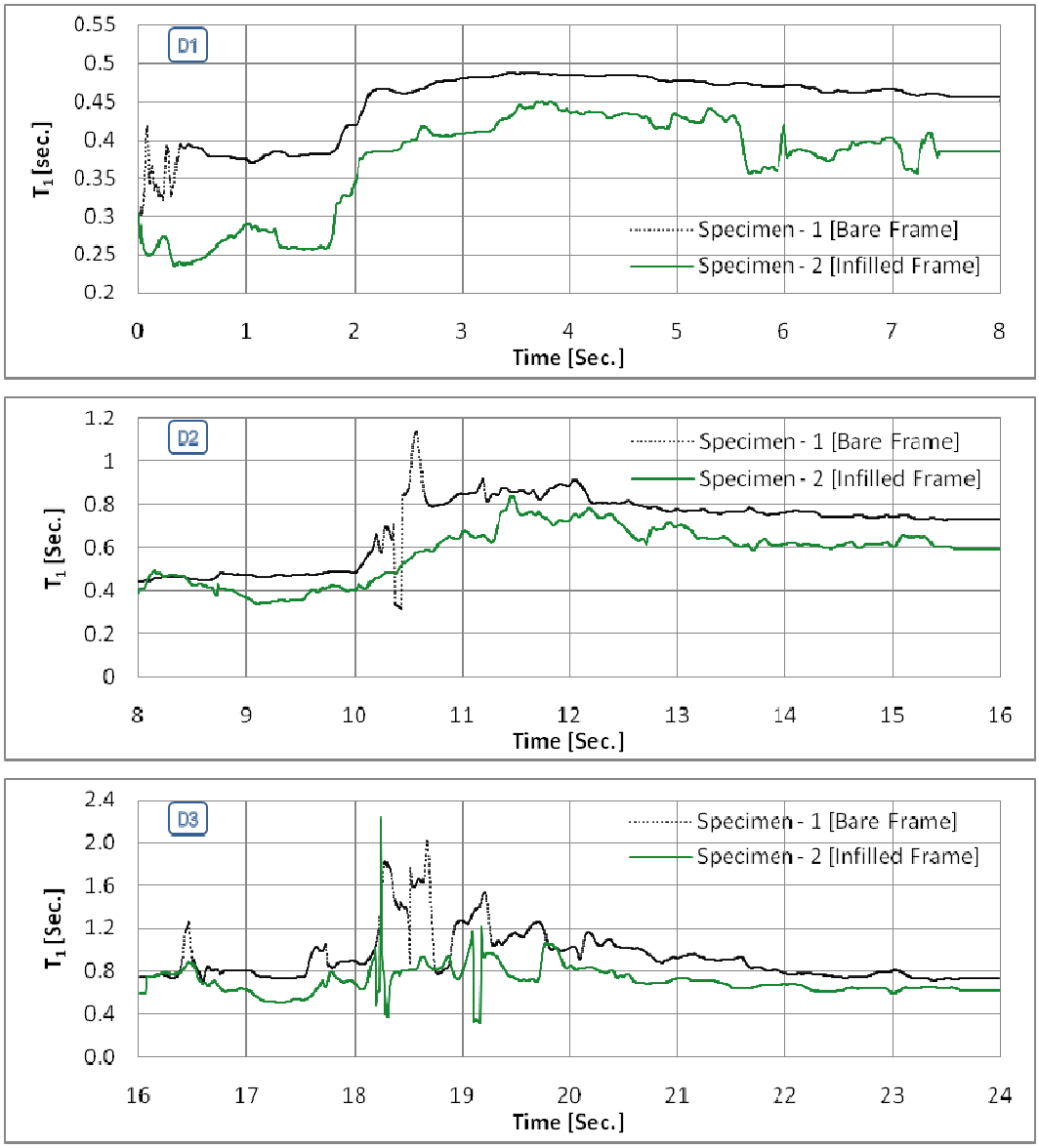

Figure 3.5: Fundamental period time-history (NC specimens)

3.2.3 Local Responses

In addition to the previously discussed global responses, certain columns and beams are also compared for end-rotations and are shown in Figures 3.6 and 3.7. Since most of the damage is concentrated at the first storey of both specimens, end rotations of one exterior and one interior member at the 1st storey are chosen for comparison for columns and beams both.

End rotations of exterior column (101) of 1st storey (Figure 3.6 a) indicates that infilled frame has similar response as the bare frame during D1 because of the absence of frame-infill composite action. It is important to note that although Column 101 is not bounding the infill panels, the local response is indirectly altered due to the alterations in overall global responses. During D2, due to the flexural cracking in columns bottom end, some residual rotations appear in bare frame which are well contained by the infills in the case of infilled frame. During ground motion D3, the peak rotations of both frames are essentially the same because of the failure of infill panels. However, the infill notably reduces the residual rotations as also evident from the global responses.

End rotations of 1st storey interior column (102) which is bounding the infill panel are shown in Figure-3.6 (b). During ground motion D1, the response of both frames is quiet similar. The point at which cracking of 1st storey infill initiates during D2 is marked in Figure-3.6 (b) with black arrow. The peak rotation of infilled frame column just before the cracking of infill is much smaller as compared to bare frame. However, at the instant of first diagonal crack in the infill panel, the rotation (both top and bottom) of infilled frame are significantly greater than bare frame probably because of the sudden reduction in the overall stiffness contributed by infills prior to cracking. The similar is also observed in the end rotation plots of column 101 in Figure 3.6 (a). Cracking and damage at the top of column 102 is also responsible for residual rotations in column 102 at the top in the infilled frame at the end of D2. During D3, the peaks as well as residual rotations of infilled frame are significantly smaller as compared to bare frame due to flexure failure of Column 102 of bare frame in an abrupt manner resulting in large drifts thereby causing large permanent deformation.

The end rotations of exterior beam (111) of 1st storey are shown in Figure-3.7 (a). It is to note that in the infilled specimen, Beam-111 is not bounding the infill panel rather it is connecting to the Beam-112 which bounds the infill panel at 1st storey. The rotation response at both ends indicates a significant increase in peak rotations of Beam-111 in infilled frame as compared to bare frame during both D2 and D3 ground motions. This can be attributed to the fact that Beam-111 is connecting to the middle bay of the frame which is much stiffer due to the presence of infill panels thereby causing larger deformations.

The end rotations of 1st storey interior beam (112) are shown in Figure 3.7 (b). In infilled frame, comparison of the j-end rotation of Beam-111 with i-end rotation of Beam-112 clarifies that due to infill panel the rotations of Beam-112 is smaller than Beam-111 at the opposite ends of the same joint. During D2, the peak rotation of infilled frame at i-end in Beam-112 is greater than the bare frame at the point of first diagonal crack in the infill panel, which is analogous to the observation in columns. At the j-end, during D3, the peak rotation of infilled frame is greater than the bare frame possibly because of the extreme damage and buckling of reinforcement in Column 103 as shown in Figure 2.12 Point-G.

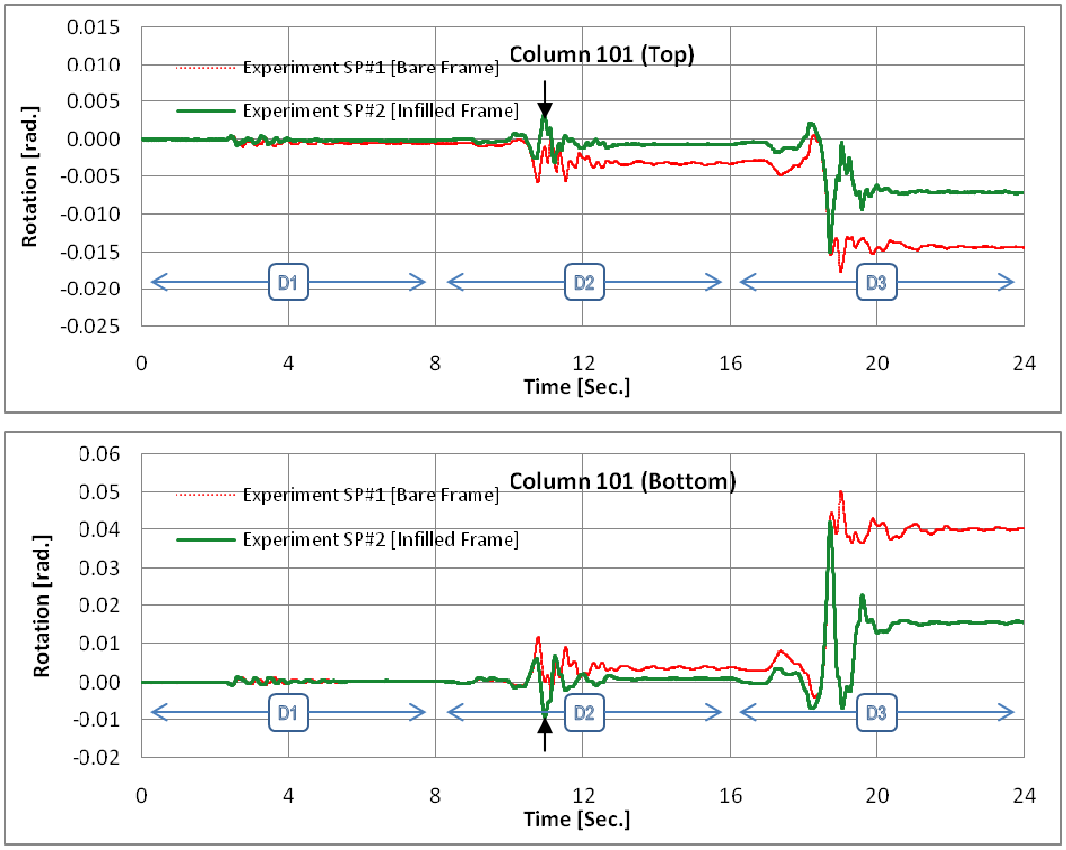

Figure 3.6(a): First storey exterior column (101) end-rotations (NC specimens)

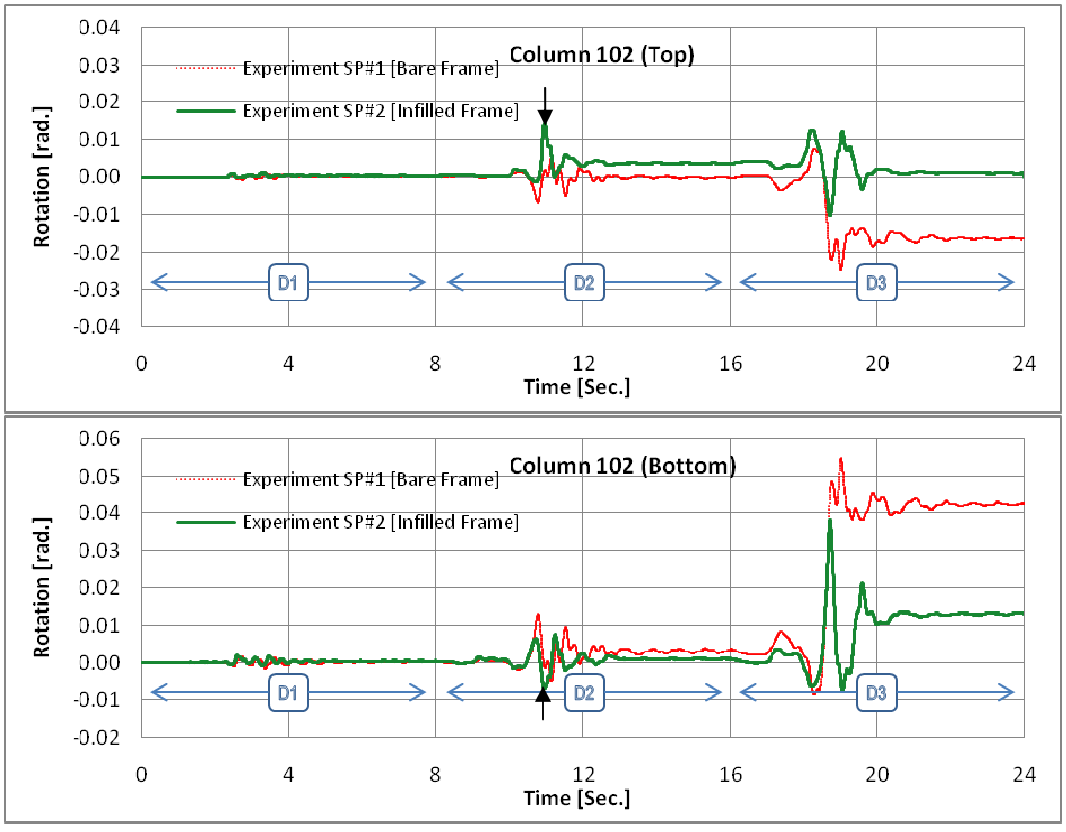

Figure 3.6(b): First storey interior column (102) end-rotations (NC specimens)

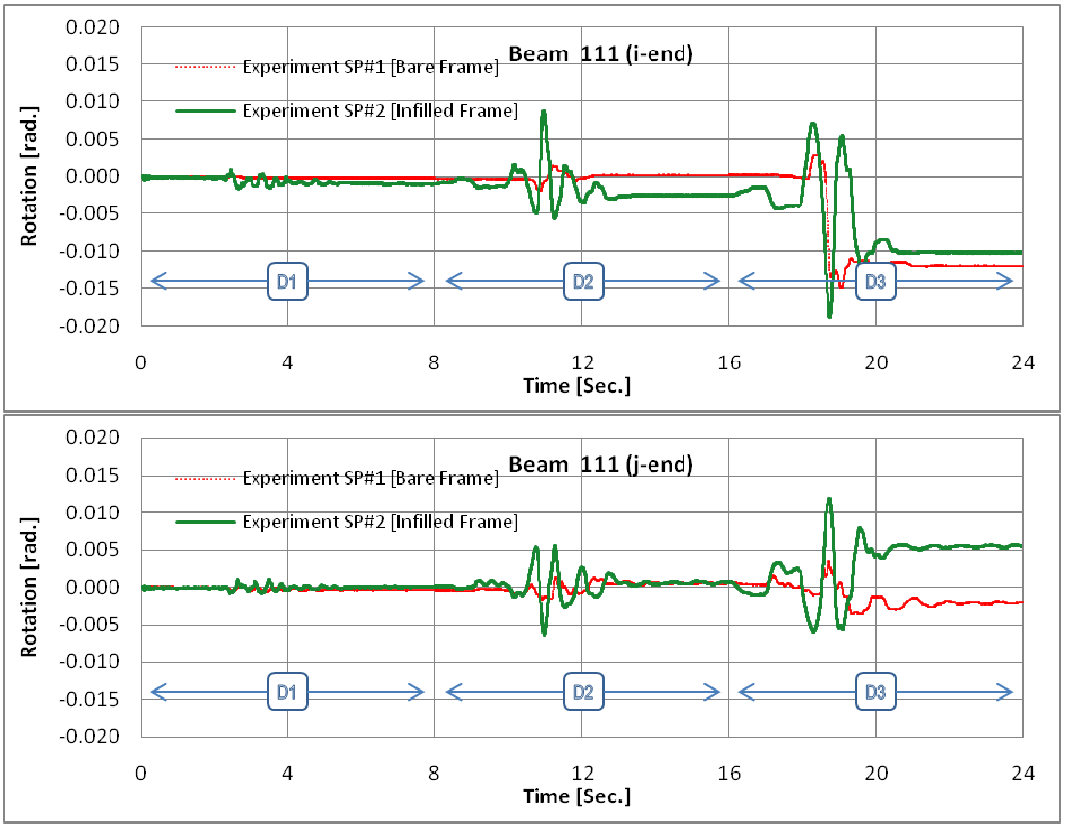

Figure 3.7(a): First storey exterior beam (111) end-rotations (NC specimens)

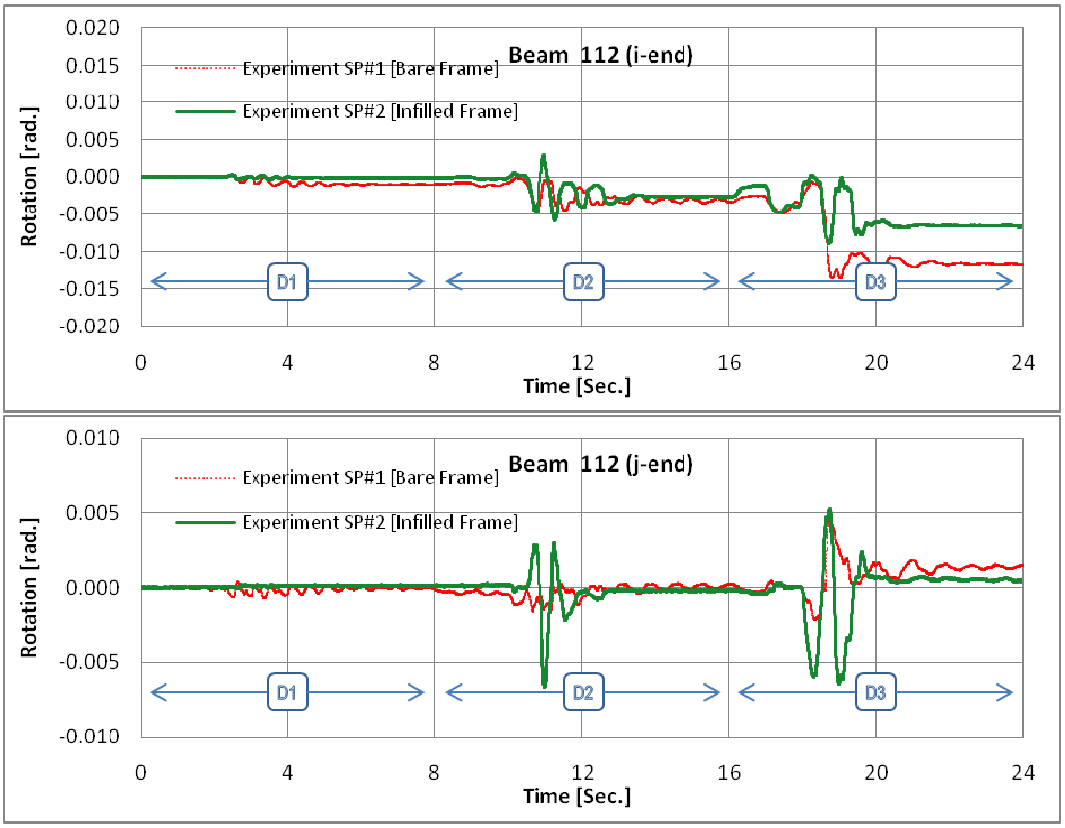

Figure 3.7(b): First storey interior beam (112) end-rotations (NC specimens)

3.3 Comparative Evaluation of the Performances of AAC Infilled and Bare Code-conforming RC Frames
(Specimen #3 vs. Specimen #4)

This section consist of the comparison of pseudo-dynamic test results between two code-conforming R.C. frames i.e. Specimen #3 and Specimen #4 in order to evaluate the effect of AAC infill on the response of RC frames. Figure 3.8 and Figure-3.9 presents the pictorial presentation of the major damages in Specimen #3 and Specimen #4 respectively, which are observed in the structural members during the three successive ground motions. Table 3.4 summarizes the observed damages with reference to these damage pictures. The global response time histories including, inter-storey drift, storey shears and fundamental period variation are presented in Figures 3.10 to 3.12. Figures 3.13 and 3.14 contain the member end rotation time histories for columns and beams respectively.

3.3.1 Performance Evaluation through Damage Observation and Failure Mode

3.3.1.1 Specimen #3 [Bare Frame – CC]

Specimen #3 is code-conforming bare frame and designed to resist both gravity and seismic loads. The observation of damage pattern at several instants of peaks during the test is presented in the Section 2.4.3 along with damage pictures in Figure-2.16 of Chapter 2. During the ground motion D1, there was no visible damage reported and the response of the frame was elastic.

During D2, diagonal cracking of joints occurred which was followed by visible flexure cracks in the 1^{st} storey exterior columns bottom. Minor flexure cracks also occurred in external beams. The specimen remains in a slight damage state.

During D3 ground motion, cracking in the joints increases and grows wider. Flexure cracks in the columns of 1^{st} storey widen and extend along the length of the column. Flexural and flexure shear cracks in the interior beams of first storey also appears. The damage was mostly concentrated in the columns, beams and joints of bottom storey which is as expected for a moment frame system, while top storey suffers very slight damage. The cracks and damage were reported in the 1^{st} and 2^{nd} storey joint region due to diagonal cracks which is unusual for a seismically designed frame. It can be attributed to the absence of confinement of the joints by the beams on the out of plane direction because in actual practice the joints are confined on all four or at least three sides. Permanent deformation in any member was not noted. Overall the specimen survived the earthquake efficiently with moderate damage. This also provides a general confidence on the design provisions of TEC 2007 for the efficient seismic design.

3.3.1.2 Specimen #4 [Infilled Frame – CC]

Specimen #4 is similar to Specimen #3 except the addition of AAC infill panels. The observation of damage pattern at several instants of peaks during the test is presented in Section 2.4.4 along with damage pictures in Figure 2.20 of Chapter 2. During the ground motion D1, no damage was observed in any of the structural members and the AAC panel also did not suffered any visible damage.

During the ground motion D2, the flexure cracks in the exterior columns and beams ends appears as well as the diagonal cracks in the joint region opened up from the previous test. Diagonal crack in the panel initiates in 1^{st} and 2^{nd} storey and continues to widen along the main compression diagonal. No secondary diagonal cracks or crushing was observed in the panel. The specimen was in a slight damage state after D2.

During D3, further diagonal cracks appeared in the 1^{st} and 2^{nd} storey masonry panel parallel to the loaded diagonal leading to the failure by crushing. Bounding columns of 1^{st} and 2^{nd} storey receives shear cracking due to the shear stresses transferred through the compression strut. Flexure cracking of exterior columns spread along the length and diagonal cracks in joint region also widens. Overall the observation suggests moderate damage to the specimen without any sign of failure in RC members.

Legends:

a Diagonal Crack at 1st storey joints – D2
b Flexure cracks at 1st storey column bottom ends – D2
c Flexure cracks at 1st storey exterior beams end – D2
d Diagonal Cracking at 1st storey joints – D3
e Flexure cracks at 1st storey column bottom ends – D3
f Overall damage to 1st storey beam, column and joint – D3

Figure 3.8: Major damages observed during D2 and D3 (SP#3)

3.3.1.3 Failure Mode

From the observations above, it is apparent that both specimens suffered moderate damage to the RC members at the end of ground motion D3. These damages resulted in notable plastic deformations in both the specimens but the specimens did not collapse. However, the dominant cause of plastic deformations for both specimens is different from each other.

In Specimen #3 the inelastic deformations both in columns and beams comprise mainly of flexural yielding. The cracking in the bottom storey columns were distributed along the length with wider cracks near the ends. No sign of brittle failure was observed. There were no notable permanent/residual deformations in any member.

Legends:

a Flexure cracks at exterior column bottom ends – D2
b Diagonal crack at 1st storey interior joints – D2
c Flexure cracks at 1st storey exterior beams end – D2
d Diagonal crack at 1st and 2nd storey infill Panel – D2
e Shear cracks at 1st storey bounding column top – D3
f Shear cracks at 1st storey bounding column – D3
g Crushing of infill panel at 1st and 2nd storey – D3
h Bond slip cracks at exterior column bottom ends – D3
i Shear-flexure cracks at 1st storey exterior beam – D3

Figure 3.9: Major damages observed during D2 and D3 (SP#4)

Table 3.4: Summary of observed performance of code-conforming specimens

Ground Motion	Observation
Specimen #3 – Code-conforming Bare Frame	
D1	• No visible damage
D2	• Minor flexure cracks in exterior columns (Figure 3.8 b) • Shear and shear-flexure cracks in beams (Figure 3.8 c) • Diagonal cracking of 1st storey joints (Figure 3.2 a)
D3	• Spread of flexure cracking at columns along the entire length (Figure 3.8 e) • Extensive diagonal cracks in joints (Figure 3.8 d) • Flexure cracks in beams (Figure 3.8 f)
Specimen #4 – Code-conforming Infilled Frame	
D1	• No apparent damage
D2	• Minor flexure cracks in exterior columns (Figure 3.8 a) • Flexure cracks in beams (Figure 3.8 c) • Diagonal crack in joints in X-pattern (Figure 3.8 b) • Diagonal crack in AAC masonry panel along the compression strut (Figure 3.8 d)
D3	• Shear cracks in 1st and 2nd storey bounding columns (Figure 3.8 e and f) • Bond slip crack at 1st storey exterior column (Figure 3.8 h) • Flexure and shear-flexure cracks in exterior columns (Figure 3.8 h) • Flexure cracks in beam widens (Figure 3.8 i) • Increase in diagonal cracking in joint regions • Multiple diagonal cracks in AAC panels leading to crushing failure of masonry at first and second storey (Figure 3.8 g)

The Specimen #4 also did not suffer any severe damage to frame members leading to collapse but the main cause of inelastic deformations in the members is different from the one observed in Specimen #3. Due to the shear stresses conveyed by the masonry panel to the bounding columns, shear cracking was observed at the interior columns, although it cannot be said that it was severe enough to cause brittle failure in the member. The exterior columns and beams received flexure and flexure-shear cracks. The joints exhibit diagonal shear cracks in X – pattern. The masonry panels yielded with the diagonal cracking pattern observed in the Specimen #2 as well. The final failure of the masonry was however different from Specimen #2. As discussed earlier, the panels of Specimen #2 failed due to extensive diagonal cracking but in Specimen #4 AAC panels failed due to compression crushing after the diagonal cracking. The final failure mechanism of the specimen however cannot be predicted due to this blend of plastic deformations as the specimen was still in moderate damage state.

3.3.2 Global Responses

This section evaluates the performance of code-conforming frames on the basis of time histories of global responses obtained after the test as well as from the comparison of peak responses during each ground motion given in Table 3.5.

The inter-storey drift responses (Figure 3.10) for infilled and bare frames during D1 indicates that AAC infills cause reduction in drift in all three storeys as compared to bare frame with least reduction in peak drift in the 1st storey and highest in the 3rd (Table 3.5), which is a similar observation as in Specimen #2. The storey shear response histories of both specimens, plotted in Figure 3.11, also indicate that the increase in storey shear of infilled frame as compared to bare frame in the 1st storey is the least due to strength contributed by the AAC infills while this increase is higher in the 2nd and

3rd storeys. This difference is also observed for peak storey shears as shown in Table 3.5. As discussed earlier, this may be attributed to the fact that after cracking of members, the effectiveness of confinement of masonry infill provided by the frame is reduced resulting in the diminishing of integral frame-infill interaction in containing the drifts.

The storey drifts plot during ground motion D2 are also plotted in Figure 3.10 with the panel cracking drift Δ_{cr} in both forward and reverse cyclic motion at the 1st and the 2nd storey (the diagonal compression struts str_1, str_3 and str_2, str_4), is marked (Point-A and B in Figures 2.19 and 2.20).

Table 3.5: Comparison of peak global responses between Bare and Infilled frames (CC)

Response Parameter "*N*"	Ground Motion	SPECIMEN		Difference [%] *
		#3 Bare - CC	#4 Infilled - CC	$\frac{(N_{SP\#4} - N_{SP\#3})}{N_{SP\#3}}$
Roof Displacement [m]	D1	0.0094	0.0051	-46.09
	D2	0.0499	0.0443	-11.30
	D3	0.0858	0.0819	-4.52
1st storey/Base shear [*kN*]	D1	46.0	48.2	4.91
	D2	115.2	129.4	12.32
	D3	131.6	182.9	39.06
2nd storey shear [*kN*]	D1	39.8	42.0	5.35
	D2	101.7	111.6	9.78
	D3	128.6	173.6	35.01
3rd storey shear [*kN*]	D1	27.8	23.8	-14.39
	D2	56.1	56.6	0.89
	D3	61.2	78.2	27.62
1st storey drift ratio [%]	D1	0.19	0.14	-28.99
	D2	1.16	1.07	-8.42
	D3	2.08	2.04	-1.96
2nd storey drift ratio [%]	D1	0.27	0.18	-33.14
	D2	1.37	1.13	-16.94
	D3	2.34	2.20	-6.05
3rd storey drift ratio [%]	D1	0.19	0.05	-75.81
	D2	0.88	0.62	-30.04
	D3	1.44	0.87	-39.68
Base shear ratio (V/W)	D1	0.15	0.16	
	D2	0.39	0.43	
	D3	0.44	0.61	

CC = Code-conforming;
*: Positive values indicate **increase** while negative values indicate **decrease.**
W = Total seismic weight of the specimens = 298 *kN*; V = Peak base shear

It can be noted that at the peak causing cracking drift, the AAC infills contained the drift very effectively in the 2nd storey as compared to bare frame; however, again at the first storey this reduction in drift is not notable due to the already present cracking and damages in the members at the first storey. Just before the first diagonal cracking of the infill, the storey drift of infilled frame at the 1st, 2nd and 3rd storeys are 1.05, 1.42 and 2.4 times lesser than that of bare frame. Table 3.6 shows the observed limiting drifts of AAC infill panel.

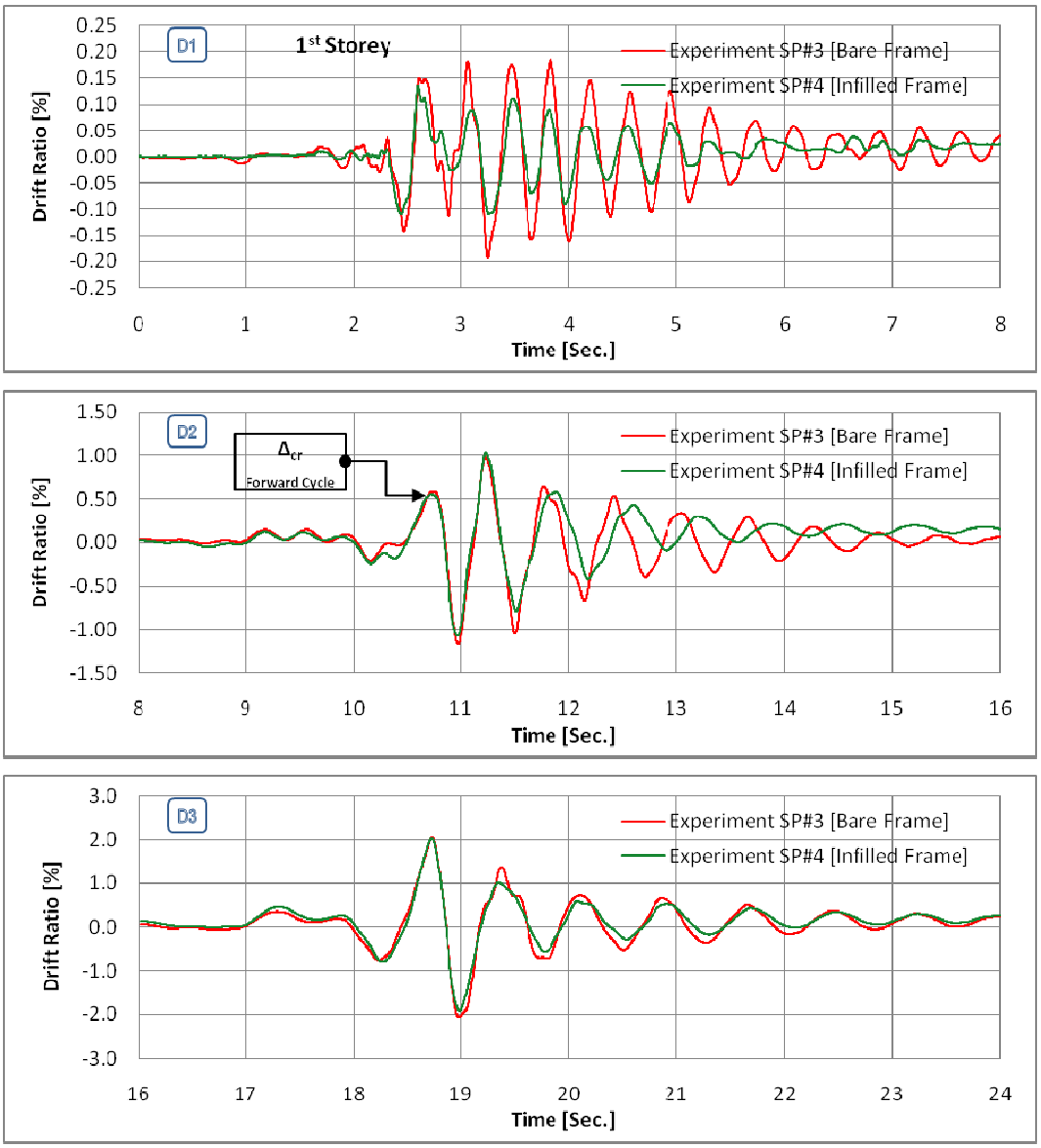

Figure 3.10(a): First storey drift ratio time-history (CC specimens)

At the 3rd storey the drift in infilled specimen during the entire ground motion is considerably smaller compared to bare frame because the infills do not show any visible damage and are fully intact. The storey shears of infilled frame increases considerably as compared to bare frame during the peak drift in D2 (Table 3.5) also indicating the integral behaviour of frame and infills in all three stories of Specimen #2.

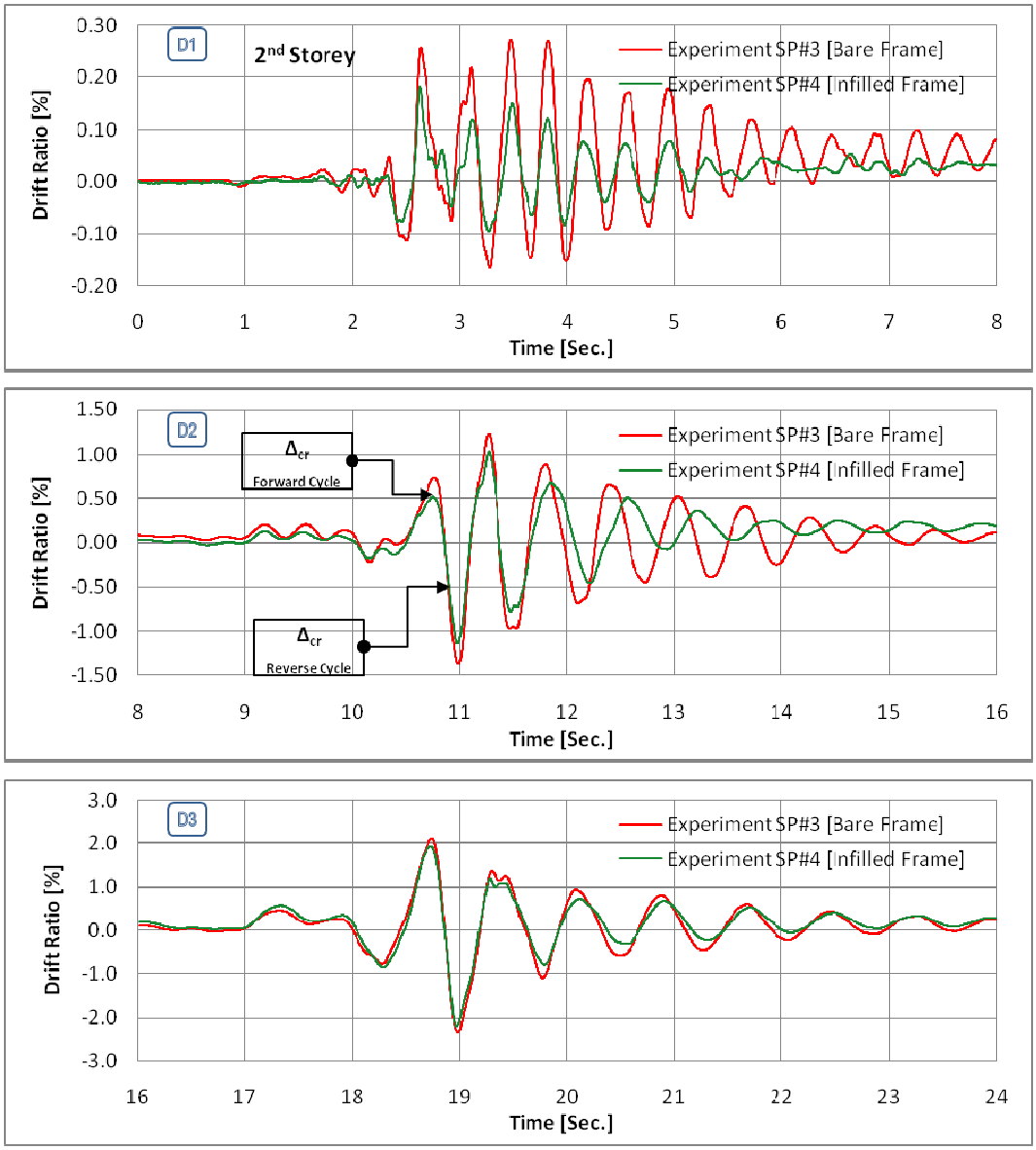

Figure 3.10(b): Second storey drift ratio time-history (CC specimens)

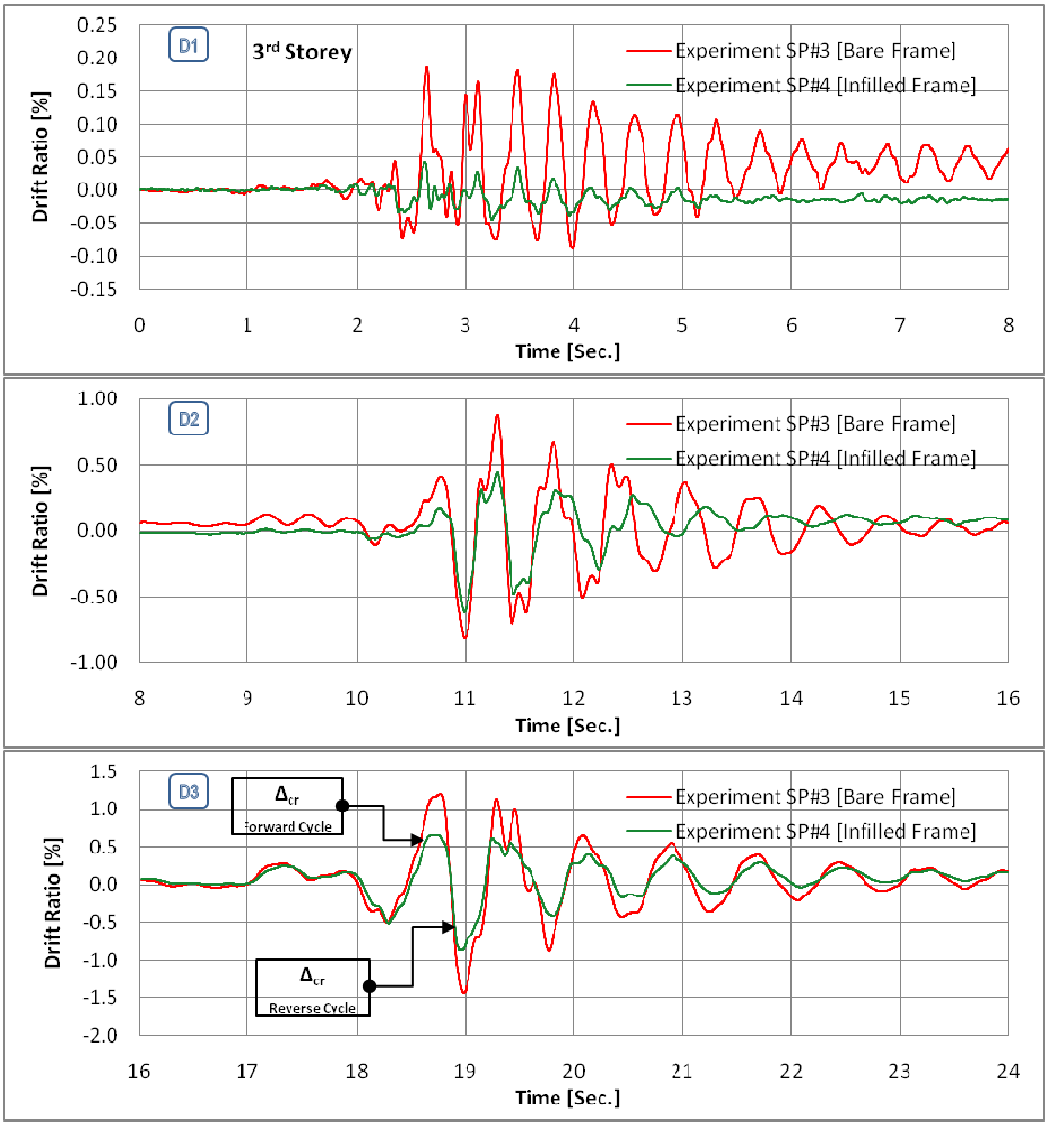

Figure 3.10(c): Third storey drift ratio time-history (CC specimens)

Table 3.6: AAC panel limiting drifts (SP#4)

Storey	Cracking Limit		Crushing Limit	
	Drift ratio [%]	Ground motion	Drift ratio [%]	Ground motion
1st storey	0.516	D2	0.789	D3
2nd storey	0.512	D2	0.847	D3
3rd storey	0.528	D3	-	-

During the ground motion D3, the infill panels at both 1st and 2nd storeys reaches the crushing limit and the peak drift responses of bare and infill frames are essentially the same after the failure of infill in both storeys (Figure 3.10 and Table 3.5). It is also worth noticing that masonry panel of the 2nd storey suffers more damage than the panel of 1st storey. Meanwhile, the panel at the 3rd storey reaches its cracking limit but however contained the drift ratio notably with reduction of 1.65 times as compared to bare frame at top storey during peak. Table3.5 indicates the highest increase in peak storey shear of infilled frame as compared to bare frame during the ground motion D3 among all three ground motions. The 1st, 2nd and 3rd storey peak shears of infilled frame increased by 1.39, 1.35 and 1.27 times as compared to the bare frame verifying the strength contribution due to infills.

Experimental observations indicate shear cracking of 1st storey bounding column at top during D3 as shown in Figures 2.19 and 2.20, point-F. In order to investigate this, shear force transferred through masonry strut into the column is calculated at this instant, by subtracting the 1st storey shear of infilled frame to that of bare frame which are 183 *kN* and 131*kN* respectively (Figure 3.11a). The difference of these, i.e. 183 – 131 = 52 *kN*, if assumed to be completely transferred to the column by the infill panel, then it is still lesser than the shear capacity of column i.e. 55.7 *kN* (refer Table 2.5). This leads to the conclusion that although the provision of confinement reinforcement provides safety against brittle shear failure of columns caused due to strut action, it does not prevent the occurrence of diagonal cracks at the region of contact between strut and column.

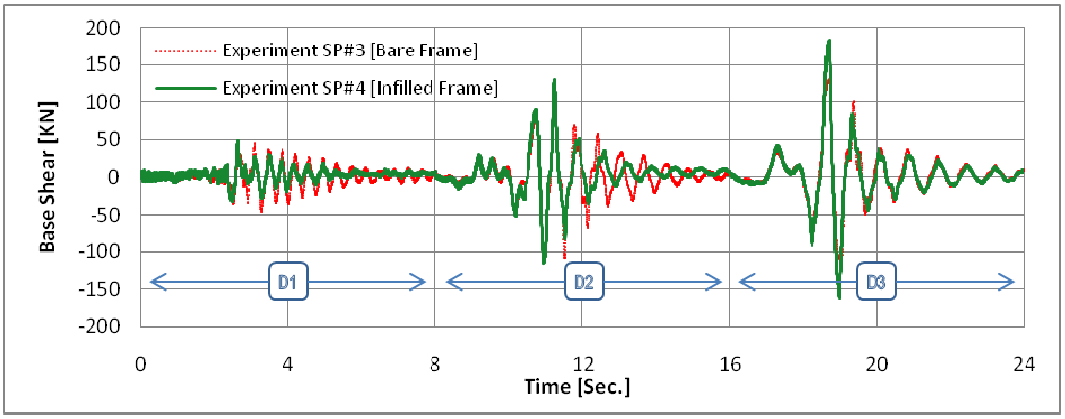

Figure 3.11(a): First storey shear/Base-shear time-history (CC specimens)

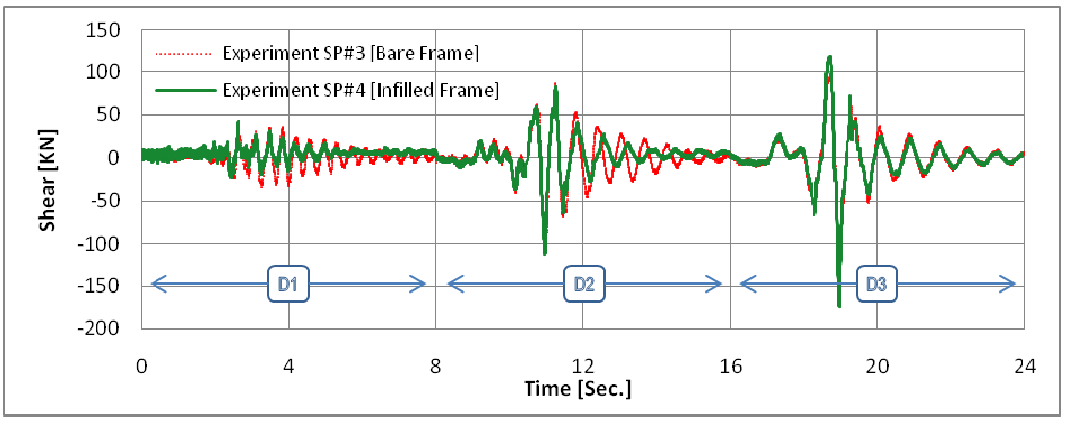

Figure 3.11(b): Second storey shear time-history (CC specimens)

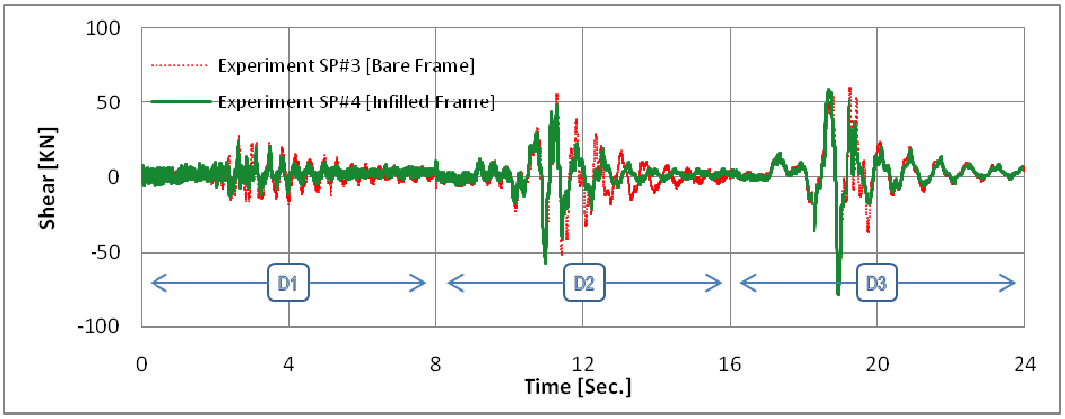

Figure 3.11(c): Third storey shear time-history (CC specimens)

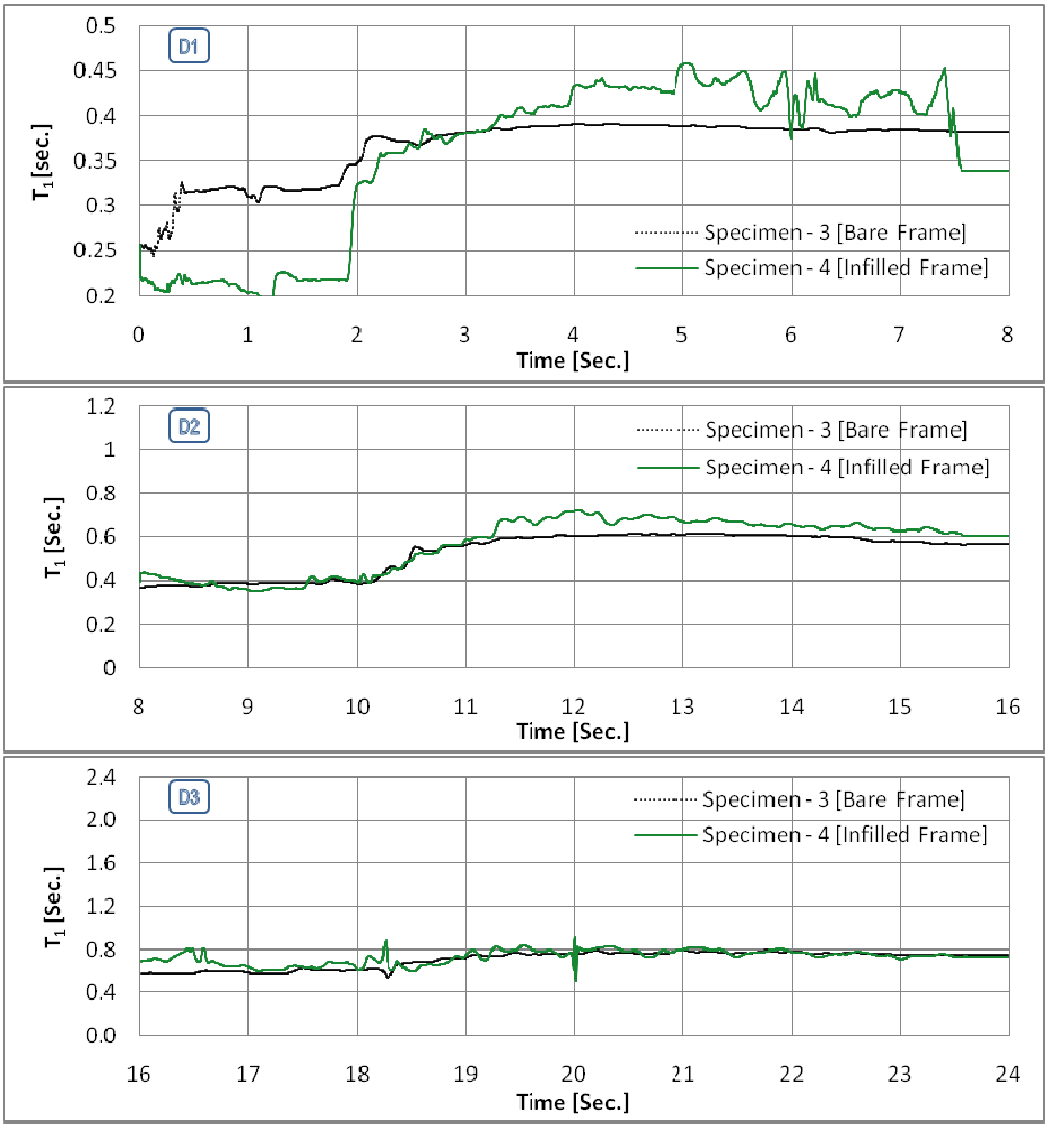

Figure 3.12: Fundamental Period Time History (CC specimens)

Fundamental period variation of the specimens during all three ground motion is shown in Figure-3.12. It is evident that fundamental period of the frames increases following the peak deformations during D1, D2 and D3 after approximately 2.5 sec., 10.5 sec. and 18.5 sec. respectively due to the cracking and damages. During D1 the time period of the infilled frame is greater than the bare frame during most of the ground motion possibly because of the fact that infilled frame is already cracked when tested and the ground motion is not strong enough to overcome the initial cracking and lack of fit and mobilize the composite infill-frame assembly. It is also evident from Table 3.5 that storey shears during D1 are essentially the same in both specimen, in fact lesser in 3rd storey. During ground motion D2, the time period of infilled frame increases as the masonry panels suffered diagonal cracks and the cracking in the joints and columns opened up. During D3, the time period of both specimens is essentially the same because the infills of the 1st and 2nd storey exhibit crushing failure while that of the 3rd storey reached cracking limit.

3.3.3 Local Responses

In addition to the previously discussed global responses, certain beams and columns are also compared for local responses. Member end rotations measured during the pseudo-dynamic test are shown in Figures 3.13 and 3.14. Bottom end rotations of exterior (101) and interior (102) columns of

1st storey are plotted in Figure 3.13 a. It can be seen that peak rotations for exterior column of infilled frame are greater than the bare frame during all three ground motions, though the difference is not very significant. It is due to the fact that the infilled frame is already cracked while tested and the exterior column is not bounded by the infills hence having no direct influence of infills. In the column 102 also, which is bounding the infill panels, the presence of infills does not seem to cause any notable reduction in the end-rotations.

The top rotations of 1st storey columns could not be presented because of the incorrect measurements caused due to the accidental defect in the measuring devices at the top end of first storey columns. Therefore, instead, the top end rotations of the 2ndstorey exterior and interior columns are shown in Figure 3.13 (b). These results will also give the similar insight since the damage to the infill panels were the same in both 1st and 2nd storeys. The infill panels cause reduction in the top end rotation of columns during ground motion D1 and D2 although the reduction is not very significant.

During ground motion D3, the end rotations of infilled frame increased abruptly as compared to bare frame at the time instant marked with black arrow in Figures 3.13 (a) and (b) which is probably due to the sudden reduction in the overall stiffness contributed by infills prior to cracking.

The end rotations of exterior beam (111) for both code-conforming frames are plotted in Figure 3.14 (a). The end rotation of beam in infilled frame are lesser than bare frame, however the difference is not very significant. The rotation response of interior beam (112) i.e. the beam bounding the infill panel, shown in Figure 3.14 (b), also shows similar response. However, in the infilled frame specimen, comparison of the j-end rotation of Beam-111 with i-end rotation of Beam-112 indicates a significant increase in peak rotations of Beam-111 at j-end as compared to i-end of Beam-112 during both D2 and D3 ground motions. This is similar to the observation in the case of Specimen #2, and can also be attributed to the fact that Beam-111 is connecting to the middle bay of the frame which is much stiffer due to the presence of infill panels thereby causing larger deformations at the weaker end of the same joint. Comparison of local responses of several members suggests that local responses are not greatly altered by the presence of AAC infill panels in case of code-conforming specimens.

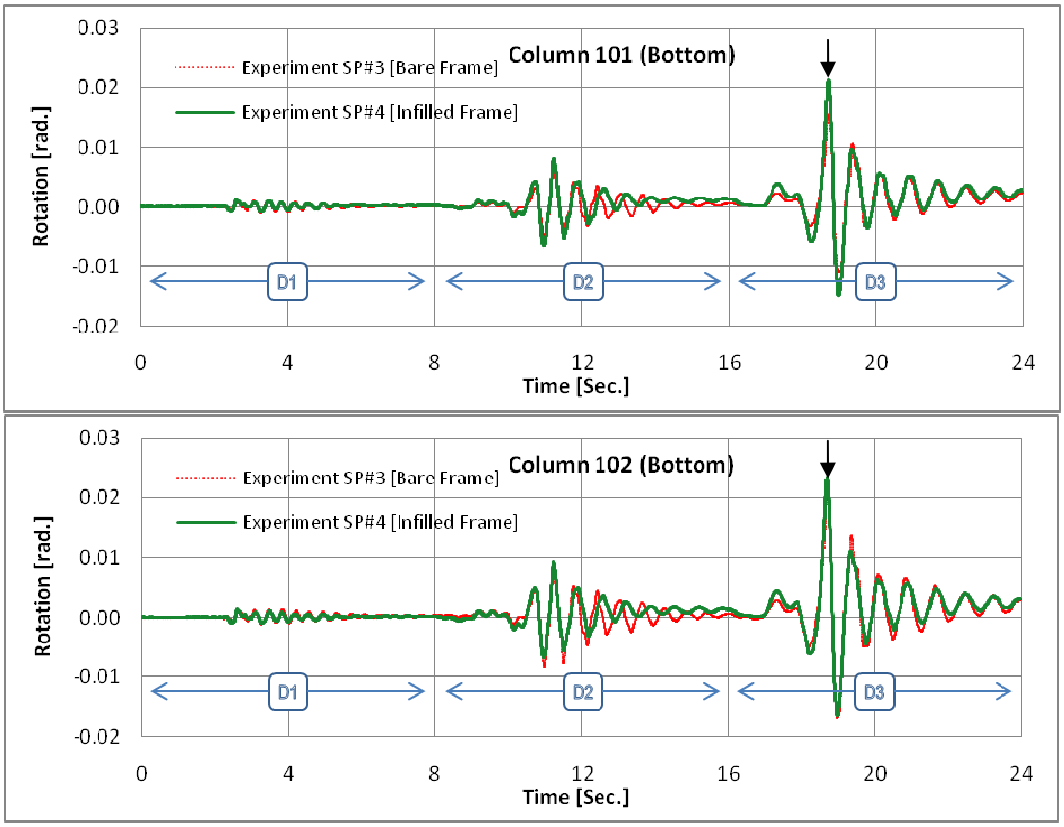

Figure 3.13(a): First storey exterior (101) and interior (102) columns bottom end-rotations

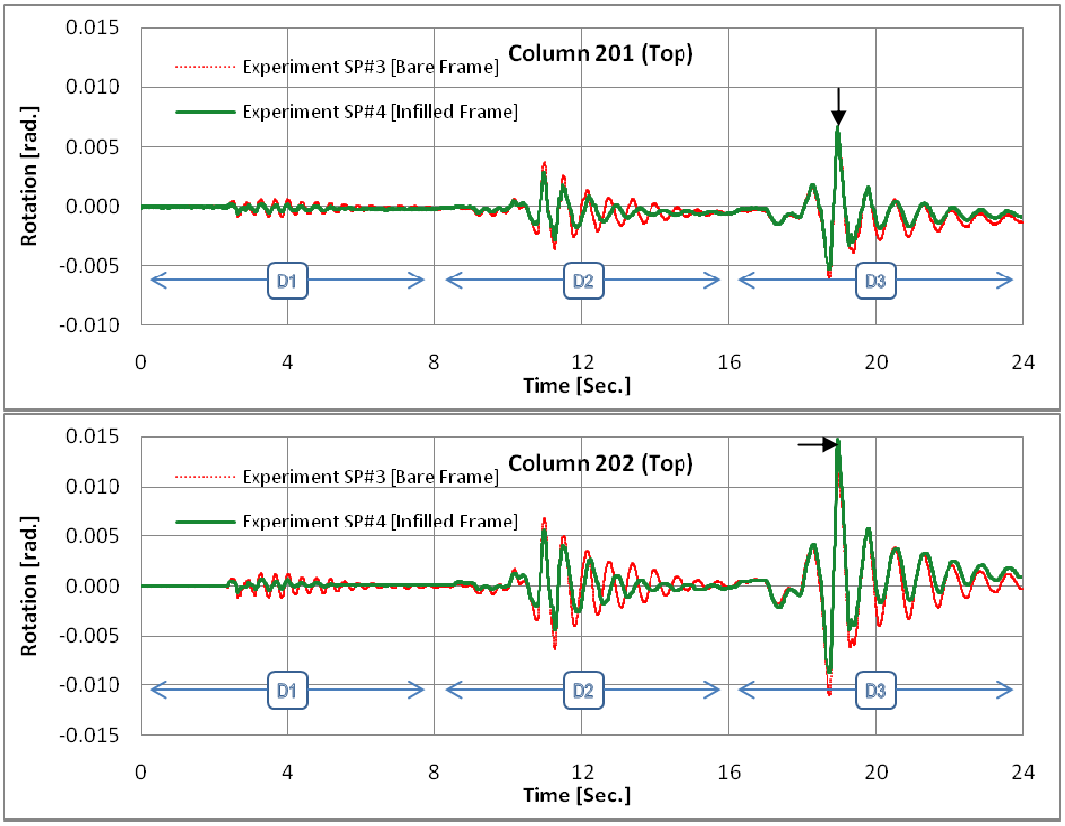

Figure 3.13(b): Second storey exterior (201) and interior (202) columns top end-rotations

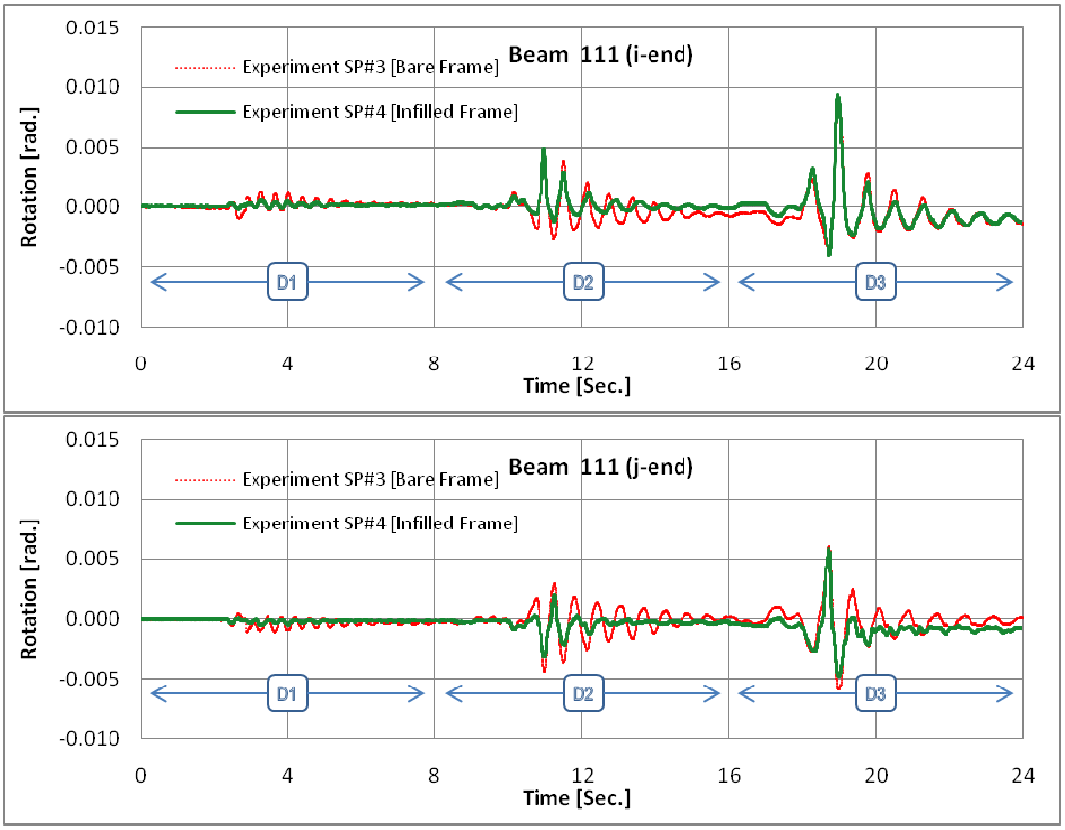

Figure 3.14(a): First storey exterior beam (111) end-rotations (CC specimens)

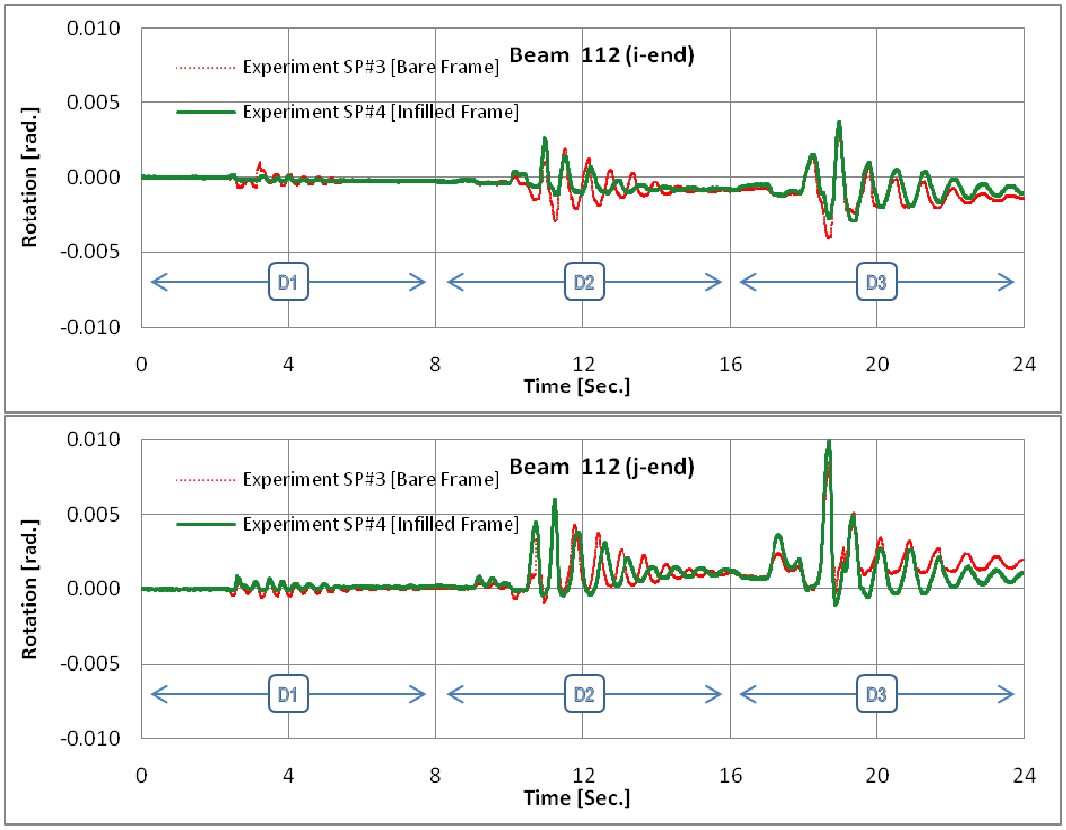

Figure 3.14(b): First storey interior beam (112) end-rotations (CC specimens)

3.4 Comparison of Results

Following the observation of the responses of frames in both non-conforming and code-conforming configuration, this section will focus on the comparison and conclusion drawn after the comparative analysis based on the experimental results and observations. Figure 3.15 plots the peak drift responses of all the specimens in separate configurations. In the code conforming specimen, the drift ratios of infilled frame in all the storeys during all the ground motion is lesser than the bare frame, with least reduction in the 1st storey and highest reduction in the 3rd storey. Non-conforming specimens indicate the same trend except at the first storey during D2, in which infilled frame drift ratio is greater than the bare frame which may be attributed, as described earlier, to the brittle failure of Column 102 at the 1st storey.

In the infilled frames, infills cause increment in storey shear during all ground motion as shown in Figure 3.16. It is worth noticing that AAC infills contribute to the increase in storey shear in the non-conforming frames while in code conforming frame the comparative increase is not very significant (Tables 3.2 and 3.5). It indicates that as the damage in the RC members increases with the increase in the magnitude of earthquake, the infills tend to attract more forces thereby causing brittle shear failures in columns if the members are not designed properly against these forces.

Ground Motion D1

Non-conforming specimens | Code-conforming specimens

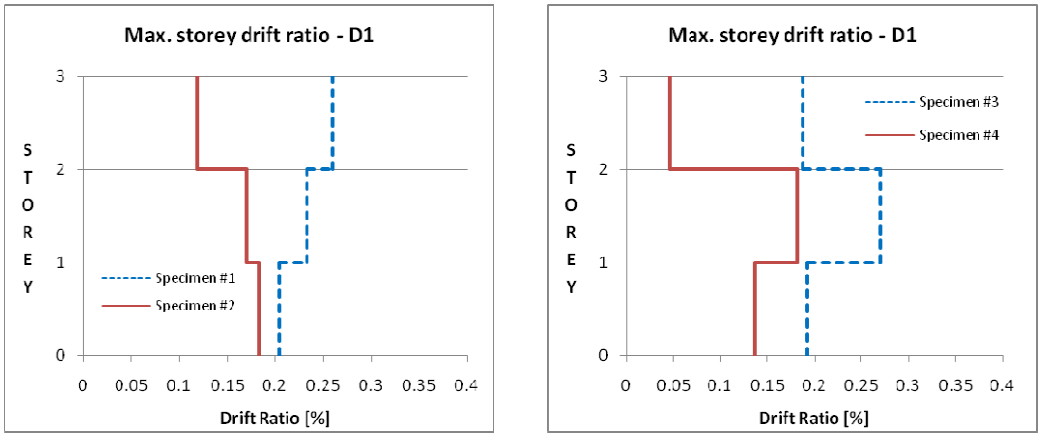

Ground Motion D2

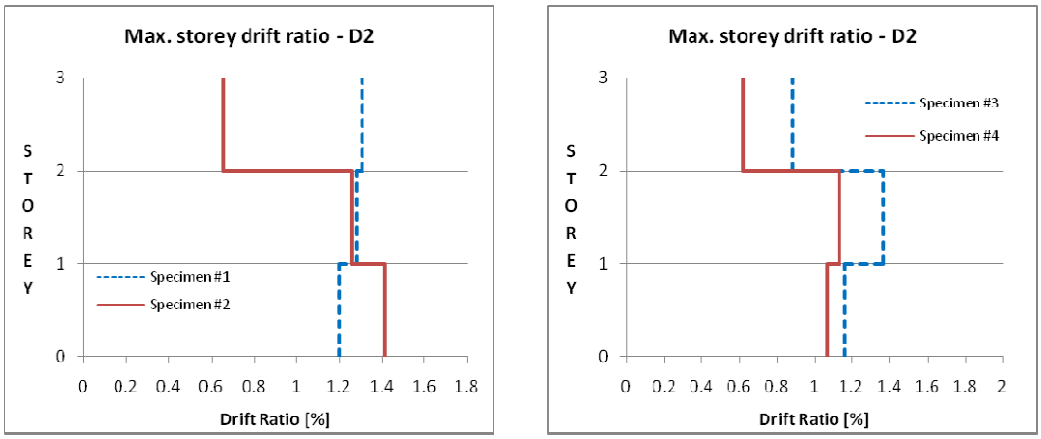

Ground Motion D3

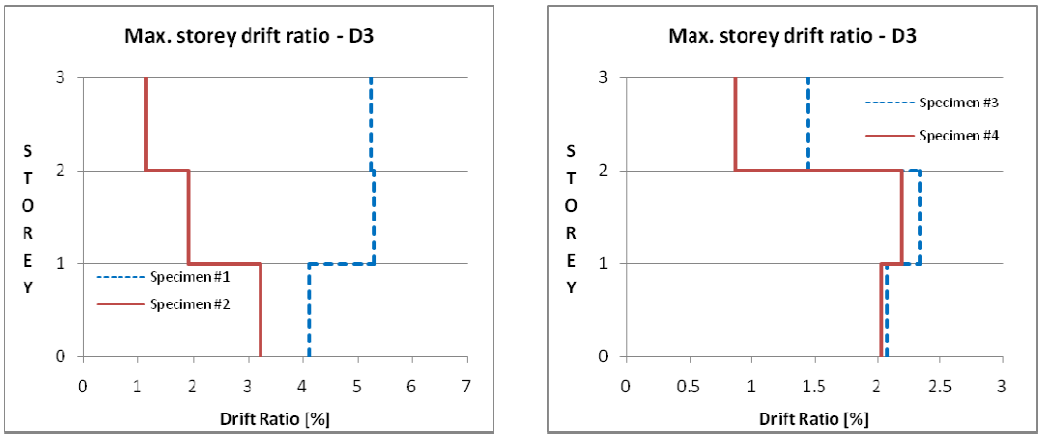

Figure 3.15: Comparison of peak inter-storey drifts

Ground Motion D1

Non-conforming specimens | Code-conforming specimens

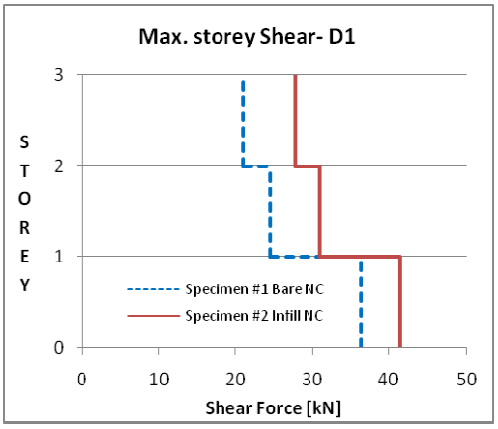

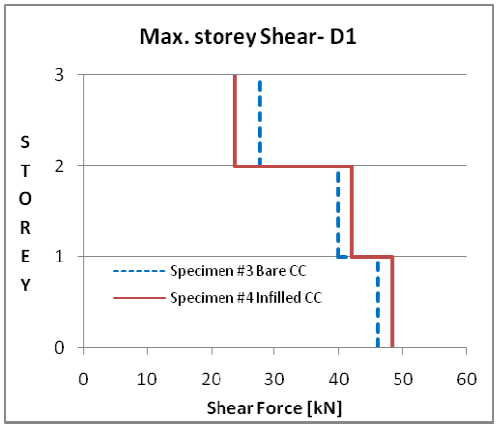

Ground Motion D2

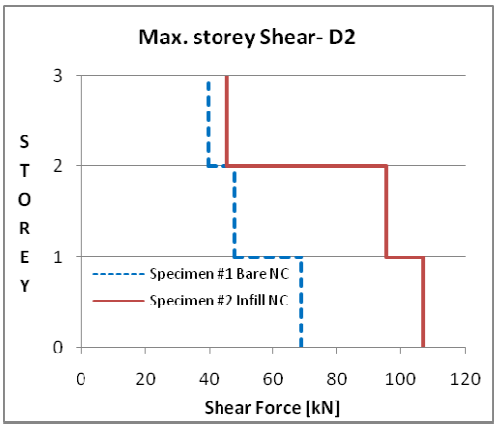

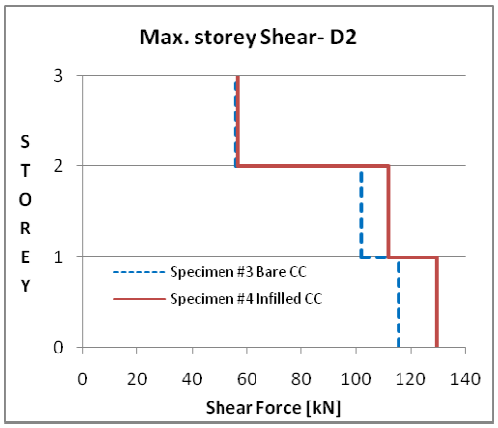

Ground Motion D3

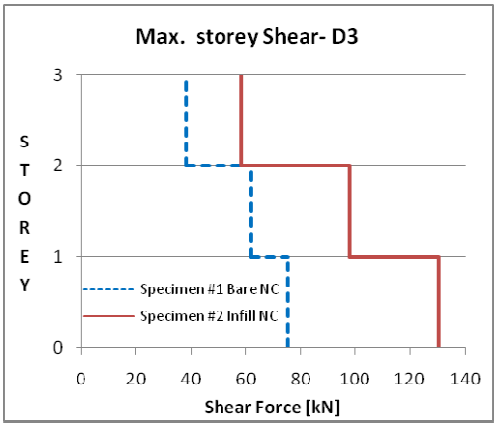

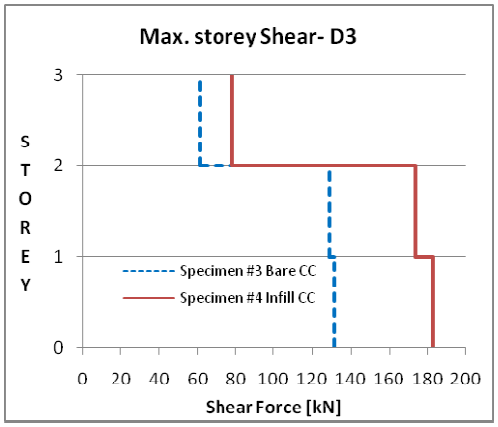

Figure 3.16: Comparison of peak storey shears

An important observation relating to the damage in infill panels is that in code-conforming frame, the infill panels experience diagonal cracks and damage even in D2 ground motion while the design ground motion for Specimen #4 is D3. Therefore, it will only increase the economic safety if necessary separation is provided between the infill panel and the bounding frame to restrict the panel damage when the ground motion is stronger but less than the design ground motion. In case of non-conforming infilled frame, this separation around the panel boundary would decrease the amount of shear forces attracted by the infill and transferred to the bounding members.

In order to investigate the response of AAC infills in the overall load carrying capacity of infilled frame, peak masonry shear vs. frame shear ratio at the 1st storey is calculated at the synchronous peaks of bare and infilled frames during ground motions D2 and D3. Shear in the masonry is calculated by subtracting the base shears of bare and infilled frame. Ratio is calculated by dividing the masonry shear to the total base shear of corresponding infilled frame. Table 3.7 lists the values for all the frames. For the non-conforming infilled frame these ratios are as high as 60% and associated with the brittle failure in the column members. For code-conforming frame, the ratio progressively increases with the magnitude of ground motion to a maximum of 26%.

Table 3.7: Infill panel shear ratio

Peak base shear	Ground Motion	SPECIMEN				V_{infill}/V_{total}	
		#1 Bare NC	#2 Infilled NC	#3 Bare CC	#4 Infilled CC	$\frac{(V_{SP\#2}-V_{SP\#1})}{V_{SP\#2}}$ Deficient	$\frac{(V_{SP\#4}-V_{SP\#3})}{V_{SP\#4}}$ Code-conforming
V	D2	43.2	107	119.298	129.206	0.598	0.077
	D3	75.226	130.41	135.652	182.746	0.423	0.258

From the above comparative analysis of the effects of AAC infills on the response of bare and infilled frames with deficient and code-conforming configurations, the following main points can be concluded:

- Frame and infill interaction is essentially through a diagonal compression strut once the ground motion is strong enough to mobilize infill-frame composite behaviour.

- Failure of AAC infill panels differs for the two different configurations. In case of deficient frame, the infill panels failed with excessive diagonal cracking, while for code-conforming frames, they failed due to crushing near the cracked diagonal.

- The drift corresponding to the cracking of AAC infill in both configurations of frames is found to be 0.5 %. The mean drift corresponding to crushing failure of infills in Specimen #4 is found to be0.8 %. The mean drift corresponding to severe damage and failure due to tension cracking is found to be approximately 1.4 %.

- AAC infills have a detrimental effect on the response of deficient RC frames in the sense that they tend to stiffen the response resulting in attraction of additional shear forces. Therefore their consideration is necessary in the performance evaluation process. However the advantage of using AAC infills is that they reduce the residual drift of the frame considerably.

- The use of AAC infills proved very beneficial in code-conforming frame as they do not tend to alter the response of the frame to a notable level while still contributing to some extent in the overall stiffness and strength.

- Analysis of AAC infill panel shear ratio indicates that in deficient construction the infill panel takeover most of the shear causing localized shear failure in bounding columns, whereas in code-conforming construction the bounding frame causes crushing in the panel reducing the detrimental effects of masonry infills during strong shaking.
- Presence of confinement reinforcement plays an important role in resisting the brittle failure of columns due to shear stresses transferred through the compression strut. The provision of adequate confinement reinforcement near the ends of columns does not guarantee the elimination of diagonal shear cracking however it may result in better performance of even the deficient RC frames once subjected to seismic loads.

- Stiffness of the frame-infill assembly decreases greatly once the infill reaches cracking limit. This effect is more pronounced in the deficient frame as compared to code-conforming frame. After the crushing of infills the response of infilled and bare frame is essentially the same.

- The provision of infill panels does not guarantee the reduction of peak deformations and drifts during a seismic event but greatly reduces the residual deformation during strong earthquake reducing the contribution of secondary forces on the columns generating from P-delta effects.

- In code-conforming construction, the provision of necessary separation between infill panel and the bounding frame may reduce the damage to the infills under ground shaking lesser than the design earthquake, thus reducing the cost of repair for the panels.

- Exterior columns i.e. columns that are not bounding the infill panels, receive most of the inelastic deformations by means of flexural yielding, however in deficient frame, this yielding is abrupt suddenly increasing the local as well as global deformations.

CHAPTER 4

NUMERICAL SIMULATION AND CALIBRATION

4.1 General

Numerical models are developed in order to evaluate the seismic performance of the test frames using non-linear time history analysis in addition to the experimental observations and results. This chapter focuses on the brief description of modelling techniques employed, parameters used and the calibration and comparison of results with those of the experiment.
The open source software OpenSees is used to create two dimensional planar structural models of the test frames. The modelling of the frame specimens is accomplished in two phases. In the initial phase, models are developed for two of the bare frames i.e. Specimen #1 and Specimen #3. Non-linear dynamic analysis or non-linear time history analysis is used to analyze and then compare the results with their corresponding experimental results. Global parameters are compared and the results from the simulation models are then calibrated with experimental observations and results by means of several parameters explained in the following sections.

In the second phase, calibrated simulation models of the bare frames prepared earlier are used to develop the models of the two infilled frames i.e. Specimen #2 and Specimen #4. As explained in Chapter-2, the main difference between the infilled and the bare frame is the provision of AAC masonry infill panels in the middle bay of the frame. In order to account for the effects of infills, the equivalent strut approach is used as described earlier in the text. Time history analysis of the developed infilled frame models are then performed in order to assess the ability of strut model in representing the response of AAC masonry infill panels. The calibrated models of all the specimens are then used to carry out the performance evaluation by using time history and pushover analyses.

4.2 Overview of the Numerical Model

The OpenSees Simulation Platform was used for generating the model of each specimen to estimate the seismic response of the test frame through performing pushover analyses and time history analyses.

Beams and columns in the OpenSees model were modelled using force-based elements defined by fibre sections at integration points. Second order geometric nonlinearity effects, i.e. P-delta effects were also considered in columns.

Formulation of the *Nonlinear Beam Column Element* follows the Euler-Bernoulli beam theory, which ignores shear deformations. For the joint regions, ASCE/SEI 41-06 provisions is applied where the rigid joint offsets are assigned to the members based on the ratio of plastic moments of columns to the beams connecting to a joint.

The concrete material model used in the model is *Concrete01*, which is the uniaxial Kent-Scott-Park (1971) concrete material model with no tensile strength and degraded linear unloading/reloading stiffness as proposed by Karsan-Jirsa (1969). Through this material model, confinement effects of transverse reinforcement were accounted for by increasing the strength and strain capacities of the unconfined concrete in order to reflect the behaviour of the concrete in the confined zones.

In order to model the behaviour of steel reinforcement, a stress-strain relation was defined by using the *uniaxial Material Reinforcing Steel* command with 90% of the yield and ultimate strength values of the reinforcing steel obtained from material tests, to provide more realistic predictions of column strengths. An onset strain hardening value of 0.01 and an ultimate strain value of 0.1 was used, as suggested by TEC 2007. The *Reinforcing Steel* material model in OpenSees is specifically created for simulating reinforcing steel in a fibre section. Perfect bond between concrete and steel was assumed because in case of Specimen #1 and #2 the reinforcements comprises of continuous bars while in Specimen #3 and #4 the lap splices are code-conforming.

Rigid end zones in the columns and beams were provided as per the provisions of ASCE/ISE 41-06 depending upon their configuration of either the joint satisfies weak column-strong beam condition or vice versa. Beam lengths are defined from centreline to centreline of the adjacent columns. Shear deformations at the beam-column connection regions are neglected in the fibre frame models.

Dynamic properties of the specimens were modelled as lumped masses at the nodes with Rayleigh damping assumed for the time history analyses.

The *Static Pushover* analysis feature in OpenSees is used to analyze the frame for nonlinear static response to the ground motions whereas *Dynamic Ground-Motion* analysis feature in OpenSees is used to perform non-linear dynamic response analysis of the frames.

The resulting model contains 9 beam elements, 12 column elements, 16 nodes, and 48 degrees of freedom. Figure 4.1 presents an overview of the modelling strategy.

The OpenSees model completes one time history analysis in approximately 3 minutes on a standard personal laptop computer. Post-processing of the results were done by using MATLAB software and are fairly straight forward as the raw output files are in terms of curvatures, member forces and end displacements**.**

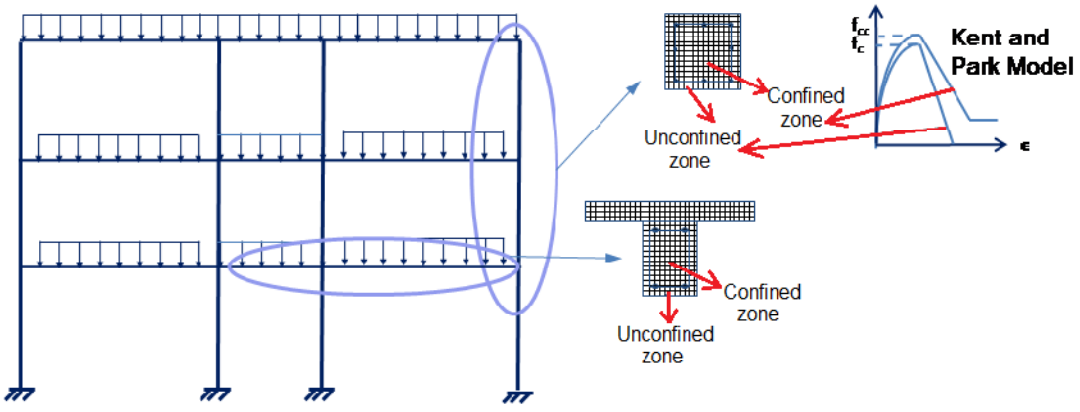

Figure 4.1: OpenSees model with force-based elements

4.3 Numerical Simulation and Model Calibration: Bare Frames [Specimen #1 and Specimen #3]

Following the development of the general numerical model for the bare frames as per the description made in the earlier section, the OpenSees model was later calibrated separately for Specimen #1 and #3 based on the observed behaviour during pseudo-dynamic test earlier detailed in Chapter-3.

4.3.1 Specimen #1 – Non-conforming Bare Frame

The following global assumptions were made in order to calibrate the Specimen #1 model time history output to match the experimental results:

- Storeys are modelled as rigid diaphragms;
- Column rigid offsets are set as zero, except for the exterior joints at the 1st and 2nd storey where the full dimension is defined;
- Beam rigid offsets are set as the full dimension, except for the exterior joints at the 1st and 2nd storey, where they are set as zero;
- Concrete strengths at each floor are defined separately based on concrete cylindrical strength test results given in Table 2.1;
- Longitudinal reinforcement steel behaviour are defined separately for beams and columns based on material strengths mentioned in Table 2.2;
- Steel strengths in columns are 90% of the nominal values determined from the material tests;
- The force-based beam and column elements have 5 Gauss-Lobatto integration points;
- P-Delta effects are considered in the column elements;
- Total load on the test specimen is applied as uniformly distributed load on the beams and calculated from the weight of steel blocks (which represents the live loads from slabs of prototype building, transverse beams and slab weight);
- Nodal masses for dynamic analyses were assigned with a factor of 1.0, representative of the physical pseudo-dynamic test; and
- The damping value is set at 2.50% for stability purposes (discussed later)

The results obtained from the analysis of the calibrated model of Specimen #1 are compared with the pseudo-dynamic results and comments are made on the accuracies obtained as well as the limitations in capabilities of the numerical model.

The initial fundamental period of Specimen #1 from OpenSees is 0.48 sec. The comparison of time histories for inter-storey drift ratio and storey shears are presented in Figures 4.2 and 4.3, respectively. Note that in Figure 4.2 the model results are unstable due to the collapse of the specimen after approximately 18.5 sec. and hence the limit of the drift plots is fixed at ±3 %.

It is evident from the plots that during ground motion D1, the model does not capture the peak drifts in all three storeys. Comparing the initial 1st mode period from experiment and model suggests that model is slightly more flexible than the physical specimen during D1 and thereby over-predicts the peak inter-storey drifts. During D2 1st storey residual drift is captured accurately however model couldn't predict the residuals accurately for 2nd and 3rd storeys while capturing some peaks better. During D3, the residuals and peak drift values are over-predicted for 1st storey while under-predicted for 2nd and 3rd storeys.

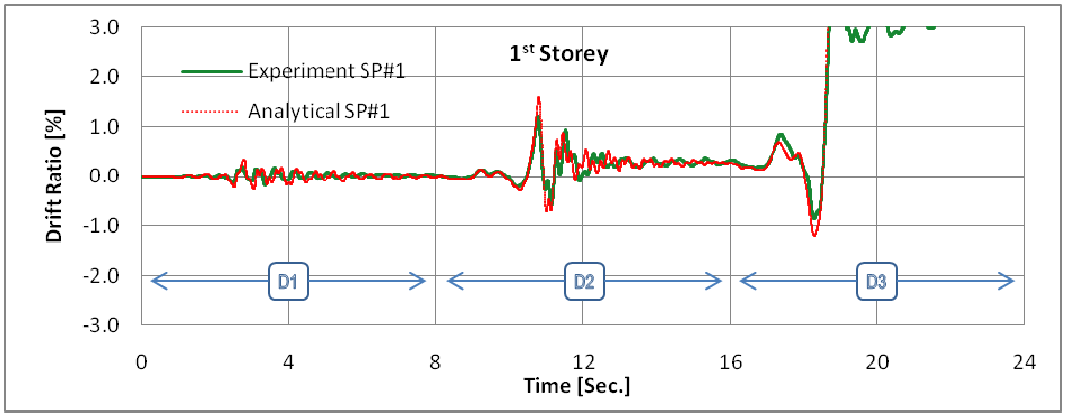

Figure 4.2(a): Comparison of first storey drift time-history (SP#1)

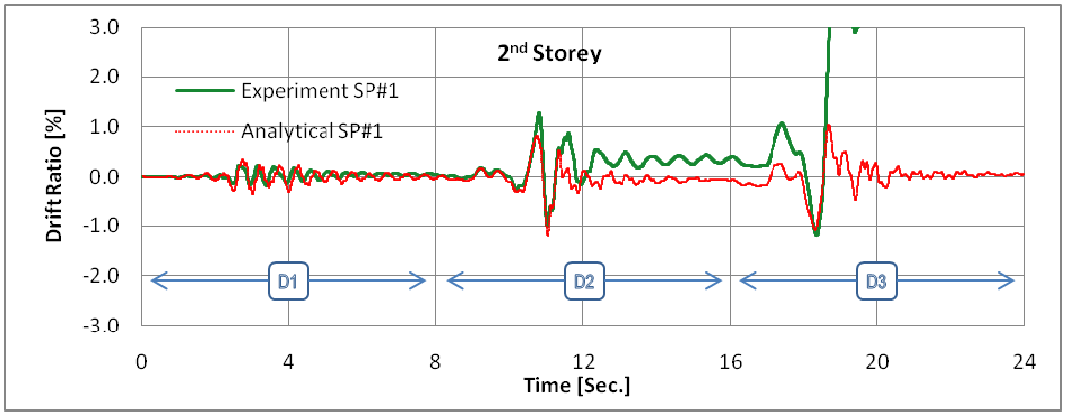

Figure 4.2(b): Comparison of second storey drift time-history (SP#1)

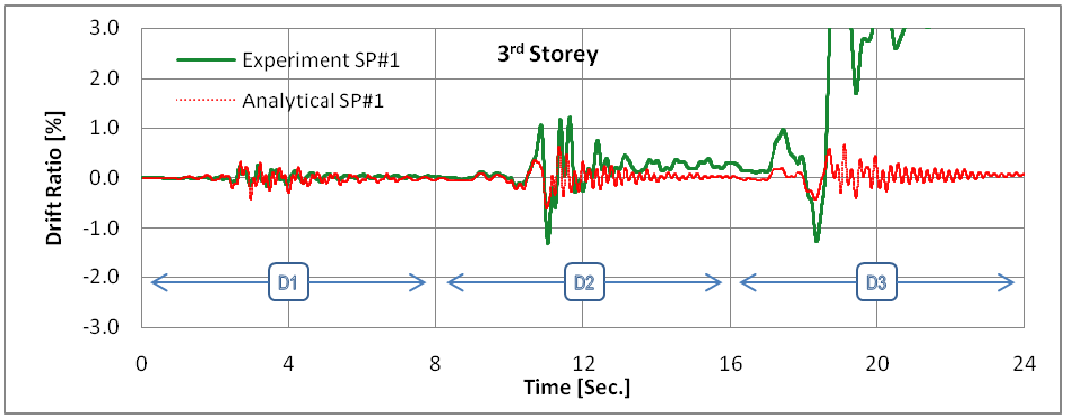

Figure 4.2(c): Comparison of third storey drift time-history (SP#1)

In order to quantitatively evaluate the accuracy of models, maximum inter-storey drift and storey shear responses are compared with experiment as these responses capture the higher mode effects better. Tables 4.1 and 4.2 give the error percentages of the peak inter-storey drifts and storey shears, respectively.

It is important to note that the model does not capture the residual and peak drifts accurately during D3. The drift plots in Figure 4.2 indicate that after approximately 18.5 seconds, the model predicts sudden increase in the drifts of the 1st storey. This implies that the model predicts significant damages which are only concentrated at the 1st storey, leading to a soft-storey mechanism, which was not observed during the experiment. The specimen showed signs of damage distributed from base to top,

mainly flexure failure of the 1st and 3rd storey columns without any warning, which is referred in this text as brittle flexure-failure. Due to this reason, the values after 18.5 seconds are discarded in the comparison of peak responses during D3 as the system indicates instability rendering the values unreliable.

An arbitrary damping value of 2.50% was selected as a value which allows the analysis to run until the very end of D3 ground motion. The damping value was not found to significantly affect the peak results during ground motions.

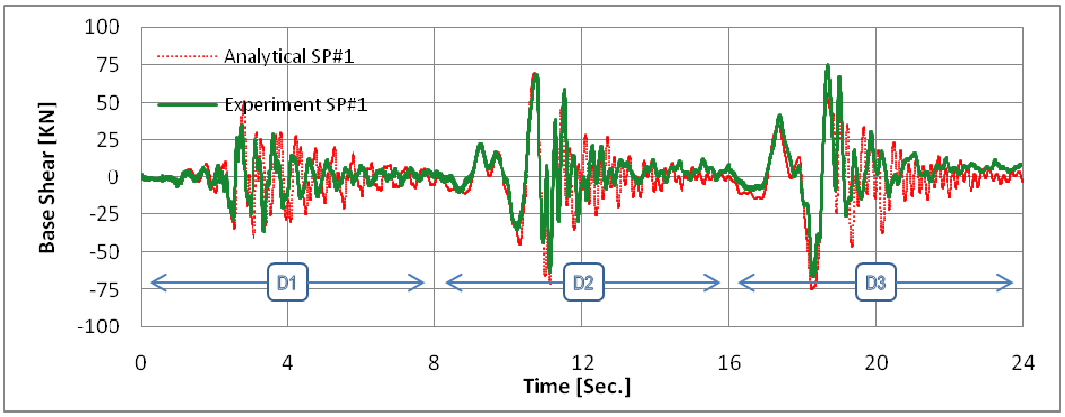

Figure 4.3 (a): Comparison of base shear time-history (SP#1)

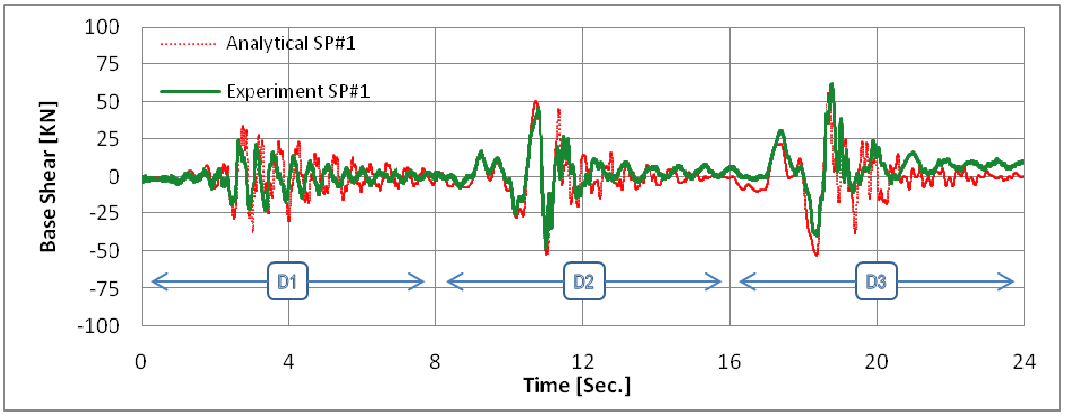

Figure 4.3 (b): Comparison of second storey shear time-history (SP#1)

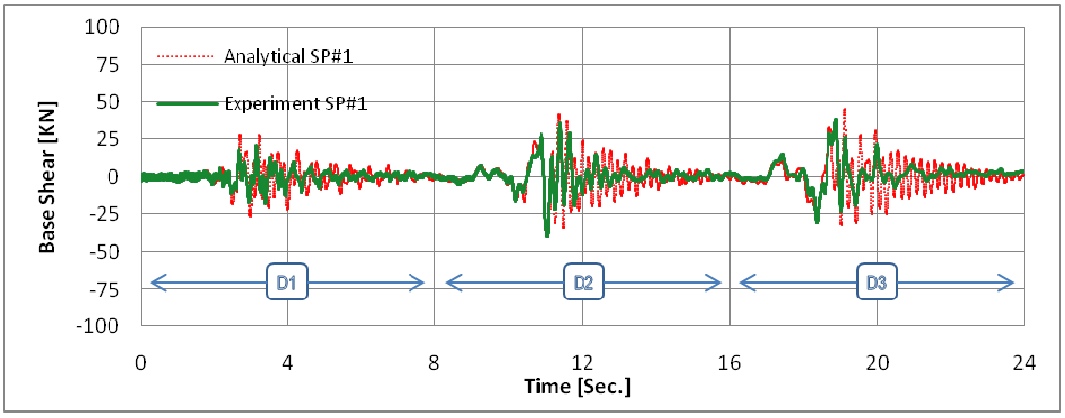

Figure 4.3 (c): Comparison of third storey shear time-history (SP#1)

Initially the model appears to be more flexible than the actual specimen hence causing over-prediction of drifts during D1 as described earlier. During ground motion D2, the drift plots indicate the signs of a soft-storey mechanism in the model, which became more prominent during D3, with over-prediction of drifts in the first storey while under-prediction in the second and third storeys, which is contrary to the experimental results. However, the error during D2 is considerably less than that of D3 because of the damage concentration and storey-mechanism in the 1st storey of the model.

The experimental observation indicates that joint regions in all three storeys of test specimen suffer shear cracking during D2 which later leads to severe damage during D3. In addition, no column mechanism usually associated with strong-beam weak column system was observed. This joint flexibility could have been a major cause of uniform drift observed in the test frame (Figure 2.9) since drift capacities are greatly influenced by the joint flexibility which in-turn is a function of the amount of transverse reinforcement, concrete strength, confinement of joint by members in all directions, shear stresses and axial loads. Thus the inability of numerical model to accurately simulate the inter-storey drifts in the 2nd and 3rd storeys could mainly be attributed to the fact that the model lacks detailed non-linear joint elements at joints other than the fixed base nodes to accurately capture rotations. Use of reduced section properties and reduced material strengths in joint end-offsets to better simulate joint flexibility and drift responses does not prove efficient. For this purpose, a more detailed non-linear spring element for joint regions could be utilized to capture the damage and deformation pattern actually observed in the tests.

Table 4.1: Peak inter-storey drift error (SP#1)

Storey	Ground Motion	Maximum Inter-Storey Drift [%]		Error [%] *
		Experiment	OpenSees	
1st	D1	0.20	0.36	+ 80.0
1st	D2	1.20	1.61	+ 34.2
1st	D3	0.86	1.19	+ 38.4
2nd	D1	0.23	0.35	+ 52.2
2nd	D2	1.28	1.21	- 5.46
2nd	D3	1.19	1.09	- 8.40
3rd	D1	0.26	0.43	+ 65.4
3rd	D2	1.20	0.62	- 48.3
3rd	D3	1.27	0.44	- 65.3

* Positive: Over-prediction, Negative: Under-prediction

Table 4.2: Peak storey-shear error (SP#1)

Storey	Ground Motion	Maximum Storey Shear [*kN*]		Error [%] *
		Experiment	OpenSees	
1st	D1	36.5	51.2	+ 40.3
1st	D2	68.5	70.8	+ 3.36
1st	D3	66.6	74.6	+ 12.0
2nd	D1	26.1	37.5	+ 43.7
2nd	D2	47.9	51.3	+ 7.09
2nd	D3	38.2	55.3	+ 44.8
3rd	D1	18.8	27.9	+ 48.4
3rd	D2	41.3	41.5	+ 0.48
3rd	D3	31.3	27.1	+ 13.4

* Positive: Over-prediction, Negative: Under-prediction

Another important factor influencing the predictions of drift responses is the effect of deficiencies present in the system. The material models listed in the software programs were developed for good quality materials with reliable mechanical properties and are unable to properly simulate the

accumulated effect of deficiencies manipulating the drift capacities as well as damage re-distribution in the upper storeys. Using reduced material strengths in order to predict the accurate behaviour seems to have little impact. The model is not capable to simulate degradation and damage during seismic loading.

The maximum storey shears are also over-predicted in the model during D1 which may be associated to inability of the model to capture micro-cracking in members during low ground shaking. The maximum error in predicting the storey shears during D2 is within 15 % indicating that results are most reliable during this ground motion. During D3, until 18.5 seconds, the results are also reliable except for the 2nd storey during D3 with greater error due to a downward shift in storey shear time history plot. The over-prediction of model values suggests that complete yielding of steel has not occurred during pseudo-dynamic tests.

In general, the unreliability of results during D1 ground motion does not influence the course of this study as the observed damage state is minimum and accompanied with completely elastic response. Therefore, performance of specimens will not be evaluated for D1. During D2, the results are most reliable to be compared for performance evaluation. During D3, until 18.5 seconds, the results are accurate for 1st storey only.

Non-linear static pushover analysis was also performed by using the calibrated OpenSees model of Specimen #1. The pushover load-pattern is applied using the first mode response. The target displacement, used in the performance evaluation discussed in the forthcoming chapter, is obtained using the response spectrum of ground motions D2 and D3 shown in Figure 2.5. Figure 4.4 presents the capacity curve super-imposed on experimental base-shear vs. roof displacement plot. It is worth noticing that pushover analysis results in slightly reduced capacity prediction than what is observed in the experimental time-history results, which is consistent with the general acceptance that due to its simplicity and ease-of-use, pushover analysis yields conservative results. The initial slope of capacity curve is similar to the slope of the base-shear vs. roof displacement plot during D2, however due to the severe damages in the specimen after peak during D3 at approximately 18.5 seconds, significant stiffness degradation and softening is observed in the specimen as evident from the plot.

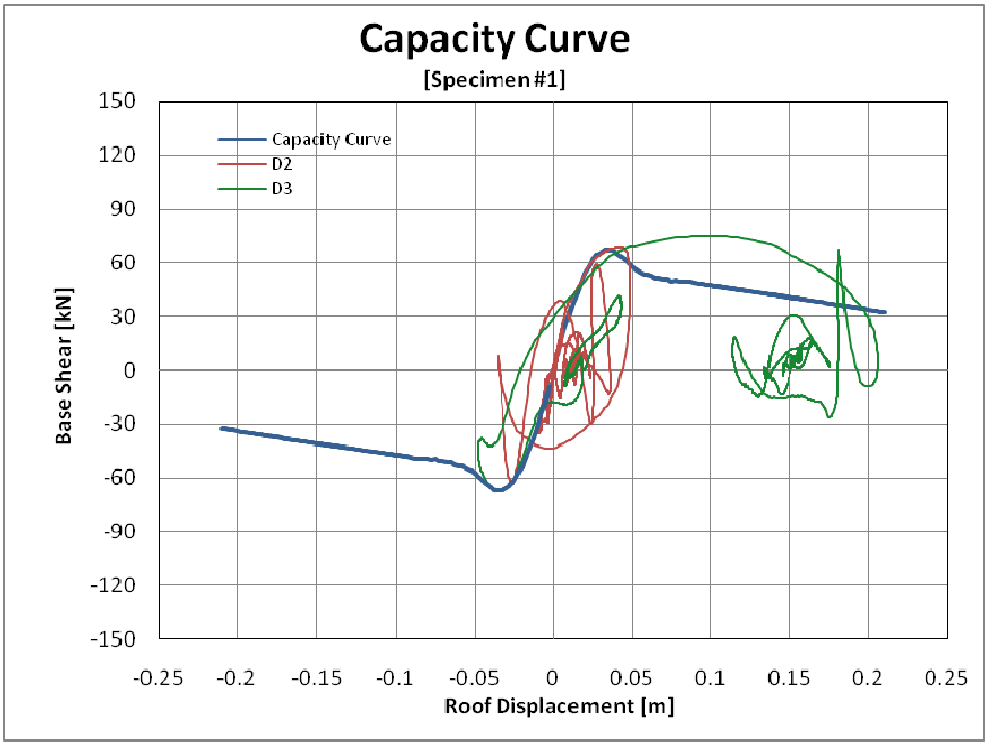

Figure 4.4: Specimen #1 capacity curve and base-shear vs. roof displacement response

4.3.2 Specimen #3 – Code-conforming Bare Frame

The following global assumptions were made in order to calibrate the model time history output to match the experimental results:

- Storeys are modelled as rigid diaphragms;
- Rigid Joint offsets for column and beams at all joints are set to zero;
- Longitudinal reinforcement steel behaviour for beams and columns are defined with steel strength set to 90 % of the nominal values determined from the material tests;
- Concrete strengths at each floor are defined separately based on concrete cylindrical strength test results;
- The force-based beam and column elements have 5 Gauss-Lobatto integration points;
- P-Delta effects are considered in the column elements;
- Total load on the test specimen is applied as uniformly distributed load on the beams and calculated from the weight of steel blocks (which represents the live loads from slabs of prototype building, transverse beams and slab weight);
- Nodal masses for dynamic analyses were assigned with load factor of 1.0, representative of the physical pseudo-dynamic test; and
- The damping value is set at 2.0% for stability purposes.

Similar to Specimen #1, the results obtained from the analysis of the calibrated model of Specimen #3 are also compared with the corresponding pseudo-dynamic test results and comments are made on the accuracies obtained as well as the limitations in capabilities of the numerical model.

The initial fundamental period of Specimen #3 from OpenSees is 0.39 sec. The comparison of time histories for inter-storey drift ratio and storey shears are presented in Figures 4.5 and 4.6, respectively.

It is evident from the plots that during ground motion D1, the model does not capture the peak drifts in all three storeys. Comparison of initial 1st mode period from experiment and model confirms that model is more flexible during D1, thus causing an over-prediction of drifts in all three storeys. Quantitative comparison of peak values, shown in Table 3.3, also suggests the same. However, as discussed earlier, the ground motion intensity for D1 is not significant enough to cause any non-linearity in the dynamic behaviour as no damages were reported during test; therefore the results of ground motion D1 will not be used for performance evaluation later discussed in the forthcoming chapter.

During D2 ground motion, the error in peak inter-storey drifts for all three storeys is less than 15%. In addition, it is important to note that experimental results indicate greater drift in 2nd storey compared to other storeys. The model is also able to capture similar response with acceptable accuracy.

During D3, the drift of 1st storey is captured fairly well, although with slight under-prediction, but the drifts of 2nd and 3rd storeys are significantly under-predicted with successively increasing error.

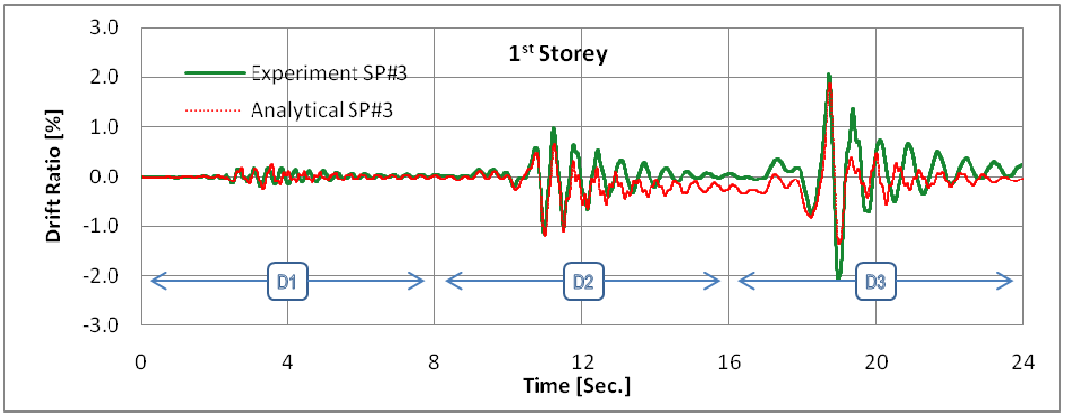

Figure 4.5(a): Comparison of first storey drift time-history (SP#3)

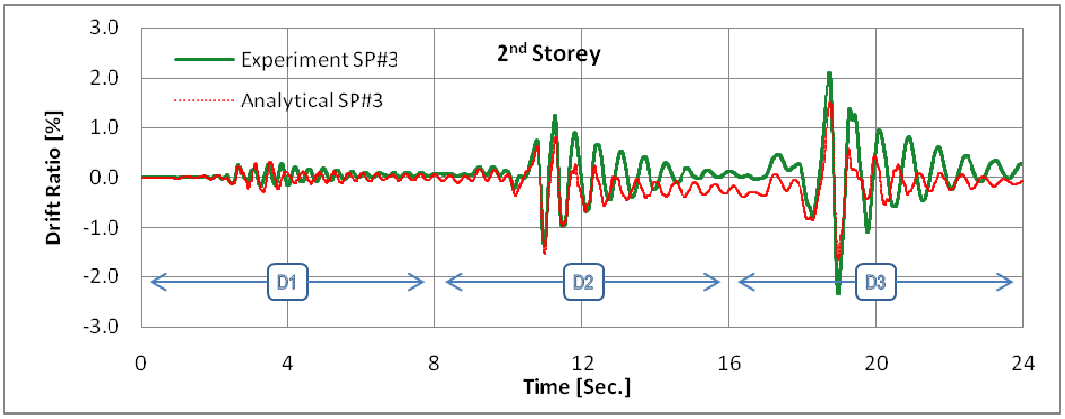

Figure 4.5(b): Comparison of second storey drift time-history (SP#3)

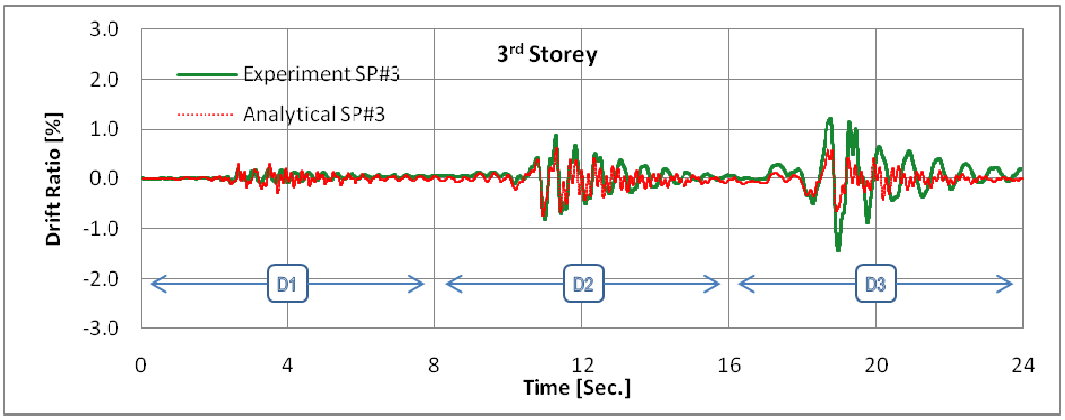

Figure 4.5(c): Comparison of third storey drift time-history (SP#3)

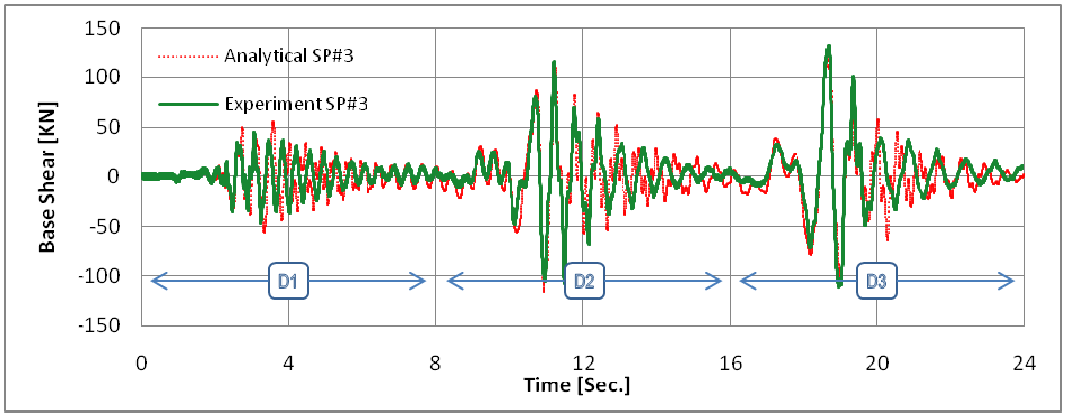

Figure 4.6(a): Comparison of base shear time-history (SP#3)

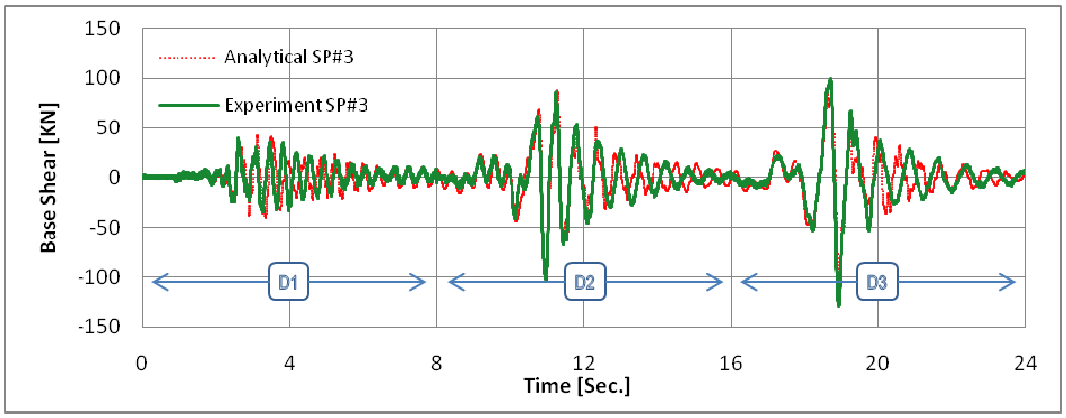

Figure 4.6(b): Comparison of second storey shear time-history (SP#3)

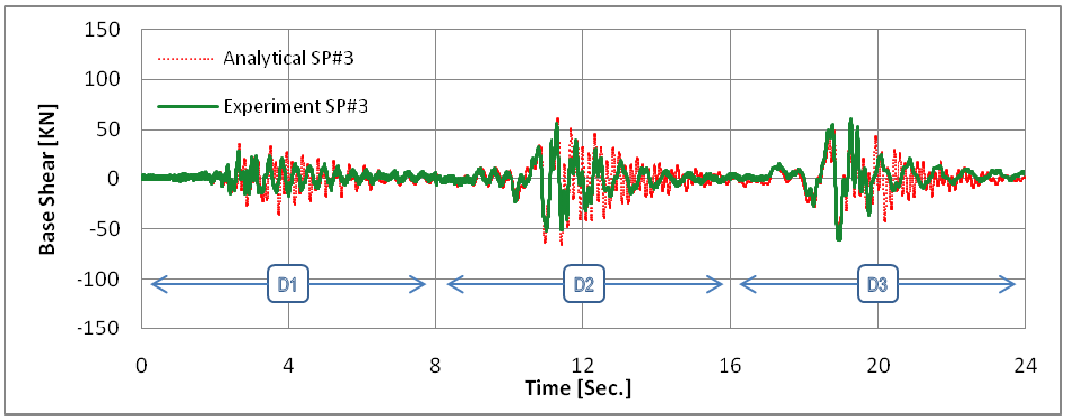

Figure 4.6(c): Comparison of third storey shear time-history (SP#3)

Storey shear response errors are shown in Table 4.4. During D1, the model predicts the storey shear with tolerable error for 1st and 2nd storey, however, over-predicts for the 3rd storey. During D2 and D3, the error percentages are mostly within 10% indicating that reduction in nominal strength of material in the model to better capture the strength response worked satisfactorily.

Table 4.3: Peak inter-storey drift error (SP#3)

Storey	Ground Motion	Maximum Inter-Storey Drift [%]		Error [%] *
		Experiment	OpenSees	
1st	D1	0.19	0.24	+ 26.3
1st	D2	1.16	1.20	+ 3.4
1st	D3	2.03	1.87	- 7.9
2nd	D1	0.27	0.32	+ 18.5
2nd	D2	1.38	1.51	+ 9.4
2nd	D3	2.34	1.62	- 30.7
3rd	D1	0.19	0.29	+ 52.6
3rd	D2	0.87	0.76	- 14.8
3rd	D3	1.44	0.66	- 54.2

* Positive: Over-prediction, Negative: Under-prediction

Table 4.4: Peak storey shear error (SP#3)

Storey	Ground Motion	Maximum Storey Shear [*kN*]		Error [%] *
		Experiment	OpenSees	
1st	D1	46.9	53.6	+ 14.2
1st	D2	115.2	113.4	- 1.6
1st	D3	131.6	126.0	- 4.3
2nd	D1	39.8	42.4	+ 6.5
2nd	D2	101.6	103.4	+ 1.8
2nd	D3	126.6	107.9	- 14.8
3rd	D1	27.7	35.9	+ 29.6
3rd	D2	56.2	61.4	+ 9.3
3rd	D3	61.3	55.4	- 9.6

* Positive: Over-prediction, Negative: Under-prediction

It should be noted that Specimen #3 is a code conforming specimen with strong-column weak-beam configuration. However, experimental observations presented earlier suggest that 1st and 2nd storey joint regions suffer shear cracking during D2 and D3 and the flexural cracking was equally observed during the test both in beams as well as in columns, without any formation of beam mechanism usually associated with strong-column weak-beam system. Therefore, similar to the Specimen #1, the joint flexibility can be deemed responsible for the observed uniform drift at 1st and 2nd storeys. The use of zero joint offsets in the model in hope to achieve joint flexibility did not prove helpful in reducing the error of under-prediction of drifts during D3. Thus, the inability of numerical model to accurately simulate the inter-storey drifts in the 2nd and 3rd storeys could mainly be attributed to lack of detailed non-linear spring element in joint regions to capture the deformation and damage pattern.

Comparison of error estimates between numerical models of Specimen #1 and Specimen #3 indicate significant improvement in capturing drift and storey forces in the model of Specimen #3. This gives an overall confidence on the hypothesis earlier made that complexity in capturing degradation and damages, associated with deficiencies due to sub-standard construction as well as modelling low quality material, are too high to be captured properly by the model. It is one of the important reasons that response of code-conforming specimen is better predicted.

Non-linear static pushover analysis was also performed using the calibrated OpenSees model of Specimen #3. Figure 4.7 presents the Capacity curve super-imposed on experimental base-shear vs. roof displacement plot. Similar to Specimen #1, the capacity curve from pushover analysis predicts lesser capacity compared to the experimental observation. The initial slope of capacity curve is similar to the slope of base-shear vs. roof displacement plot during both D2 and D3, indicating that pushover analysis has captured the behaviour accurately since it is a first mode dominant structure.

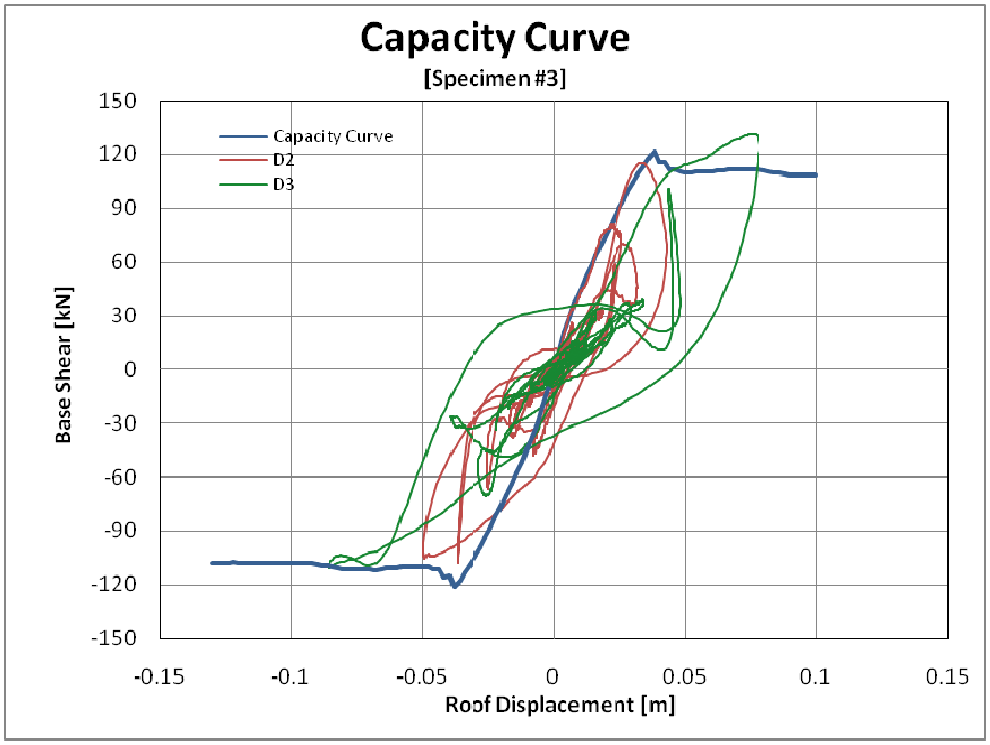

Figure 4.7: Specimen #3 capacity curve and base-shear vs. roof displacement response

4.4 Numerical Simulation and Model Calibration: Infilled Frames [Specimen #2 and Specimen #4]

Following the development of numerical models for non-conforming and code-conforming bare frame specimens, their respective infilled counterparts will be simulated by using the same model but with addition of compression struts in the middle bay of the frames in order to simulate the infill panels. The comparison of numerical models and respective experiments in terms of global responses is conducted later, followed by the error analysis.

4.4.1 Modelling of Autoclave Aerated Concrete Masonry Infill Panels

Equivalent strut methodology, earlier discussed in the literature, is used to model the AAC infill panels in the infilled RC frame models of bare frames earlier developed. It is already known that the strength and stiffness properties plays vital role in the performance of equivalent strut method. The following section presents the necessary description of the modelling of AAC masonry infill modelling.

4.4.1.1 Width of Equivalent Compression Strut

With regards to strength, compression tests on masonry prisms are conducted to investigate the mechanical properties as earlier presented in Chapter-2. In terms of stiffness, the width of equivalent compression strut b_{inf} is estimated by using the provisions of ASCE-41/06 section 7.4 given below in Equation 4.1. It is based on the characteristic parameter λ (Equation 4.2) first proposed by Stafford Smith. Similar formulation is also adopted in TEC 2007 Annex-7F for strengthened masonry panels.

$$b_{inf} = 0.175\left(\lambda\, h_{inf}\right)^{-0.4} d_{inf} \tag{4.1}$$

where;

b_{inf} = Width of equivalent compression strut
λ = Characteristic parameter calculated as;

$$\lambda = \left[\frac{E_{inf}\, t_{inf} \sin 2\theta}{4\, E_{fr} I_{col} h_{inf}}\right]^{0.25} \tag{4.2}$$

h_{inf}	=	Height of infill panel	=	1325	*mm*
t_{inf}	=	Thickness of infill	=	150	*mm*
d_{inf}	=	Diagonal length of infill panel	=	2039	*mm*
θ	=	Inclination from horizontal to d_{inf}	=	0.707	*rad.*
I_{col}	=	Inertia of bounding column	=	$1x10^8$	mm^4
E_{fr}	=	Modulus of elasticity of frame $[4780 \times \sqrt{\sigma_{c\,fr}}]$ *ACI 318-08*			
	-	Specimen #2	=	18289	*MPa*
	-	Specimen #4	=	25066	*MPa*
σ_{cfr}	=	Concrete compressive strength of frame			
E_{inf}	=	Modulus of elasticity of infill [from prism test]	=	1182	*MPa*

Substituting the above values yields;

λ	=	Characteristic Parameter SP #2	=	0.00206	*mm*
λ	=	Characteristic Parameter SP #4	=	0.00191	*mm*
b_{inf}	=	Width of Equivalent Strut SP #2	=	227	*mm*
b_{inf}	=	Width of Equivalent Strut SP #4	=	234	*mm*

The average width of strut $b_{inf} = 230$ *mm* is used and thickness of strut is taken equal to the thickness of infill panel in the numerical models.

4.4.1.2 Material Model

Another important factor is the assignment of force-deformation (F-D) relationship for the masonry compression strut. Several relations are proposed in the literature, however, in this study; three material models are presented to represent the F-D relation of AAC masonry equivalent compression strut in the OpenSees models. The time history analysis results from the numerical model of both infilled frames using each of the three material models for equivalent strut are then compared with experimental results and errors are evaluated. The selected model is later used for performance evaluation using pushover analysis. A necessary description of each material model is given below.

First of these models utilizes the concrete material representation with zero tensile strength using the *1D-Concrete material* command in the OpenSees, hereinafter denoted as "***1D-Concrete***". The initial slope for this material model is $2 \times {}^{\sigma_{c\,inf}}/_{\varepsilon_{c\,inf}}$. The crushing strength of infill is assumed equal to 0.2 *MPa* for solution-convergence purpose. Strain at the crushing limit is calculated from the experimental observation of drift responses presented in Chapter-3. The drift at which the crushing of panel occurs is approximately equal to Δ_f = 0.8% as given in Table-3.6. From this observation, the strain at the crushing of infill panel is calculated using the Equation 4.3, shown below.

$$\varepsilon_{cr\,inf} = \left(\frac{\Delta_f \times h_{inf}}{100}\right) \times \frac{\cos\theta}{d_{inf}} \tag{4.3}$$

Figure 4.8 presents the "*1D-Concrete*" material model with input parameters involved are given below:

σ_{cinf}	=	Compressive strength of infill	=	2.6	*MPa*	(from prism test, Figure 2.24)
ε_{cinf}	=	Strain at maximum stress	=	0.0022		(from prism test, Figure 2.24)
σ_{crinf}	=	Crushing stress of infill	=	0.2	*MPa*	(assumed)
ε_{crinf}	=	Strain at crushing stress	=	0.0039		(from Equation-4.3)

Second one of these material models is developed using one of the several F-D relationships already present in the literature and hereinafter referred as "***Literature***". Assuming the diagonal compression failure, also observed in the experiments, the ultimate shear force V_u in the compression strut can be given by Equation-4.4 as suggested by Stafford Smith.

$$V_u = b_{inf} t_{inf} \sigma_{c\,inf} \cos\theta = 68.2\ kN \tag{4.4}$$

The displacement S_u at maximum force is given by Equation-4.5, proposed by Madan et al (1997).

$$S_u = \varepsilon_{c\,inf} \times \frac{d_{inf}}{\cos\theta} = 5.9\ mm \tag{4.5}$$

It is worth noticing here that, the drift observed in Specimens #2 and #4 during experiments at the cracking of infill panel Δ_{cr} is approximately 0.5 %, which gives the maximum displacement in the infill $= \Delta_{cr} \times h_{inf}/100 = 6.6\ mm$ which is quite close to the value of S_u obtained from Equation-4.5.
The initial stiffness can now be obtained from Equation 4.6 as follows;

$$k_1 = 2 \times \frac{V_u}{S_u} = 23119\ kN/m \tag{4.6}$$

Using the post yield stiffness co-efficient α = 0.2, the shear force at yield can be calculated as follows;

$$V_y = \frac{V_u - \alpha k_1 S_u}{1 - \alpha} = 51.2\ kN \tag{4.7}$$

The displacement at yield can be given by $S_y = V_y/k_1 = 2.2\ mm$. Assuming the residual shear force V_r equal to 0.1 x V_y and the displacement S_r = 3 x S_u, we have V_r = 5.12 *kN* and S_r = 17.7 *mm*. The F-D relationship is converted to stress-strain using geometric and cross-section properties of equivalent strut obtained earlier and plotted also in Figure 4.8 with the parameter values given below;

σ_{cyinf}	=	Yield stress	=	2.0	*MPa*
ε_{cyinf}	=	Yield strain	=	0.00083	
σ_{cuinf}	=	Ultimate strength	=	2.6	*MPa*

ε_{cuinf}	=	Ultimate strain	=	0.0022	
σ_{crinf}	=	Residual stress	=	0.2	*MPa*
ε_{crinf}	=	Residual strain	=	0.006	

The "*hysteretic material"* command in OpenSees is used with above mentioned compressive stress-strain values while negligible values are used for tension regime.

The third material model, proposed in this study, utilizes the stress-strain curve obtained from the compression test of prisms shown in Figure2.24. It is evident from the tests that AAC infill material depicts a brittle response without a definite yield point and definite post-yield stiffness degradation, unlike the above mentioned material models predicts. Therefore, in view of this observation, the material model, hereinafter referred as "***Calibrated***", is developed by calibrating the stress-strain curve of masonry prism such that the initial slope is equal to secant modulus of elasticity of AAC infill material as shown in Figure4.8. The post-failure stiffness is found negligible in the tests, however; minimum value is used in the model to achieve solution convergence. The "*hysteretic material"* command in OpenSees is used with compressive stress-strain values mentioned below while negligible values are used for the tension regime.

σ_{cuinf}	=	Ultimate strength	=	2.6	*MPa*
ε_{cuinf}	=	Ultimate strain	=	0.0022	
σ_{crinf}	=	Residual stress	=	0.2	*MPa*
ε_{crinf}	=	Residual strain	=	0.0023	

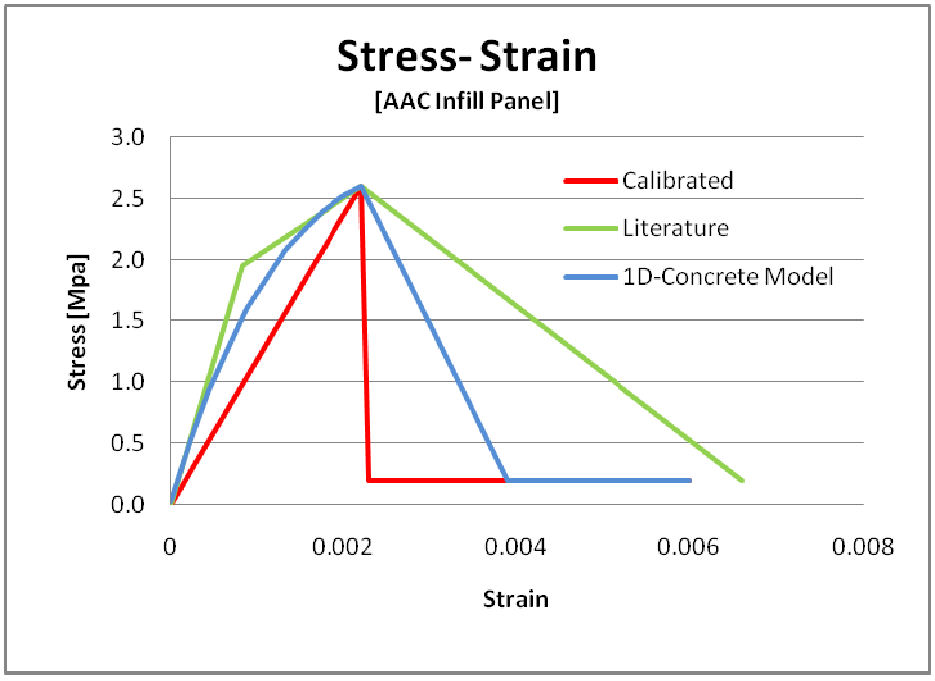

Figure 4.8: Material models for equivalent compression strut

4.4.1.3 Modelling of Strut Members

The definition of strut cross-section and its material model is followed by implementing the strut elements into the numerical models. The equivalent struts are modelled with diagonal axial force member using “truss” element in the OpenSees model. Two truss elements are connected node to node in the middle bay at each floor to represent the AAC infill panel with concentric struts active in each direction. Similar methodology is used for both infilled frames.

In the forthcoming sections, the analysis results for the infilled frame specimens are presented in separate sections and compared with the experimental results. Three numerical models of each infilled frame specimen are prepared with the only difference between the three is the material model used to represent equivalent compression strut.

4.4.2 Specimen #2 – Non-conforming Infilled Frame

The results obtained from the analysis of the calibrated model of Specimen #2, which is developed using the model of Specimen #1 after modelling infills, are compared with the pseudo-dynamic results and comments are made on the accuracies obtained as well as the limitations in capabilities of the numerical model. Comparative analysis is also performed among the three material models used for masonry infill equivalent strut.

The initial fundamental period of Specimen #2 obtained from OpenSees using *Calibrated*, *1D-Concrete* and *Literature* material models are 0.29 seconds, 0.24 seconds and 0.24 seconds respectively. The comparison of time histories for inter-storey drift ratio and storey shears are presented in Figures 4.9 and 4.10, respectively.

It is evident from the inter-storey drift plots that overall the model captures the response for first storey accurately however under-prediction of responses increase in the 2^{nd} and 3^{rd} storeys. The quantitative evaluation of the accuracy of model predictions in terms of peak inter-storey drifts and peak storey shears is shown in Table 4.5 and 4.6 respectively. It can be noted that during D1, the *Calibrated* material model over-predicts the storey drifts in all three storeys while *1D-Concrete* and *Literature* material models predict the drifts accurately. The over-prediction of drifts in *Calibrated* model can be attributed to the fact that this model has much reduced initial stiffness of equivalent struts than the other two models. However, the results of ground motion D1 are insignificant as no observed damage was recorded in any member during the test and the specimen behaviour was nearly elastic.

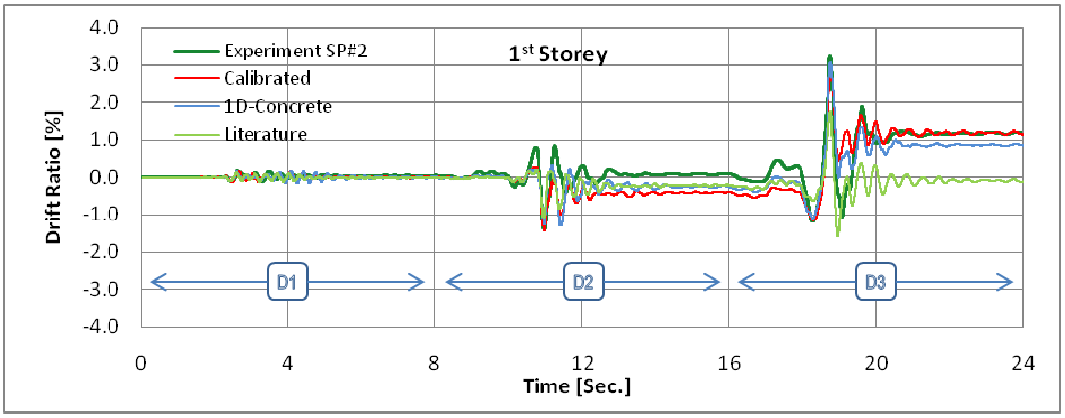

Figure 4.9 (a): Comparison of first storey drift time-history (SP#2)

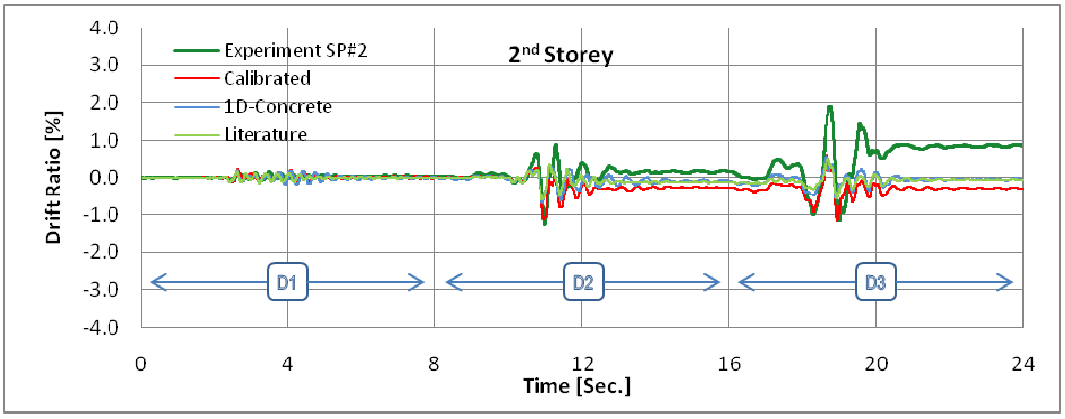

Figure 4.9 (b): Comparison of second storey drift time-history (SP#2)

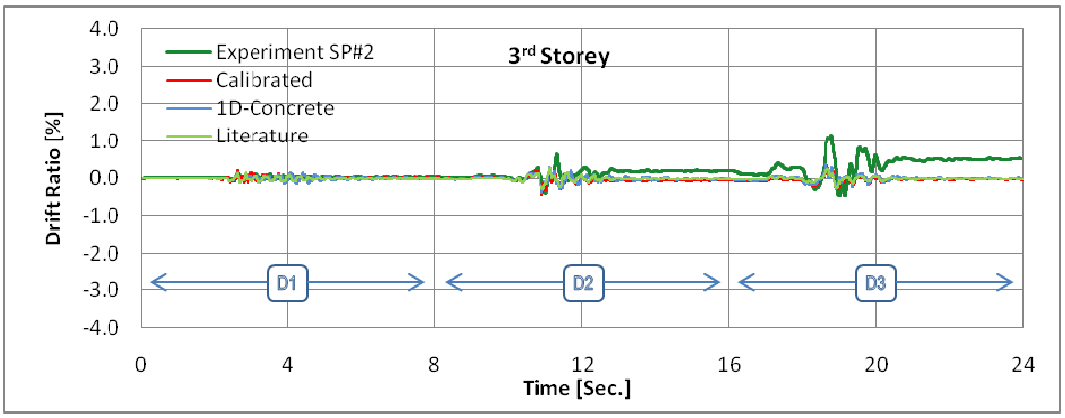

Figure 4.9 (c): Comparison of third storey drift time-history (SP#2)

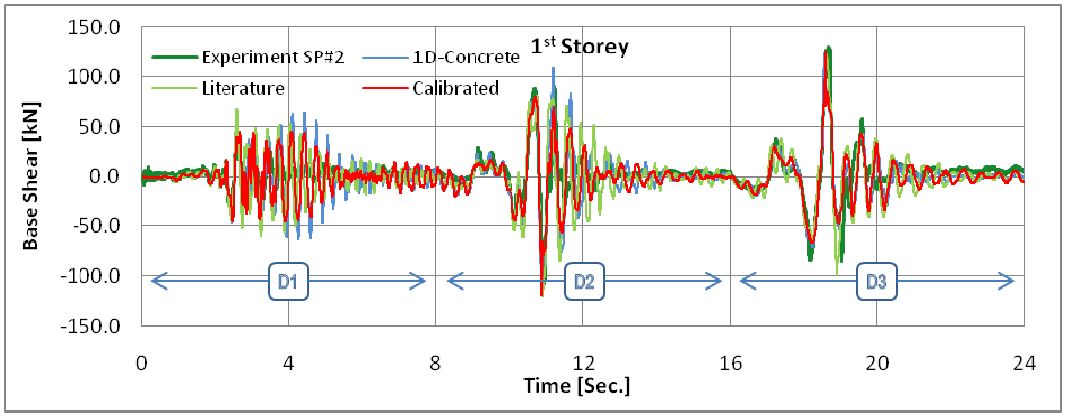

Figure 4.10 (a): Comparison of first storey shear time-history (SP#2)

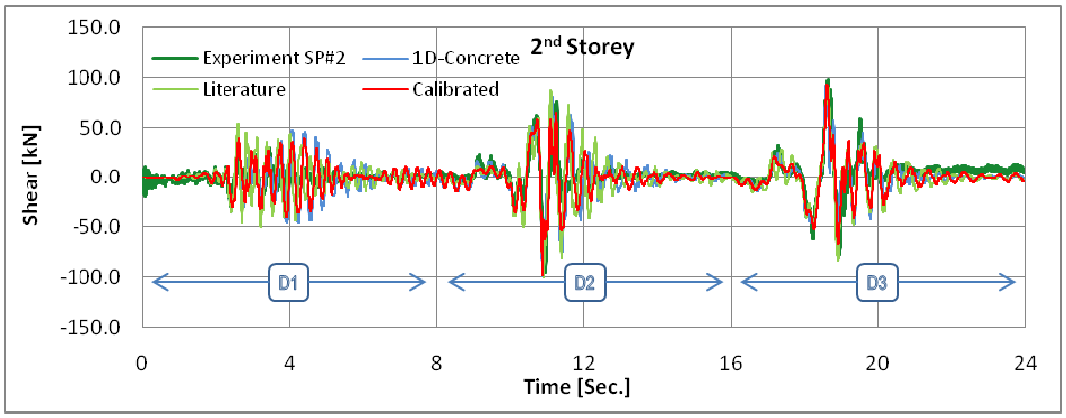

Figure 4.10 (b): Comparison of second storey shear time-history (SP#2)

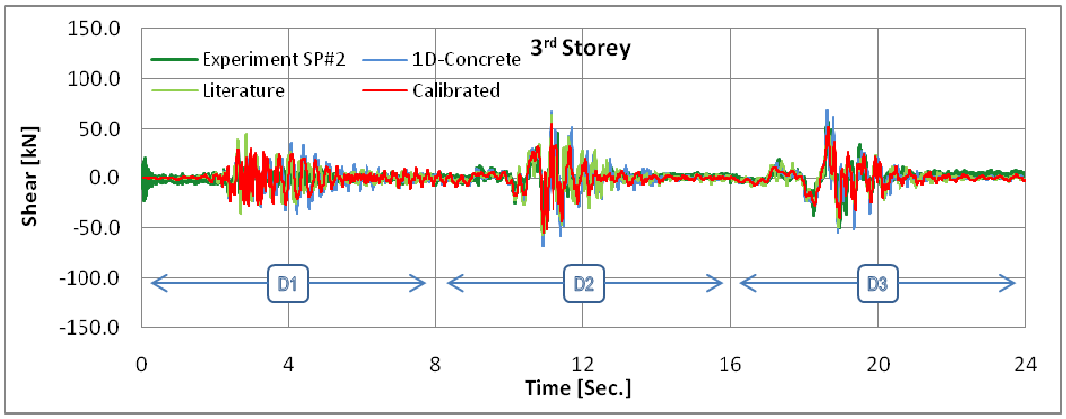

Figure 4.10 (c): Comparison of third storey shear time-history (SP#2)

During ground motion D2, the *Calibrated* material model predicts the drifts in the 1st and 2nd storeys accurately with much lesser error percentages as compared to other two models. The drift for the 3rd storey is under-predicted in all models though with the *Calibrated* model, prediction is better than the other two.

Table 4.5: Peak inter-storey drift error (SP#2)

Storey	Ground Motion	Maximum Inter-Storey Drift [%]				Error [%] *		
		Experiment	OpenSees					
			Calibrated (a)	1D-Concrete (b)	Literature (c)	(a)	(b)	(c)
1st	D1	0.18	0.175	0.17	0.15	- 2.8	- 7.8	- 15.6
1st	D2	1.41	1.43	1.29	1.09	+ 1.6	- 8.4	- 22.9
1st	D3	3.22	3.11	3.04	1.74	- 3.4	- 5.6	- 46.1
2nd	D1	0.17	0.24	0.19	0.17	+ 42.4	+ 16.2	+ 0.04
2nd	D2	1.26	1.14	0.69	0.61	- 9.3	- 45.3	- 51.6
2nd	D3	1.89	1.17	0.56	0.55	- 38.5	- 70.3	- 70.9
3rd	D1	0.12	0.21	0.15	0.14	+ 78.2	+ 29.5	+ 21.9
3rd	D2	0.65	0.44	0.37	0.28	- 32.2	- 43.5	- 57.4
3rd	D3	1.14	0.39	0.36	0.27	- 65.7	- 67.9	- 76.4

* Positive = Over-prediction, Negative = Under-prediction

Table 4.6: Peak storey shear error (SP#2)

Storey	Ground Motion	Maximum Storey Shear [*kN*]				Error [%] *		
		Experiment	OpenSees					
			Calibrated (a)	1D-Concrete (b)	Literature (c)	(a)	(b)	(c)
1st	D1	41.4	45.9	64.1	66.9	+ 10.9	+ 54.7	+ 61.7
1st	D2	107.1	119.2	117.3	119.7	+ 11.3	+ 9.6	+ 11.8
1st	D3	130.4	125.1	124.3	122.1	- 4.1	- 4.6	- 6.3
2nd	D1	30.9	40.3	53.3	53.4	+ 30.1	+ 72.3	+ 72.6
2nd	D2	95.5	97.4	99.6	100.6	+ 2.1	+ 4.3	+ 5.3
2nd	D3	97.9	92.4	91.8	89.5	- 5.6	- 6.2	- 8.5
3rd	D1	27.7	30.1	36.9	44.1	+ 8.3	+ 33.2	+ 62.1
3rd	D2	45.7	52.6	67.7	63.4	+ 15.0	+ 48.1	+ 38.7
3rd	D3	58.6	51.9	68.8	48.6	- 11.3	+ 17.5	- 17.0

* Positive = Over-prediction, Negative = Under-prediction

During ground motion D3, until approximately 18.5 seconds (Figure-4.9), the *Calibrated* material model captures the drift response at several peaks quite accurately, however, after that instant the results differ considerably for higher storeys, probably due to the brittle failure of columns at 1st storey. Table 4.5 also indicates that the peak drift for 1st storey is predicted accurately while for 2nd and 3rd storeys the drifts are successively under-predicted. This indicates that models for specimen #2 are predicting first storey mechanism in D3 which was not observed explicitly in the experiments.

This is the similar behaviour as observed in the results of Specimen #1 models, which again can be attributed to the similar reasons that the model is unable to capture damage distribution in a deficient specimen with sub-standard concrete material and plain reinforcing bars. In-addition, the inability of model to simulate joint flexibility observed in the experiment due to diagonal cracking in the joints is another cause of increasing errors in the upper storeys.

The maximum storey shear response errors shown in Table-4.6 indicate that *Calibrated* model captures the peak storey shears in all three ground motion with acceptable accuracies within 15 % errors as compared to other two models, except in the case of D1 in the 2nd storey where the error is high probably because of the inability to capture micro-cracks.

Non-linear static pushover analysis was also performed using *Calibrated* and *1D-concrete* OpenSees models of Specimen #2. The resulting capacity curve along with base shear vs. roof displacement

from the experimental test for ground motion D2 and D3 is plotted in Figure 4.12. The capacity curve from the respective bare frame of Specimen #1 is also superimposed in the same figure. It is worth noticing that pushover analysis results in reduced capacity prediction than what is observed in the experimental time-history results, which is consistent with the general acceptance that due to its simplicity and ease-of-use pushover analysis yields conservative results.

Comparison of capacity curves from bare and infilled frames indicates an abrupt drop in the capacity of infilled frame which is due to the failure of equivalent struts at the 1st and 2nd storeys. Note that a little later, after the cracking of 3rd storey infills as well, the capacity of infilled frame again drops abruptly and almost coincides the capacity curve of Specimen #1 at its peak, indicating that after the failure of all masonry struts, the capacity of infilled frame reduced to that of the bare frame. It should be noted that this reduction in capacity is abrupt in the case of deficient infilled frame, regardless of whether the material model used for representing the equivalent struts has abrupt post-peak degradation as in the case of *Calibrated* model, or it has gradual degradation like in the case of *1D-Concrete* material model (Figure 4.8). The experimental results also prove this hypothesis since an abrupt reduction can also be seen in base-shear vs. roof displacement plot during D3 in the same figure. The stiffness of the infilled frame is also considerably larger than the bare frame according to the model predictions due to the contribution of infill panels. The initial slope of capacity curves from pushover analysis compares well with the slope from time-history hysteretic curve of experiment.

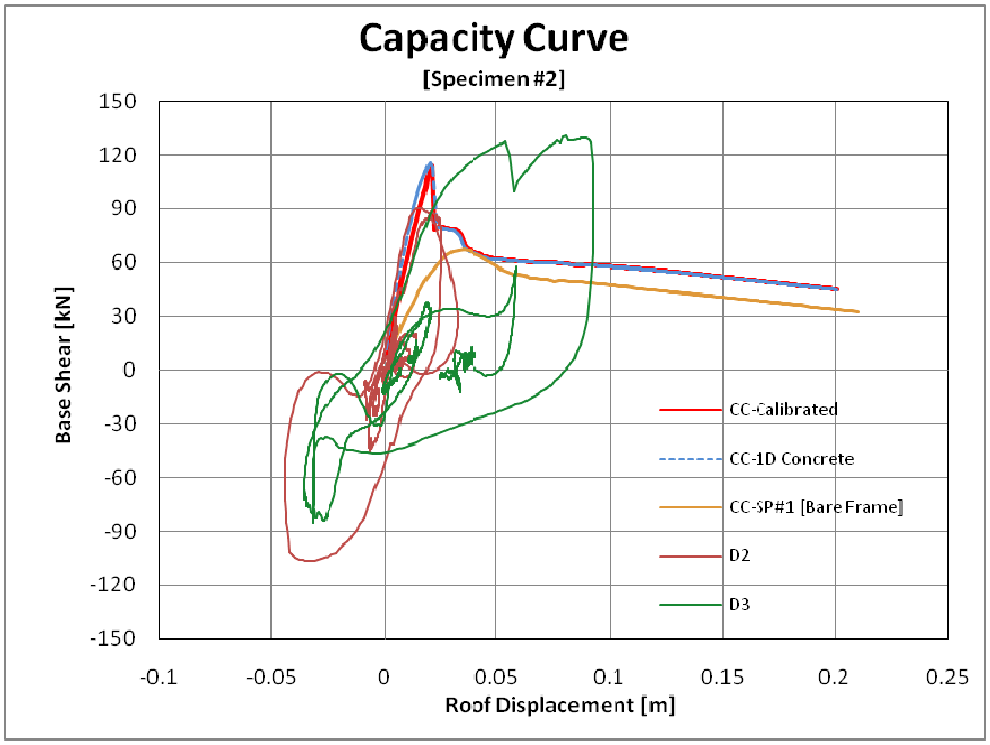

Figure 4.11: Specimen #2 capacity curve and base-shear vs. roof displacement response

4.4.3 Specimen #4 – Code-conforming Infilled Frame

The results obtained from the analysis of the calibrated model of Specimen #4, which is developed using the model of Specimen #3, are compared with the pseudo-dynamic results and comments are made on the accuracies obtained as well as the limitations in capabilities of the numerical model. Comparative analysis is also conducted among the three material models used for masonry infill equivalent strut.

The initial fundamental periods of Specimen #4 from OpenSees using *Calibrated*, *1D-concrete* and *Literature* material models are 0.25 seconds, 0.22 seconds and 0.22 seconds respectively. The comparison of time histories for inter-storey drift ratio and storey shears are presented in Figures 4.12 and 4.13, respectively.

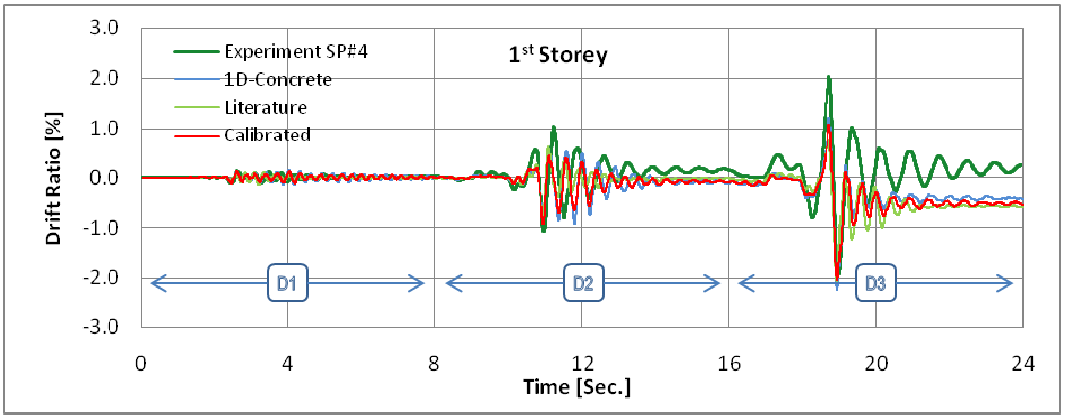

Figure 4.12 (a): Comparison of first storey drift time-history (SP#4)

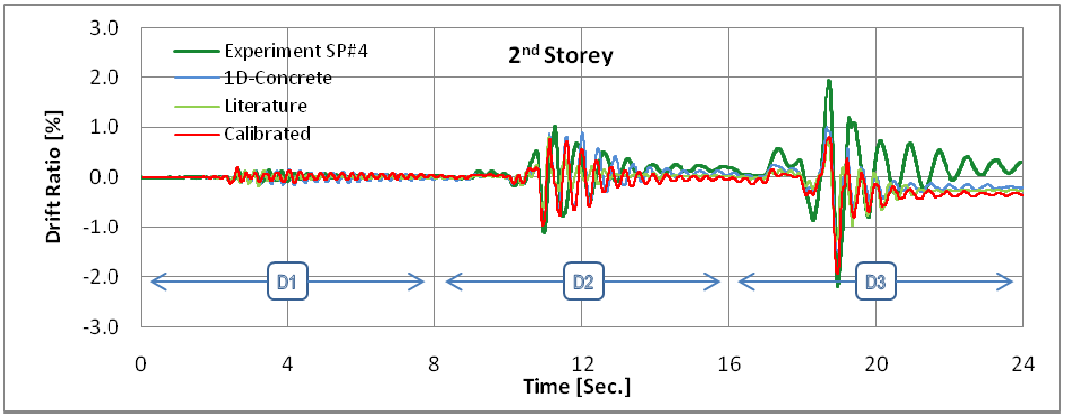

Figure 4.12 (b): Comparison of second storey drift time-history (SP#4)

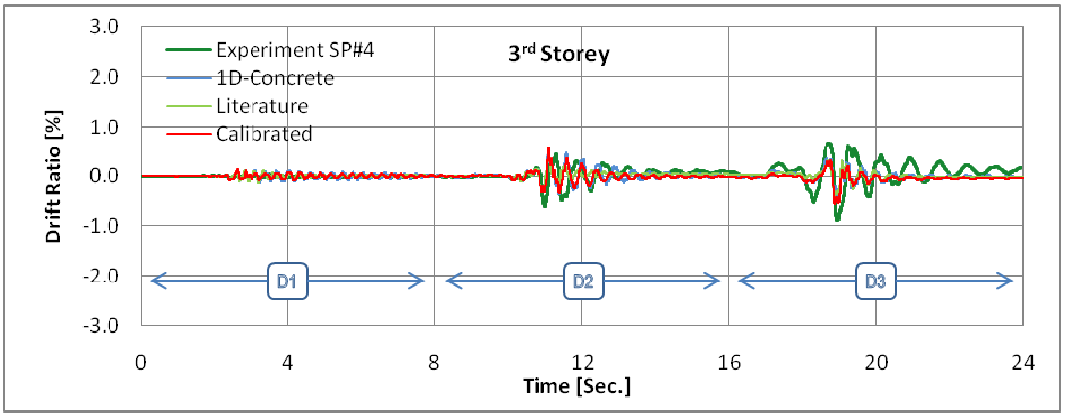

Figure 4.12 (c): Comparison of third storey drift time-history (SP#4)

It is evident from the inter-storey drift plots that overall the models capture the response peaks quite accurately in the 1st and 2nd storeys during D2 and D3. The quantitative evaluation of the accuracy of model predictions in terms of peak inter-storey drifts and peak storey shears is shown in Tables 4.7 and 4.8 respectively. The error percentages for drifts during D2 and D3 ground motions are within an acceptable range for *Calibrated* material model giving an overall confidence on the use of proposed material model for AAC infills, except in the case of third storey for which the model predicts stiffer response than the experimental observation during D3. This could again be attributed to the inability of capturing joint flexibility in the model due to the absence of specific joint elements.

The error percentages for peak storey shear response, shown in Table 4.8, also indicate that OpenSees model of Specimen #4 using *Calibrated* material model captures the response with better accuracy than other two material models during both D2 and D3. However, the storey shears in the 3rd storey during D2 are over-predicted indicating a stiffer response, which is also similar to the drift response.

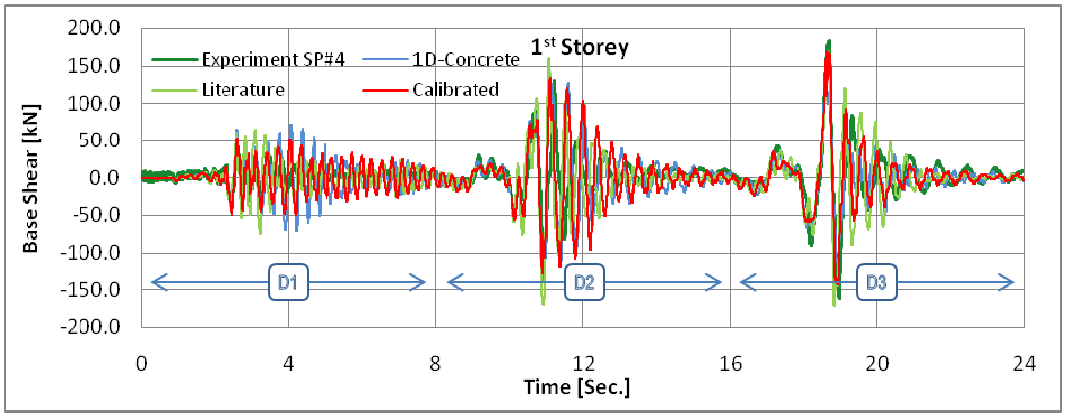

Figure4.13 (a): Comparison of first storey shear time history (SP#4)

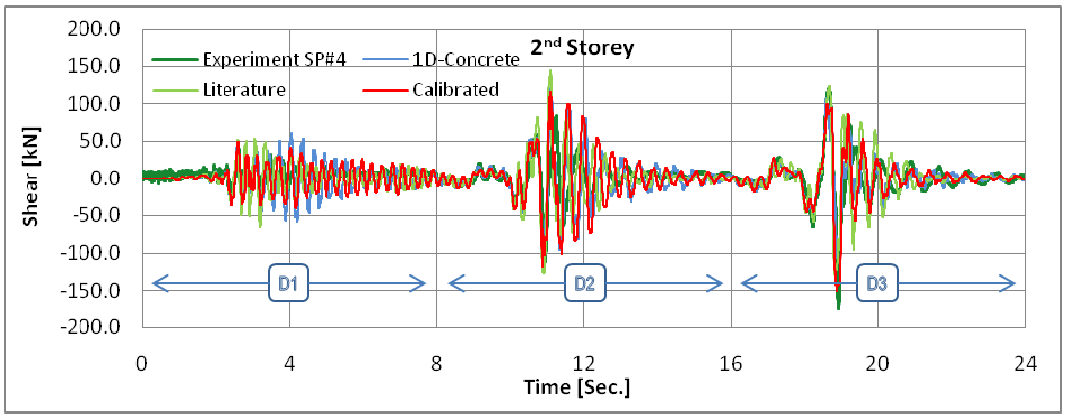

Figure 4.13 (b): Comparison of second storey shear time-history (SP#4)

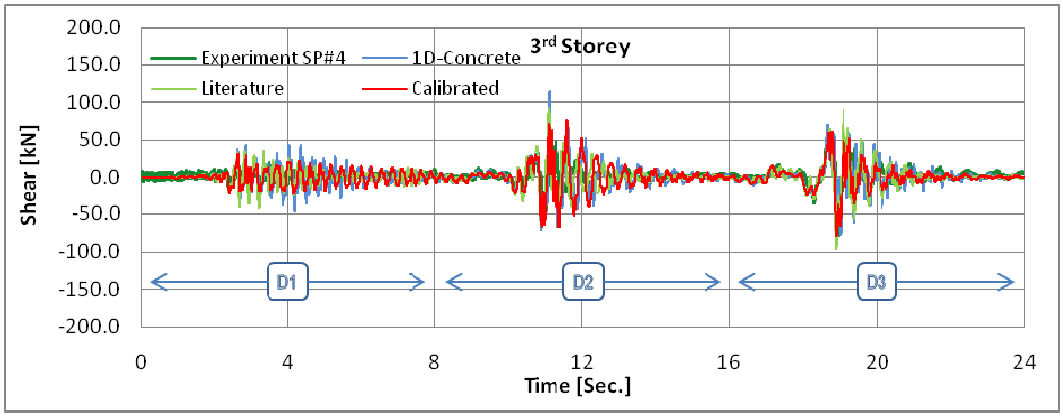

Figure 4.13 (c): Comparison of third storey shear time-history (SP#4)

Table 4.7: Peak inter-storey drift errors (SP#4)

Storey	Ground Motion	Maximum Inter-Storey Drift [%]				Error [%] *		
		Experiment	OpenSees					
			Calibrated (a)	1D-Concrete (b)	Literature (c)	(a)	(b)	(c)
1st	D1	0.14	0.138	0.133	0.15	+ 1.4	+ 5.0	+ 9.4
1st	D2	1.07	0.93	0.92	0.75	- 13.3	- 13.6	- 29.2
1st	D3	2.04	2.04	2.24	2.1	+ 0.26	+ 9.9	+ 1.6
2nd	D1	0.18	0.21	0.16	0.18	+ 13.1	+ 10.0	+ 0.7
2nd	D2	1.13	0.97	0.89	0.79	- 14.5	+ 21.8	- 30.1
2nd	D3	2.2	1.95	1.51	1.29	- 11.3	+ 31.4	- 41.2
3rd	D1	0.05	0.15	0.14	0.13	+ 223.5	+ 204.7	+ 193.1
3rd	D2	0.62	0.58	0.55	0.41	- 6.1	+ 10.8	- 33.7
3rd	D3	0.87	0.55	0.47	0.47	- 36.7	- 45.8	- 46.3

* Positive = Over-prediction, Negative = Under-prediction

Table 4.8: Peak storey shear errors (SP#4)

Storey	Ground Motion	Maximum Storey Shear [*kN*]				Error [%] *		
		Experiment	OpenSees					
			Calibrated (a)	1D-Concrete (b)	Literature (c)	(a)	(b)	(c)
1st	D1	48.2	52.4	70.9	75.3	+ 8.7	47.2	+ 56.0
1st	D2	129.4	133.1	138.5	170.2	+ 2.8	7.0	+ 31.5
1st	D3	182.9	167.1	130.9	172.2	-8.7	-28.4	-5.9
2nd	D1	42.0	48.3	60.5	66.3	+ 15.2	44.1	+ 57.9
2nd	D2	111.6	117.9	119.9	143.9	+ 5.6	+ 7.4	+ 28.9
2nd	D3	173.6	150.8	106.2	128.8	-13.1	-38.8	-25.8
3rd	D1	23.8	30.7	46.1	42.3	+ 29.3	+ 93.9	+ 77.8
3rd	D2	56.6	75.0	113.5	91.5	+ 32.4	+ 100.5	+ 61.6
3rd	D3	78.2	80.1	82.6	97.3	+ 2.5	+ 5.7	+ 24.5

* Positive = Over-prediction, Negative = Under-prediction

Capacity curves from non-linear static pushover analysis of Specimen #4 using all three materials models in OpenSees are shown in Figure 4.14 along with the base shear vs. roof displacement from the experimental tests under ground motion D2 and D3. The capacity curve of the respective bare frame i.e. Specimen #3 is also superimposed in the same figure. Similar conservative prediction of capacity from pushover analysis is observed in this specimen also as compared to the time-history analysis.

The capacity curves from different material models of infilled frame have now shown differences in terms of post-peak response, i.e. post strut-failure response. The *Calibrated* model indicate an abrupt reduction in capacity after successive failures of 1st and 2nd storey compression struts while *1D-Concrete* and *Literature* models results in gradual capacity degradation. The abrupt capacity reduction is not observed in the experiment (SP#4).

It is worth noticing that none of the capacity curves of Specimen #4 models are able to accurately predict the stiffness from time history hysteretic curve of experiment. The capacity curves indicate significant increase in the stiffness of infilled frame while experimental results indicate no considerable alteration in the stiffness of code-conforming bare and infilled frames (see Figures 2.18 and 2.22). However, the comparative increase in capacity due to contribution of AAC infills in the code-conforming frame is lesser than that of deficient frame which also confirms that AAC infills tends to contribute and alter the response in deficient frames much more as compared to the code-conforming frames. The same can be said for the abrupt degradation in the capacity of infilled frames after the failure of infills which is more prominent in the deficient infilled frame.

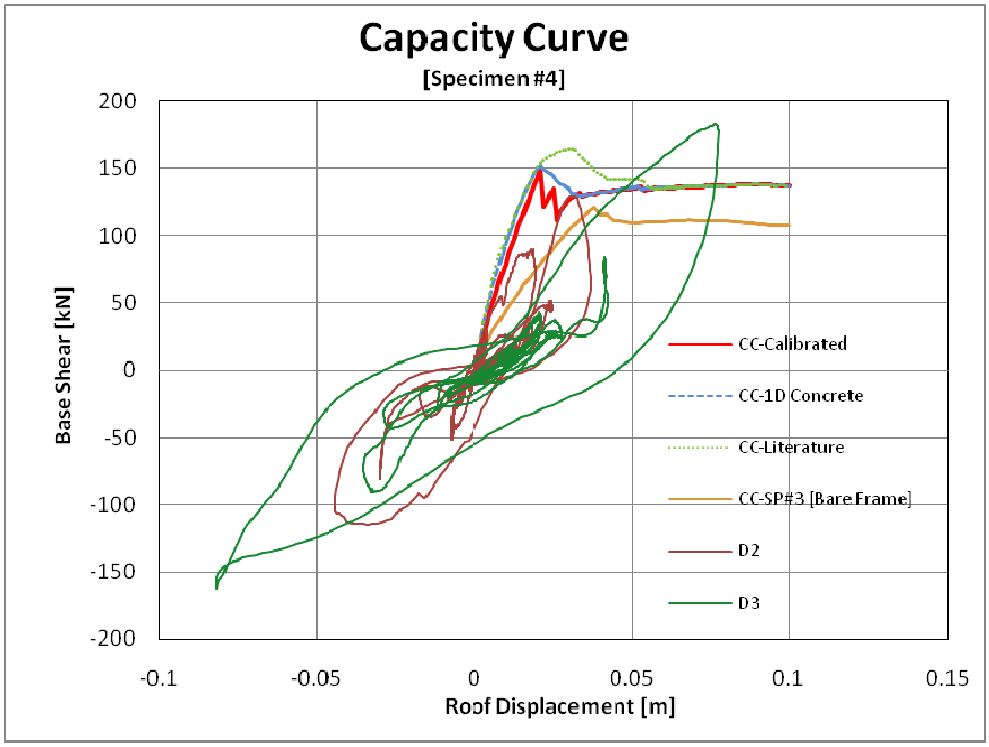

Figure 4.14: Specimen #4 capacity curve and base-shear vs. roof displacement response

CHAPTER 5

PERFORMANCE EVALUATION

5.1 General

The evaluation of performance assessment procedures mentioned in TEC 2007 and ASCE-41/06 in the light of experimental data is the focus of this chapter as stated in the problem statement as well. In this regards, the performance evaluations of all four specimens is carried out. Numerical models earlier developed are used to evaluate the seismic performance of the test frames using non-linear static and non-linear time history analyses in addition to the experimental observations and results.

5.2 Performance Evaluation of Specimens

Performance evaluation of all four specimens is conducted using experimental measurements as well as the results of time history and pushover analysis in the OpenSees platform. The aim is to compare the non-linear assessment procedures of TEC 2007 and ASCE/SEI 41-06. Visual assessment of selected members during the tests is also used for comparison purposes. It should be noted that assessment is strictly focused on the column members and the effect of infills on the performance of frames since the infills mainly affected the response of column members as observed in the pseudo dynamic test.

The assessment procedure of TEC 2007 comprises of strain-based performance limits while that of ASCE/SEI 41-06 is rotation-based performance limits. Three performance limit states for ductile members defined in TEC 2007 at member level are: Minimum Damage (MD), Safety Limit (SL), and Collapse Limit (CL). Similar performance limits defined in ASCE/SEI 41-06 for ductile members are: Immediate Occupancy (IO), Life Safety (LS), and Collapse Prevention (CP). In this text, the notation for performance limit states similar to ASCE/SEI 41-06 is used. The damage regions between these performance limits specified in both TEC 2007 and ASCE/SEI 41-06 are Minimum Damage (MD), Significant Damage (SD), Heavy Damage (HD), and Collapse (CP). Figure 5.1 shows the performance limits and the damage regions specified in both codes.

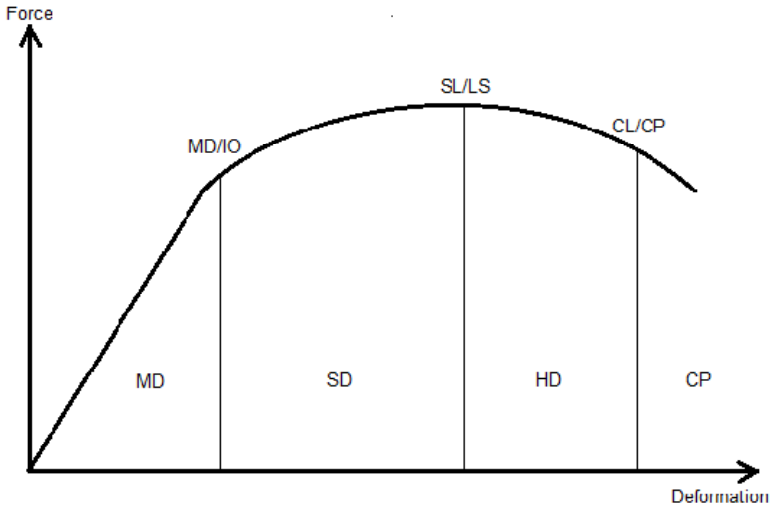

Figure 5.1: Performance limits and damage states

The formulation for limit state strain values for longitudinal steel in tension and concrete in compression for columns of both code-conforming and non-conforming specimens is shown in Table 5.1 in accordance with TEC 2007, Chapter #7. These performance limits depends on the ratio of the provided confinement reinforcement ratio "ρ_s" vs. required confinement reinforcement ratio "ρ_{sm}" with an upper bound of ratio ρ_s/ρ_{sm} equal to 1. For columns of non-conforming frames, the ratio ρ_s/ρ_{sm} is 0.3 whereas for columns of code-conforming frames it is 0.95. Columns in all specimens satisfy the requirements of ductile behaviour.

Table 5.1: TEC 2007 limiting strain values

	Limiting strains		
	MD	***SL***	***CL***
Longitudinal Steel	0.01	0.04	0.06
Concrete (compression)	0.0035	$0.0035 + 0.01(\rho_s/\rho_{sm})$	$0.004 + 0.013(\rho_s/\rho_{sm})$

The limiting values of plastic rotations for column members given in ASCE/SEI 41-06 in Table 6-8 are presented here in Table 5.2. These values are interpolated bi-linearly based on two parameters which are axial load ratio and confinement reinforcement ratio as calculated from Equations 5.1 and 5.2 respectively.

$$\frac{P}{A_g f_c'} \tag{5.1}$$

$$\rho = \frac{A_v}{b_w S} \tag{5.2}$$

Table 5.2: ASCE/SEI 41-06 limiting values for plastic rotations

Specimen	**Column**	**Plastic rotations**		
		IO	***LS***	***CP***
Specimen #1 Bare Frame NC	Exterior	0.0033	0.0063	0.0073
	Interior	0.0029	0.0057	0.0065
Specimen #2 Infilled Frame NC	Exterior	0.0034	0.0064	0.0076
	Interior	*	*	*
Specimen #3 Bare Frame CC	Exterior	0.0049	0.024	0.032
	Interior	0.0048	0.022	0.030
Specimen #4 Infilled Frame CC	Exterior	0.0047	0.016	0.020
	Interior	*	*	*

* Refer to Table 5.3

These limits are applied to plastic rotations obtained at potential plastic hinge regions of members from experimental measurements as well as from OpenSees models assuming uniform strain distribution in these regions.

It should be noted that unlike TEC 2007, ASCE/SEI 41-06 provides separate performance limits for frame elements bounding the infill panels. These assessment limits are based on total strain (compression/tension) in the member and are provided in Table 6-16 of ASCE/SEI 41-06. The tensile strain limits are based on adequate/inadequate splicing whereas strain limits for concrete in compression depend on adequate/inadequate confinement. In our case, columns of Specimen #2 are inadequately confined whereas columns of Specimen #4 are properly confined. Table 5.3 presents the limiting strain values for bounding columns of the infilled frames.

Table 5.3: ASCE/SEI 41-06 limiting strain values for RC members bounding the infill panel

Specimen		**Total Strain**		
		IO	***LS***	***CP***
Specimen #2 NC	Tension	0.01	0.03	0.04
	Compression	0.002	0.002	0.003
Specimen #4 CC	Tension	0.01	0.03	0.04
	Compression	0.003	0.015	0.02

In case of infill panels, the performance limits are specified in both codes based on maximum inter-storey drifts. The limiting values are indicated in Table 5.4 for TEC and ASCE guidelines. It should be noted that in TEC 2007, these limits are defined for strengthened infill panels. However, in ASCE/SEI 41-06 these limiting values are for unreinforced masonry infill panels.

Table 5.4: Limiting drift values for infill panel

Specimen		**Limiting drifts (%)**		
		IO	***LS***	***CP***
Specimen #2 NC	TEC 2007	0.15	0.35	-
	ASCE 41-06	-	0.3	-
Specimen #4 CC	TEC 2007	0.15	0.35	-
	ASCE 41-06	-	0.6	-

In addition to these limiting drift values for infill panels, ASCE/SEI 41-06 also defines the acceptance criteria based on observed damage which is as follows; for immediate-occupancy: significant visual cracking of an unreinforced infill panel occurs, for life-safety: substantial cracking of infill panel occurs and the potential is high for the panel, or some part of it, to drop out of the frame. In this study, this approach will be used to determine the performance based on the observations during experimental tests because the drift limits are not comparable due to difference in applicability.

5.2.1 Assessment using Non-linear Analysis Procedures

Non-linear time history and non-linear static pushover analyses are performed on OpenSees models for the performance assessment of column members. Capacity curves obtained from pushover analysis and demand curves from response spectra of D2 and D3 ground motions are used to estimate the target displacements (inelastic deformations) in accordance with the procedure defined in TEC 2007. In this approach, the multi-degree of freedom system (MDOF) is reduced to an equivalent single-degree of freedom system (SDOF).

The procedure can be outlined as follows:

- Using the pushover load-pattern based on the first mode response, obtain the capacity curve of the MDOF system
- Bi-linearize the capacity curve and convert MDOF system to equivalent SDOF system
- Convert the capacity curve to spectral acceleration-spectral displacement format
- Convert the response spectrum to acceleration-displacement response spectrum (ADRS) to obtain the demand curve
- Plot the demand and capacity curves in the ADRS format on the same graph and determine the inelastic displacement demand of the SDOF system at the control node
- Convert the displacement demand of SDOF system to the global roof displacement (target displacement) of MDOF system at the control node.
- Push the structure up to the target displacement and record member deformations.

The fixed pushover load pattern which is based only on the first mode response may influence the reliability of this method. It is important to note that for ground motion D3, the evaluation based on pushover does not take into account prior damage to the specimen due to ground motions D1 and D2. It should also be noted that target displacement used in pushover analysis is calculated from the respective response spectrum of the ground motions and it may differ from the experimental target displacement.

For the assessment using time history analysis, the peak values of strain and rotation time-histories recorded at member ends are used to compare with the limiting values mentioned above. Similar procedure is also adapted for experimental time histories.

Evaluation procedures based on permanent residual displacements of structure from the analytical model have also been proposed by several researchers such as Dazio and Yazgan (2011). However, the developed simulation models are not sophisticated enough to accurately capture the residuals and therefore the only procedure applicable here for evaluation is based on peak responses during the response time history.

In addition to the experimental and analytical performance evaluation using TEC 2007 and ASCE 41-06 procedures, certain columns are also assessed through visual observations during the physical test. The judgement is purely objective with the aim to compare the methods of these codes with damages observed during the experiment.

It should be reminded here again that evaluation is only performed for D2 and D3 ground motions and focus strictly on column members as well as infill panels.

5.3 Performance Assessment of Specimen #1

Performance evaluation of Specimen #1 is conducted as explained above for experimental and numerical results using the procedures of TEC 2007 and ASCE 41-06 and the outcome is given in Figure 5.2 and Figure 5.3 under the ground motions D2 and D3 respectively. Assessment using experimental time histories from pseudo-dynamic test is referred hereinafter as "Experiment", whereas assessment results using OpenSees time history and pushover analysis are referred hereinafter as "Time History" and "Pushover" respectively.

Comparing the evaluation using experimental results, we observe that TEC 2007 procedure is conservative as compared to ASCE 41-06 evaluation under both D2 and D3. Among the time history and pushover evaluation, ASCE procedure gives conservative results compared TEC 2007 during both D2 and D3.

Comparing the two analysis methods using OpenSees model, pushover procedure overestimates the damages in the members as compared to time history and indicate complete collapse after D2, which is contrary to the experimental evaluation by using any of the procedures. During D2 ground motion, where the response is stable, the assessment of OpenSees time history using TEC 2007 limit states compares fairly acceptable with the corresponding experimental evaluation outcome while evaluation using ASCE 41-06 over-predicts the damage. During D3, since the specimen reaches collapse rendering the response unstable, none of the model results are comparable due to the soft storey mechanism formed at the 1st storey in the analytical model, therefore the damages at higher stories are not predicted accurately by the model.

As presented in Chapter 3 and Chapter 4, most of the damage is concentrated in the first storey. Model results also compare well with experimental results for the first storey, we therefore objectively compare first storey evaluation results from experimental, analytical time history and analytical pushover analysis of TEC 2007 and ASCE 41-06 with that of visually observed damages during the physical test. It is important to remind here that since the analytical model was not capable to accurately capture the response from experimental time histories, the comments here are focused on the experimental assessment results. The comparison for D2 and D3 ground motion is shown in Figure 5.4 and Figure 5.5 respectively. Using experimental data, TEC assessment compares quiet well with the observed damages while ASCE 41-06 mostly under-predicts the damages. The OpenSees time history and pushover assessment using ASCE procedure is conservative while that of TEC 2007 compares good with observation during D2 while better than ASCE 41-06 during D3.

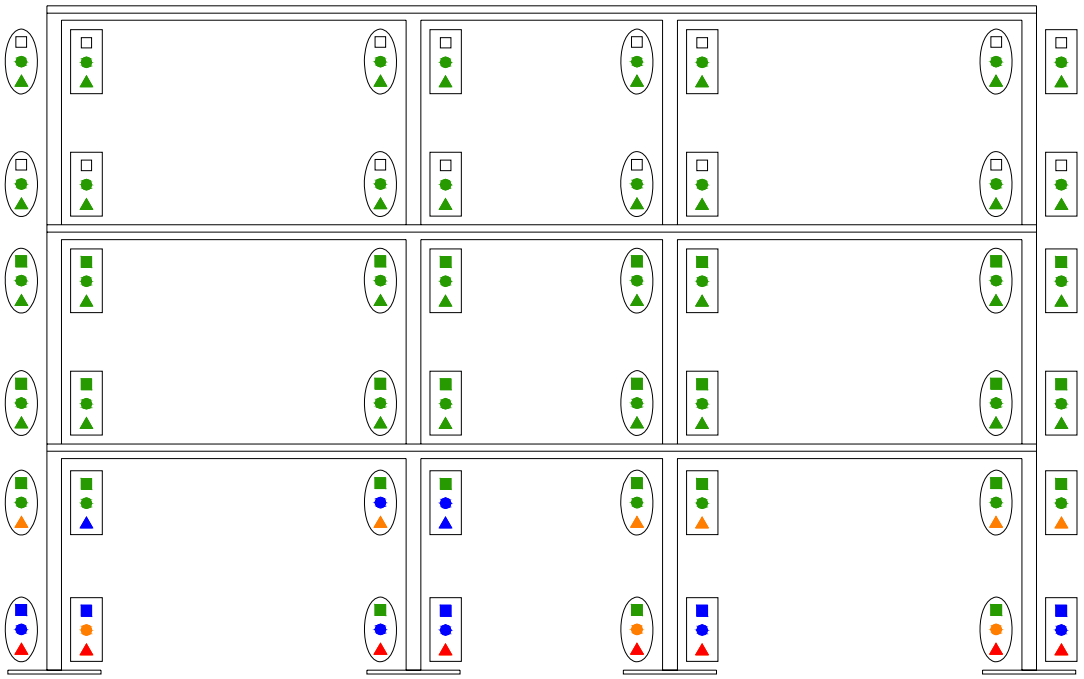

Figure 5.2: Specimen #1 performance assessment [D2]

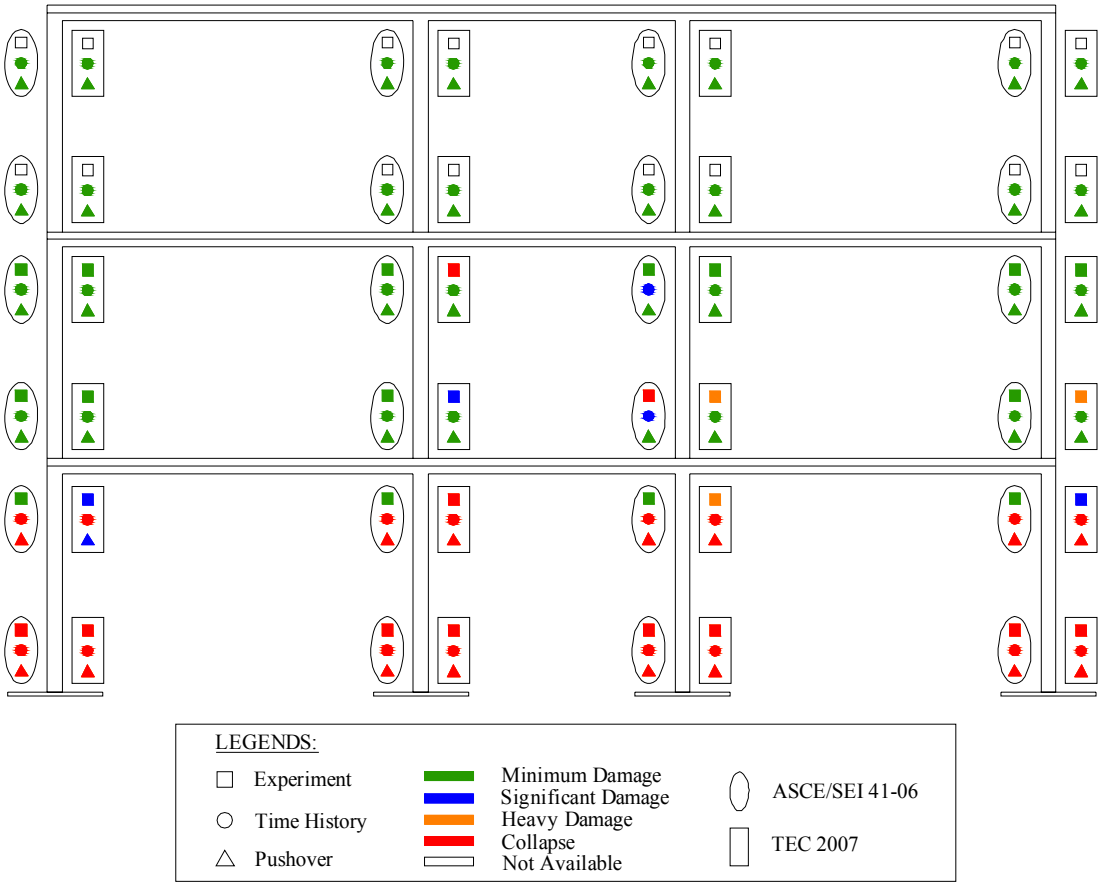

Figure 5.3: Specimen #1 performance assessment [D3]

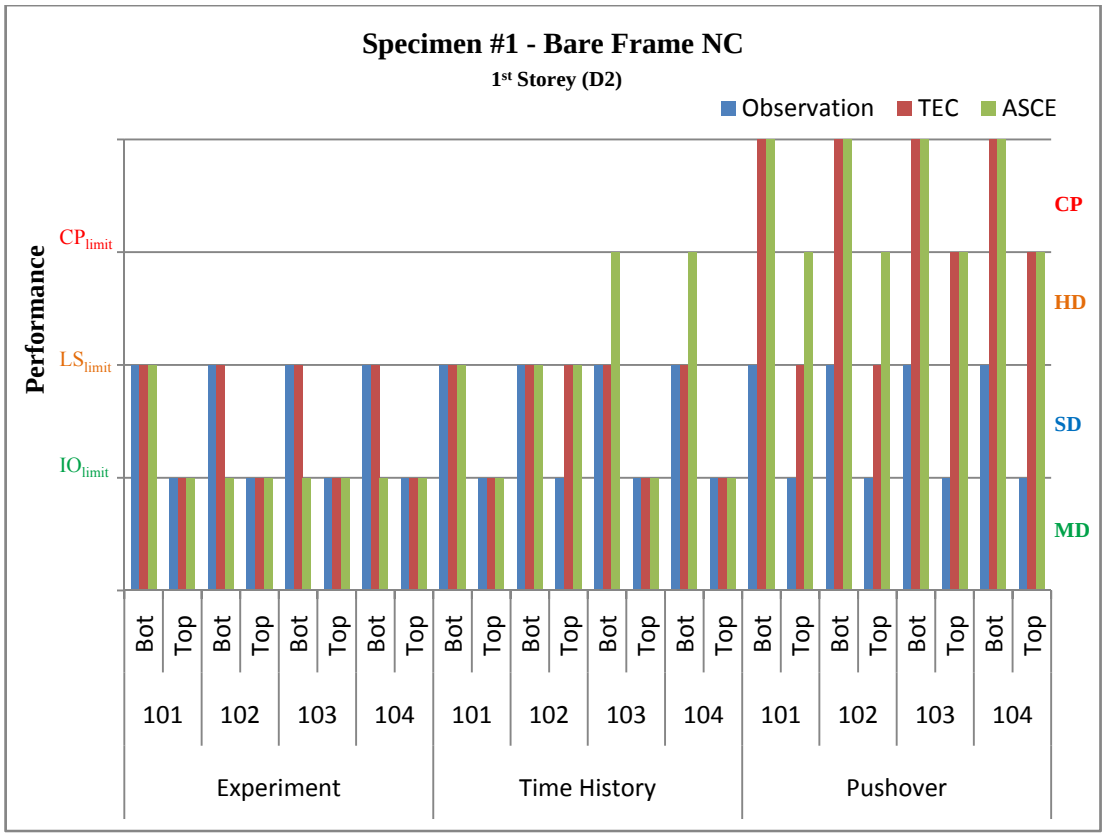

Figure 5.4: Observed and evaluated damages - SP #1 [D2]

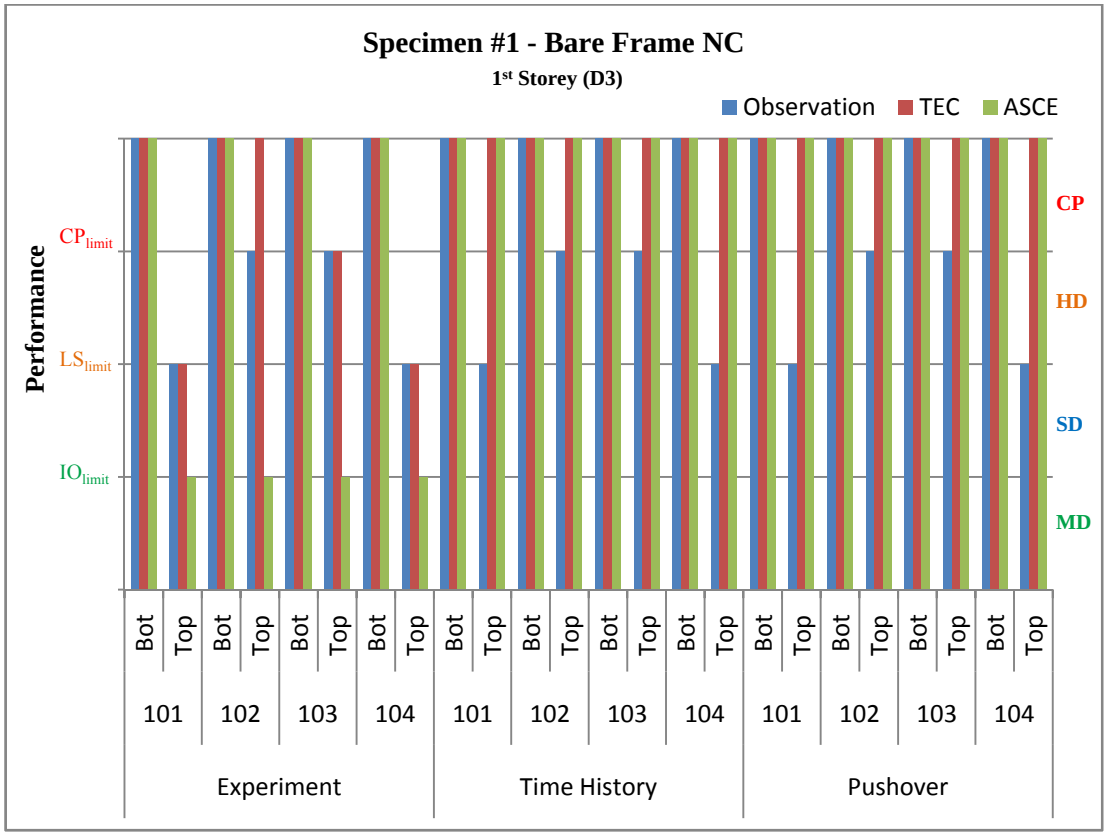

Figure 5.5: Observed and evaluated damages - SP #1 [D3]

5.4 Performance Assessment of Specimen #2

Performance evaluation of Specimen #2 is conducted similar to the Specimen #1and the outcome is given in Figure 5.6 and Figure 5.7 for ground motions D2 and D3 respectively.

The assessment using experimental results indicates that for exterior columns, TEC 2007 procedure is conservative as compared to ASCE 41-06 as for the previous Specimen #1 while for bounding columns, i.e. columns bounding the infill panels, ASCE/SEI 41-06strain-limits conservatively predicts the damages as compared to TEC 2007 during both D2 and D3.

The results of assessment using OpenSees model for both D2 and D3 do not comply with experimental evaluation specially for bounding column from any of the two procedures. The reason could be the inability of concentric strut model to capture local deformations and representing the damage caused by transfer of shear from the columns. For this purpose, a more detailed multi-strut model could be used.

Similar to Specimen #1, the first storey assessment results are compared with observation and presented in Figure 5.8 and Figure 5.9 for D2 and D3 ground motions. During D2, TEC 2007 gives accurate prediction of observed damages in the exterior column while under-predicts the damages in the bounding column. On the other hand, ASCE 41-06 accurately predicts the damages in the bounding columns as compared to observation while under-predict the damages in exterior columns. The difference can be attributed to the fact that TEC 2007 provides general performance limits for both bounding and non-bounding RC frame members while ASCE 41-06 provides separate strain based limits for RC columns which are bounding the infill panel, treating them as tension and compression chords under lateral loads. These limits are significantly strict than TEC 2007 limits which general for all column elements.

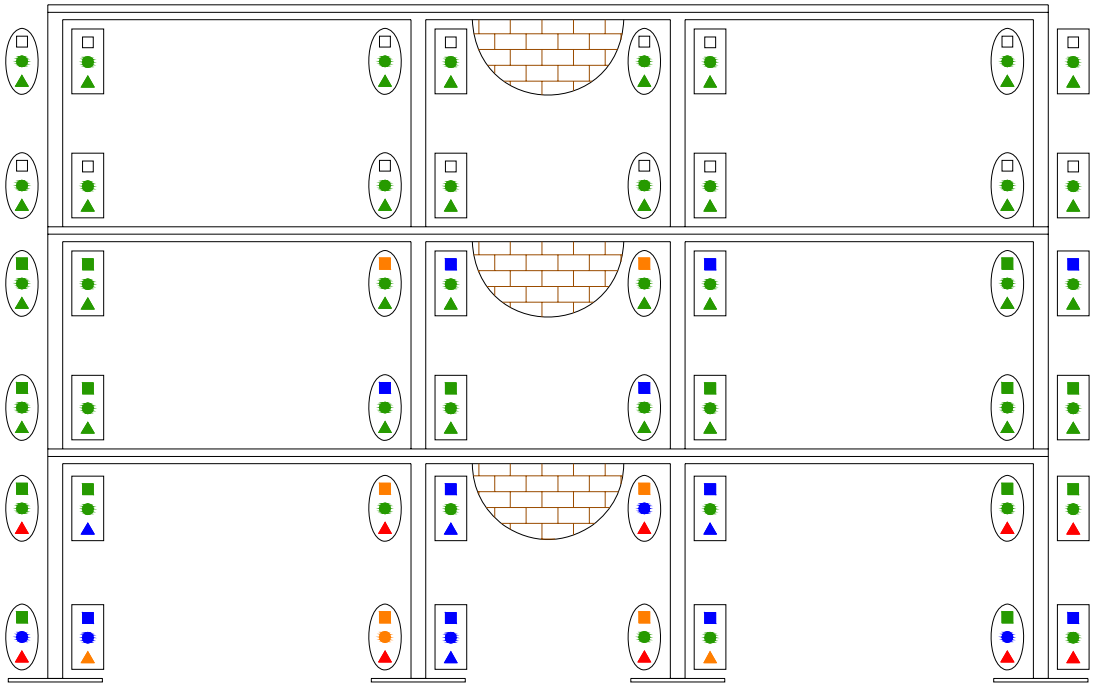

Figure 5.6: Specimen #2 performance assessment [D2]

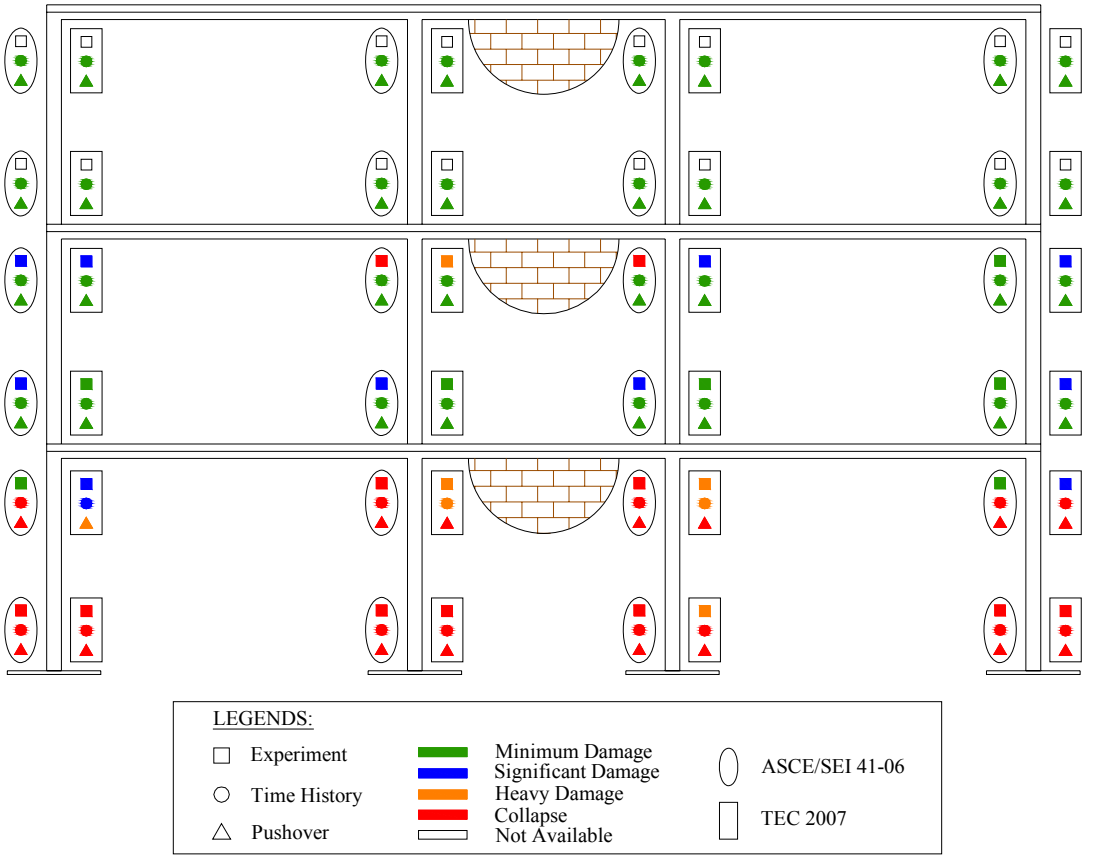

Figure 5.7: Specimen #2 performance assessment [D3]

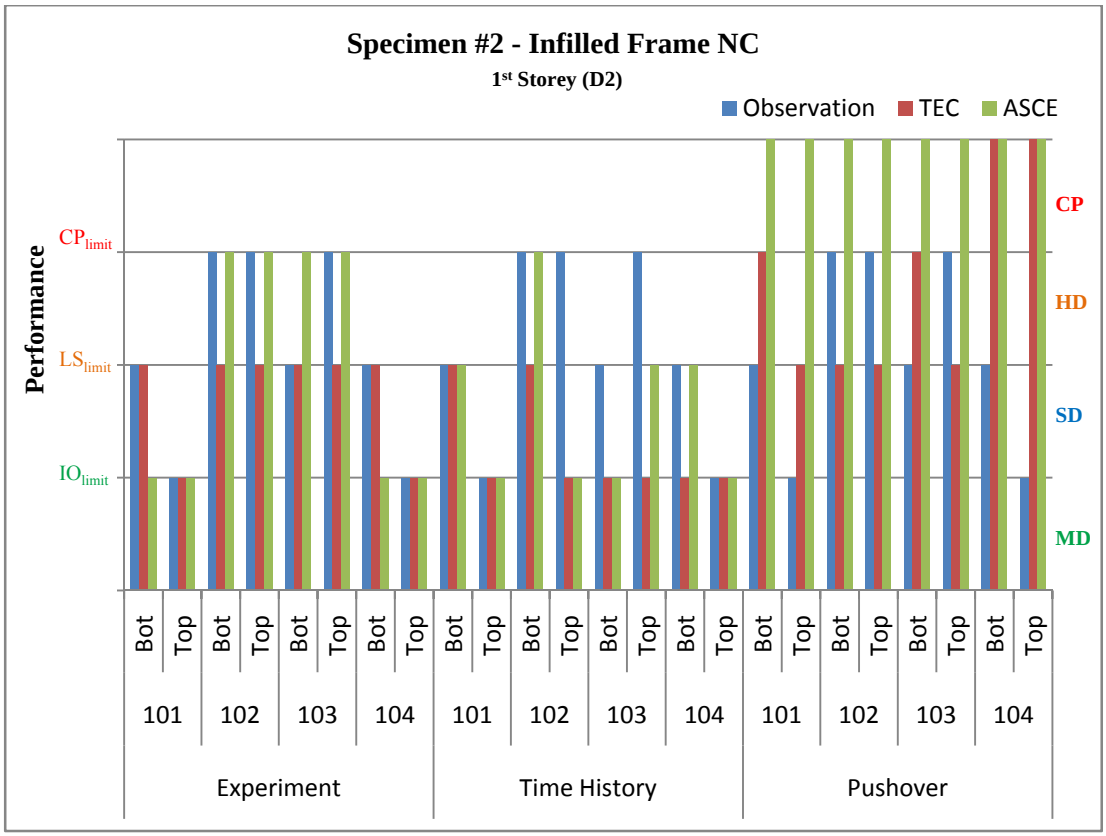

Figure 5.8: Observed and evaluated damages - SP #2 [D2]

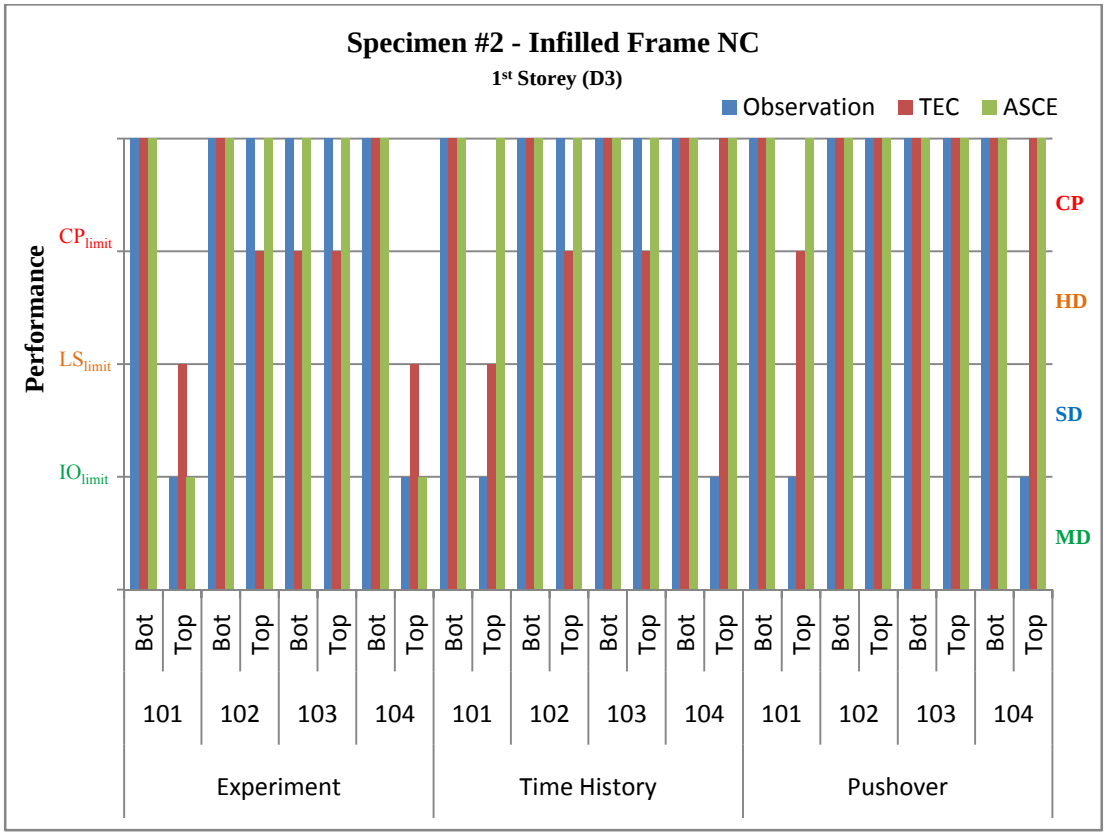

Figure 5.9: Observed and evaluated damages - SP #2 [D3]

Based on the limiting drift values given in Table 5.4, the infill panel already reached collapse point at the end of D2 according to both TEC and ASCE, however, since the limits in TEC are valid for strengthened infill walls; the evaluation criteria will not be consistent for both codes in order to perform comparison of two approaches. Therefore, the infill panel assessment is done, as explained earlier, based on the visual-observation acceptance criteria explained in the ASCE/SEI 41-06 and the results are tabulated below:

Table 5.5: Performance evaluation of infill panels (SP#2)

Ground motion	Storey	Damage	Performance Level
D2	1	Significant multiple diagonal cracking	LS
	2	Significant diagonal cracking	LS
	3	No visible cracks	IO
D3	1	Wide see-through cracks with spalling of fragments	CP
	2	Wide see-through cracks with spalling of fragments	CP
	3	Significant diagonal cracking	LS

Considering the performance of the AAC infill panels, comparison of the cracking and crushing/failure drift values of panel for Specimen #2 given in Table 3.3 with the limiting drift values of Table 5.4, it reveals that AAC infill panels performed much better than the expected response. According to TEC 2007, life-safety limit is assumed to be reached and the panel is considered in collapse range when inter-story drift reaches 0.35%, whereas during pseudo-dynamic test, the first visible diagonal crack appears at approximately 0.5% drift value. Similar comments can be made in the case of ASCE/SEI 41-06 limits.

5.5 Performance Assessment of Specimen #3

For Specimen #3, performance assessment outcomes are presented in Figure 5.10 and Figure 5.11 for ground motions D2 and D3 respectively.

For evaluation using experimental results, similar to Specimen #1, TEC 2007 procedure yields conservative assessment of damage compared to ASCE/SEI 41-06 during both D2 and D3.

The assessment using OpenSees model indicates that during D2, TEC and ASCE assess similar damage distribution in time history and pushover analysis with pushover being conservative and indicate significant damage in some column ends. During D3, the evaluation using time history and pushover analysis through ASCE procedure yields similar results with the corresponding experimental evaluation. However; using the TEC 2007 procedure the damages are mostly under-predicted compared to corresponding assessment using experimental results.

Comparing the first storey assessment results with observed damages presented in Figure 5.12 and Figure 5.13 for D2 and D3 respectively indicate that during D2, evaluation using ASCE from experimental and analytical data predicts minimum damage in all columns as observed while TEC 2007 experimental evaluation indicate some members to be in significant damage region contrary to observation. During D3, similar to D2, experimental evaluation from ASCE 41-06 procedure matches accurately with observation while TEC procedure results in over-prediction of damage.

It is evident that time history analysis seems to work better in predicting the observed performance compared to pushover however the difference among them is insignificant.

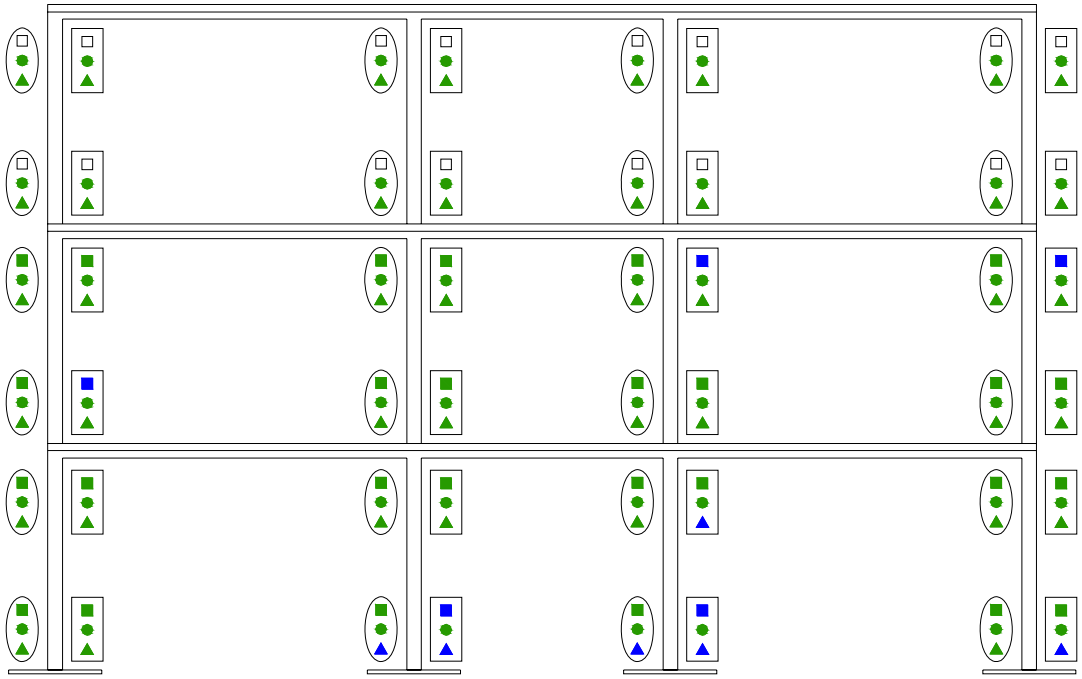

Figure 5.10: Specimen #3 performance assessment [D2]

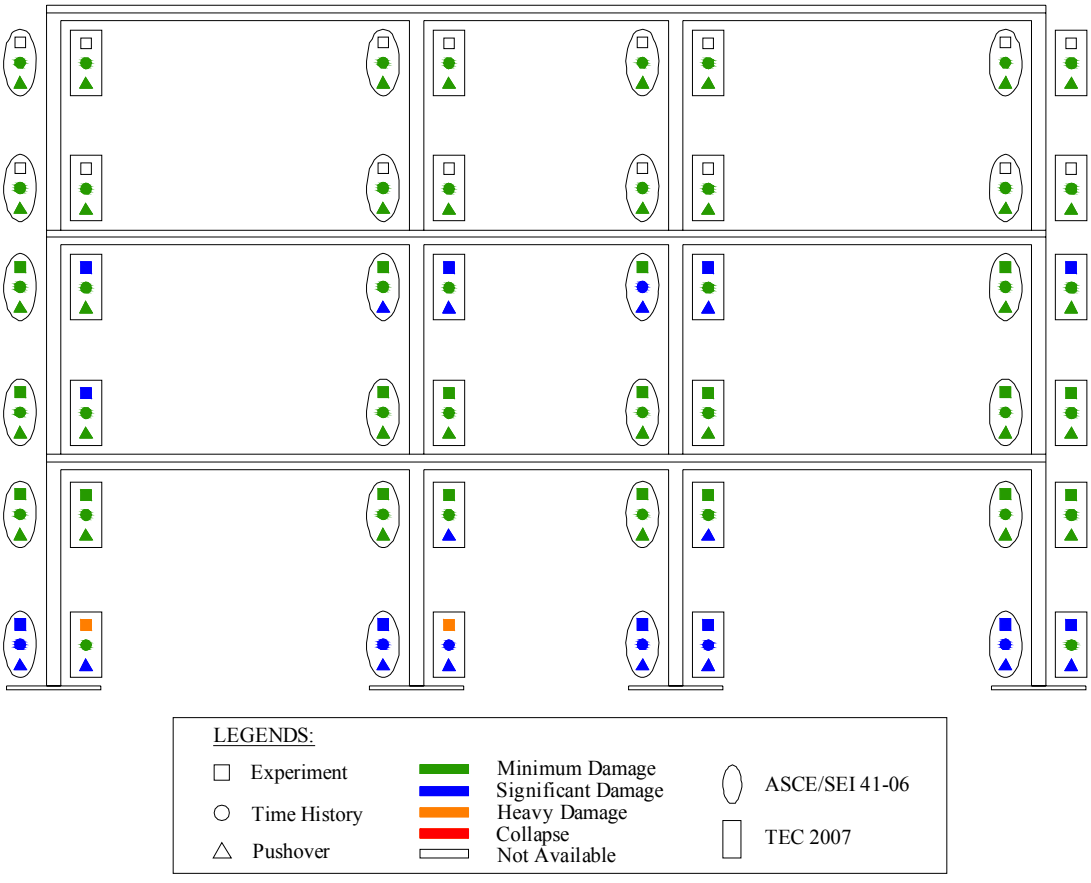

Figure 5.11: Specimen #3 performance assessment [D3]

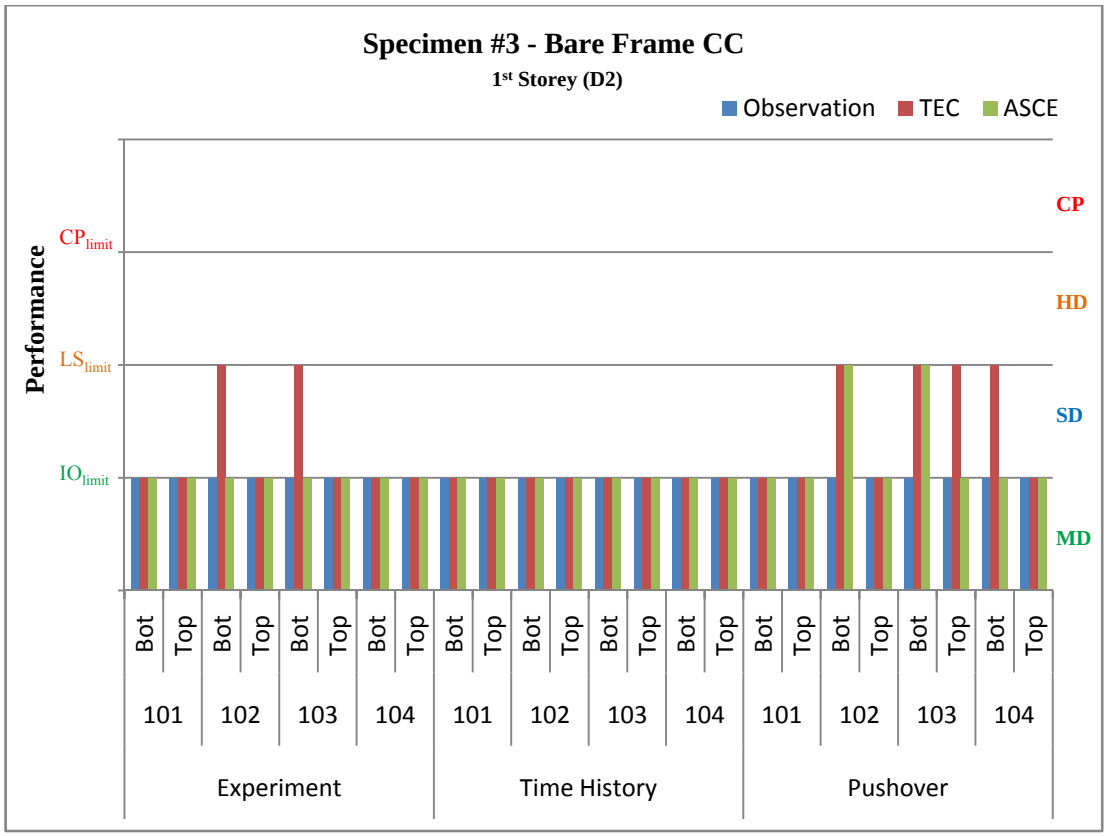

Figure 5.12: Observed and evaluated damages - SP #3 [D2]

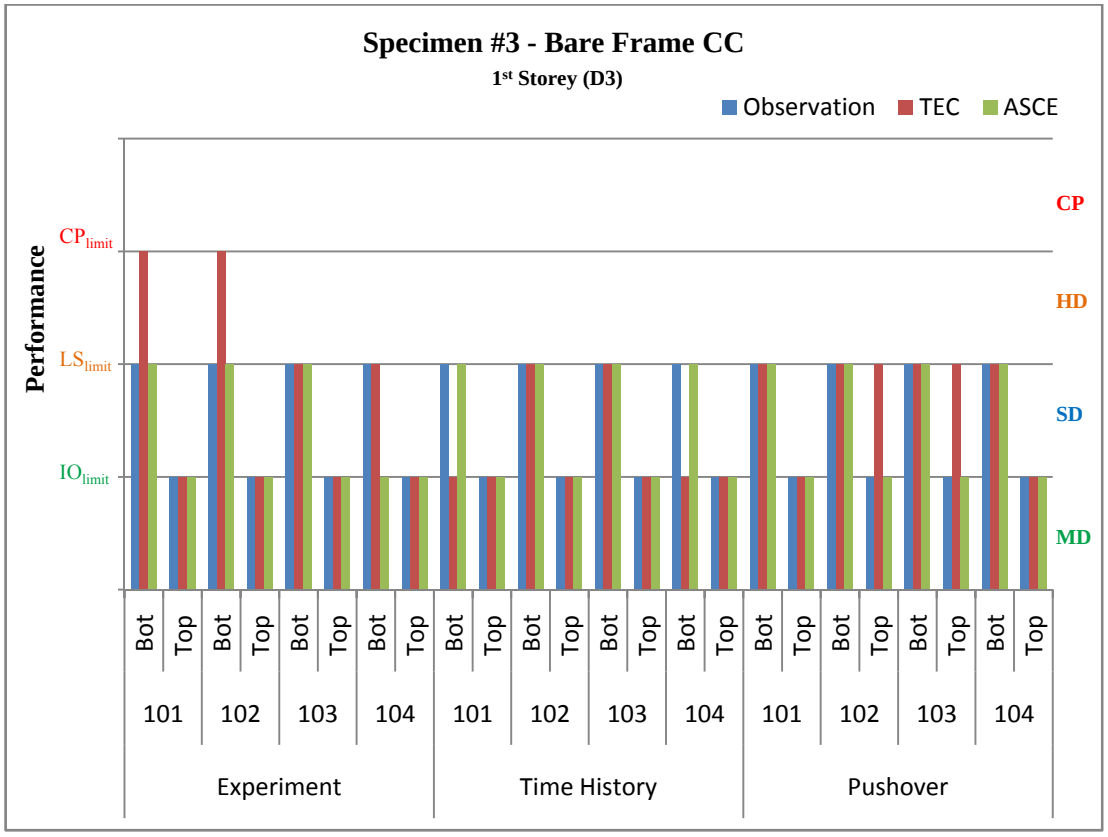

Figure 5.13: Observed and evaluated damages - SP #3 [D3]

5.6 Performance Assessment of Specimen #4

The results of performance evaluation for Specimen #4 are presented in Figure 5.14 and Figure 5.15 for ground motions D2 and D3 respectively.

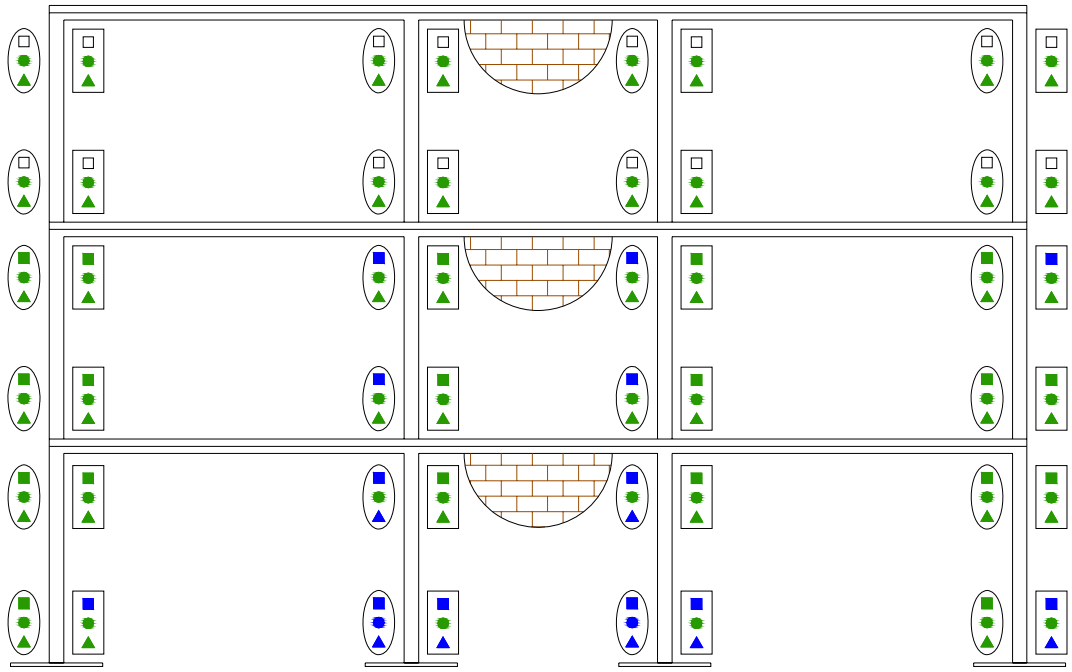

Figure 5.14: Specimen #4 performance assessment [D2]

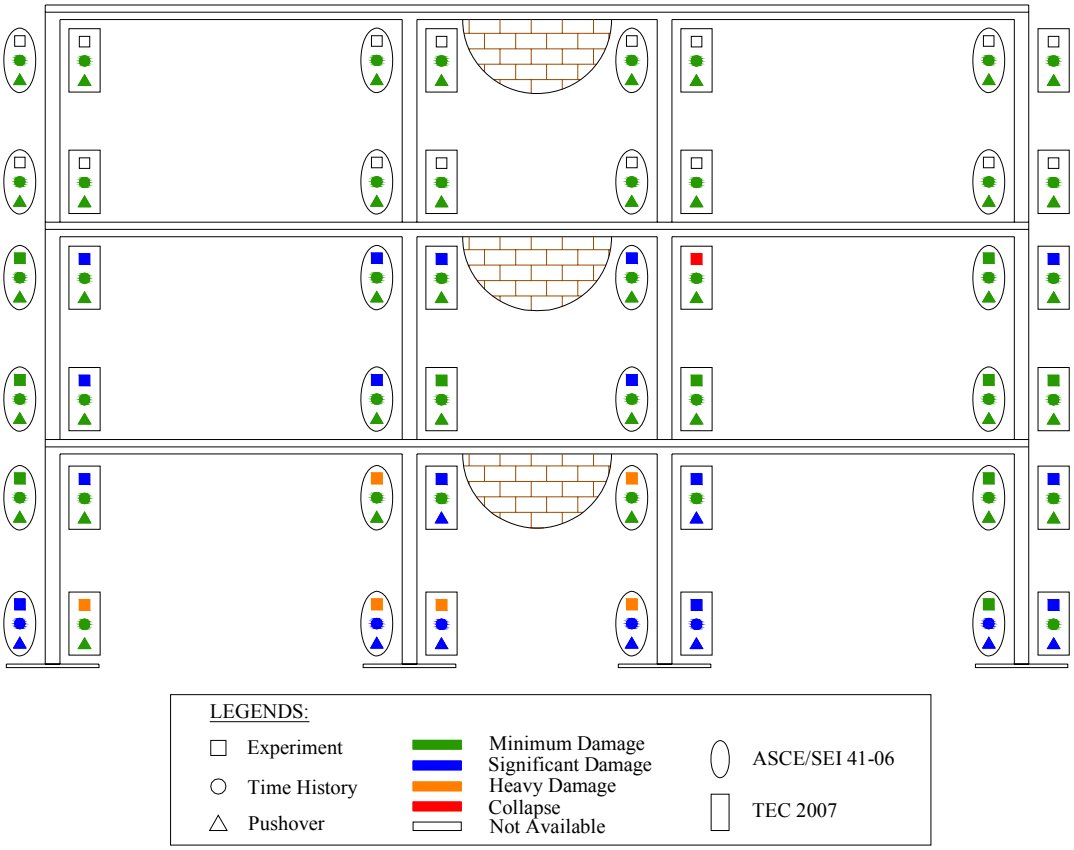

Figure 5.15: Specimen #4 performance assessment [D3]

Comparing the evaluation using experimental results, the TEC 2007 procedure gives conservative evaluation of damage state for exterior columns, as in Specimen #3, whereas ASCE 41-06 provides conservative evaluation for bounding columns, as in Specimen #2.

Using time history and pushover analysis of OpenSees with *Calibrated* strut model for equivalent strut, the damages in the bounding columns are under-predicted as compared to experimental assessment using both procedures due to the same reason as explained in the case of Specimen #2; the limitation of concentric strut model to capture local responses despite the accurate capturing of global responses of Specimen #4. However, due to the strict limits of ASCE for bounding column members, ASCE limits are is more conservative than the TEC limits for time history as well as pushover methods under both ground motions.

Comparison of assessment results with visual observation during test for first storey columns is presented in Figure 5.16 and Figure 5.17 for D2 and D3 ground motions, respectively. During both D2 and D3, TEC 2007 over-predicts the damages for non-bounding columns, as in Specimen #3, while under-predicts the damages in bounding columns. On the other hand, ASCE 41-06 accurately predicts the damages in all columns at each ends. This gives an overall confidence on the judgement that strain-based performance limits of ASCE for bounding columns predicts the damages accurately, regardless of the configuration of frame being deficient or code-conforming.

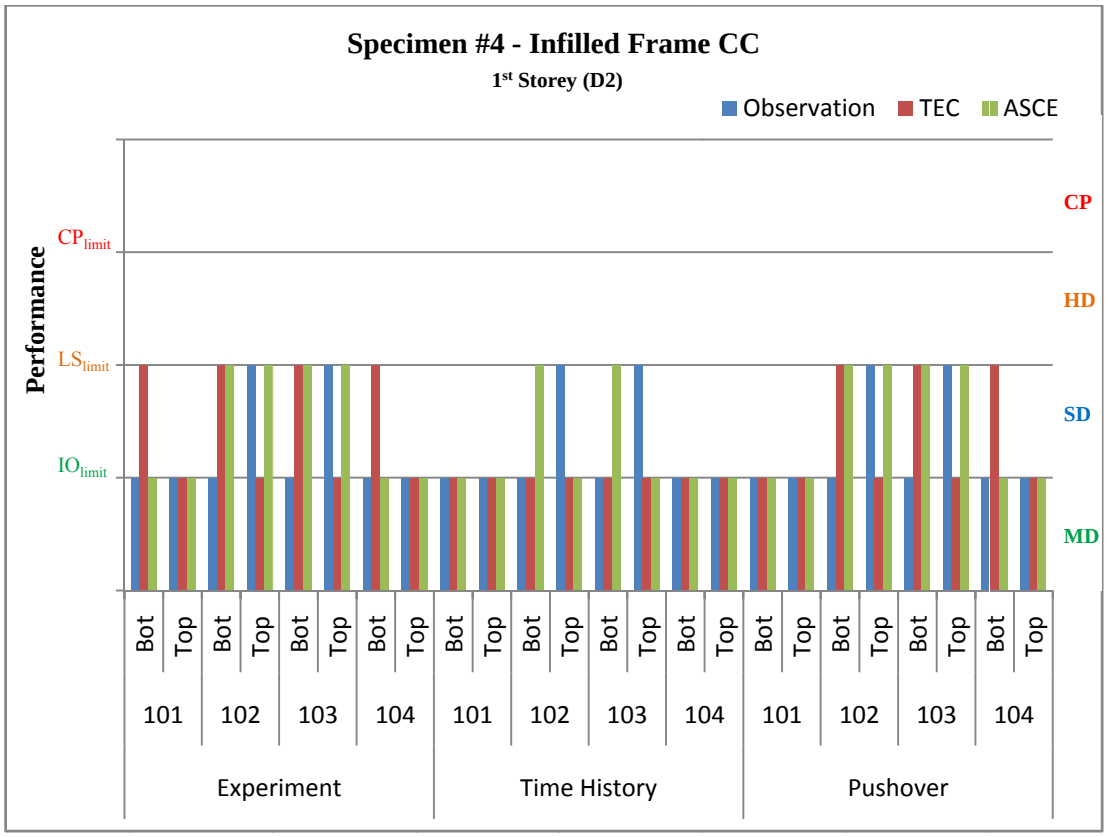

Figure 5.16: Observed and evaluated damages - SP #4 [D2]

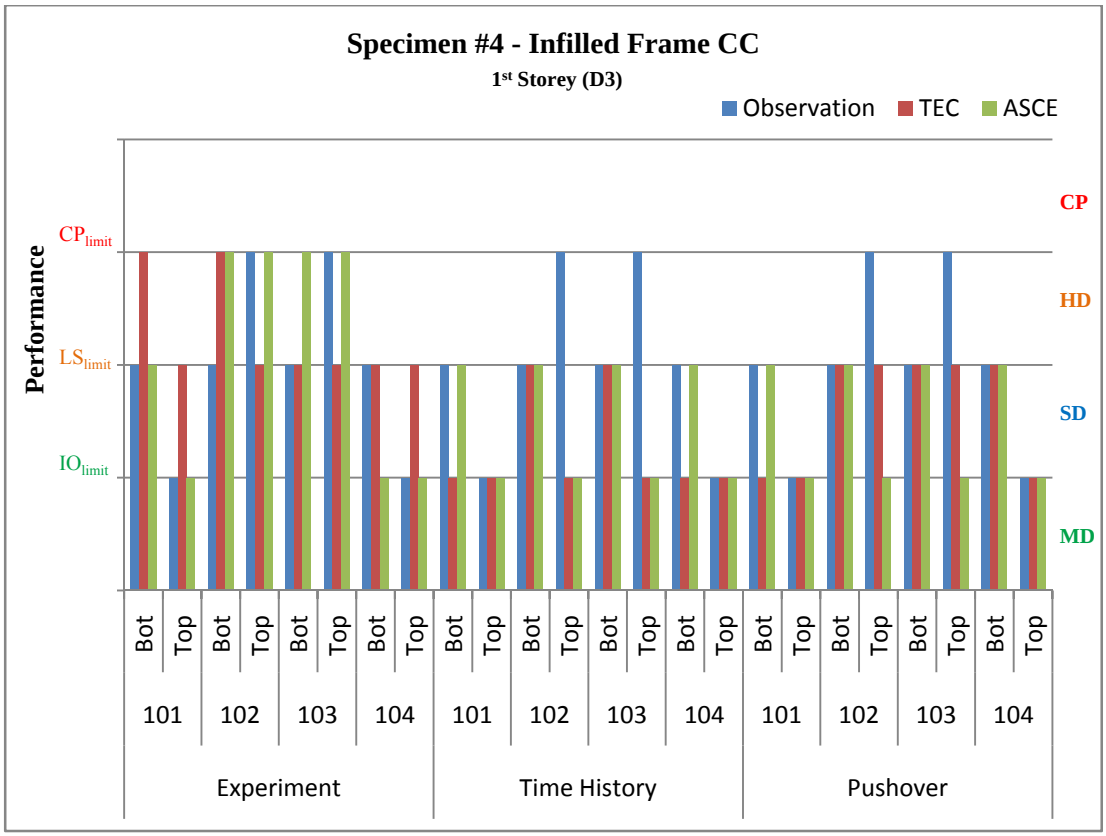

Figure 5.17: Observed and evaluated damages - SP #4 [D3]

Similar to Specimen #2, the assessment of the infill panels of Specimen #4 is performed as explained before, and the outcome is presented in Table 5.6.

Table 5.6: Performance evaluation of infill panels (SP#4)

Ground motion	Storey	Damage	Performance Level
D2	1	Visible crack along the primary diagonal	IO
	2	Visible crack along the primary diagonal	IO
	3	No visible cracks	IO
D3	1	Significant diagonal cracking and crushing	LS
	2	Significant diagonal cracking and crushing	LS
	3	Visible crack along the primary diagonal	IO

The performance of AAC infills are assessed by comparing the cracking and crushing/failure drift values of panel for Specimen #4 given in Table 3.6 with the limiting drift values of Table 5.4. Once again it is confirmed that AAC infill panels performed much better than expected. The life-safety limit is assumed to be reached and the panel is considered in collapse range when inter-story drift reaches: 0.35% as per TEC 2007, whereas 0.6% as per ASCE 41-06. However, the first visible diagonal crack appears at approximately 0.5% drift value while the specimen reached crushing at about 0.8% drift during Pseudo-dynamic test which is clearly greater than either of the limits.

5.7 Comments

From the results obtained for several test specimens the following comments can be made:

- The performance evaluation limits of TEC 2007 are more conservative in all specimens as compared to ASCE 41-06 limits for all column members not bounded by infills. For columns bounding the infill panels (interior columns of Specimen #2 and #4), ASCE limits are more conservative than the TEC 2007 limits.

- For bounding columns, ASCE's separate provisions accurately assess the observed damage in both infilled frames while TEC's generalized provisions failed to predict performance for bounding columns and under-predict their damage.

- For non-conforming specimens (Specimen #1 and #2), TEC limits accurately predict the damages in exterior columns while ASCE results in under-prediction. For bounding columns, ASCE provisions works accurate while TEC limits under-predicts the damages.

- For code conforming specimens (Specimen #3 and #4), ASCE performance evaluation limits accurately predicts the damage in exterior and interior columns while TEC performance limits over-predicts the damage in exterior column while under-predict for bounding columns.

- For bare specimens, the analytical model of Specimen #1 is unable to capture the damage in columns due to instability and formation of first storey mechanism while it predicts damage state fairly accurately for Specimen #3 as compared to observation and experimental measurement.

- For infilled specimen, the models for both specimens are unable to capture the damage distribution and damage state in the column members due to limitation of strut model in capturing local responses.

- AAC infill panel of both infilled specimens performed significantly better than the expected performance based on limiting inter-storey drifts specified in both codes.

CHAPTER 6

CONCLUSIONS

Investigation of the influence of autoclave aerated concrete masonry infills on the seismic response of 3-storey, 3-bay RC frames tested by pseudo-dynamic testing procedure is presented in this thesis. The investigation on the frames is carried out in pairs of two: the Non-conforming frames with material and detailing deficiencies; and the "Code-conforming" frames compliant with TEC 2007. Each of these pairs contains one bare frame while another frame infilled with AAC masonry panels in the entire middle bay. The comparison is made between the bare frame and the corresponding infilled frame using experimental test results in terms of primary failure mode, global responses such as inter-storey drifts and storey shears and local responses such as end-rotations. Numerical modelling of the frames is conducted on the OpenSees platform following guidelines of TEC-2007 and ASCE/SEI 41-06. Models, calibrated with experiments using time-history results, are used for assessment using pushover and time-history methods in accordance with procedures of TEC-2007 and ASCE/SEI 41-06.

The comparative analysis indicates that AAC infills detrimentally influence the response of deficient RC frames by stiffening the structure thereby attracting additional shear force which is on average twice as high as the column shear capacity, resulting in localized shear failure in bounding columns. The infills cause overall increase in the capacity of the system, however; after the failure of infills, the capacity of infilled frame reduces significantly. This drop in capacity is abrupt in deficient frames as compared to code-conforming frame which causes sudden increase in lateral deformation causing abrupt flexure failure in non-bounding columns. In code conforming specimens, the AAC infill panels does not tend to dominate the response in a detrimental manner and during strong shaking the bounding frame causes crushing of the panel after which frame behaves similar to the bare frame. This leads to the conclusion that providing adequate confinement reinforcement may result in better performance of even the deficient RC frames infilled with AAC masonry. In addition, AAC masonry infills may prove advantageous in code-complaint new construction which is designed by neglecting the influence of masonry infills.

Modelling and calibration of deficient systems, which constitutes majority of existing building stock in major cities, using reduced nominal material strengths and modified joint-offsets, in order to predict accurate seismic response and damage distribution, is not very efficient. To capture the deformation pattern on local scale, joint flexibility and frame-infill interaction needs to be explicitly accounted for using detailed joint-elements and eccentric strut models respectively. In terms of global response of infilled frames, modelling of AAC masonry material using "*Calibrated*" material model proposed in this study appears to work better than using either the concrete material representation or the force-deformation relationships already proposed in the literature.

Performance evaluation of frames using strain-based limits of TEC 2007 generally results in more conservative evaluation of damage as compared to rotation-based limits of ASCE/SEI 41-06. In deficient frames, TEC evaluates the damages accurately whereas ASCE under-predicts the damages whereas in code-conforming frames; ASCE evaluates the damages accurately while TEC overestimates.

In particular to the columns bounding the infill panels, the separate strain-based provisions of ASCE accurately assess the observed damages in both infilled frames while the general strain-based limits of TEC failed to predict performance for bounding columns and under-predict their damage. This leads to the conclusion that strain-based limits in TEC 2007, which are general for all RC members

regardless of the presence of infills, do not capture the damage state in bounding members thus addition of separate provisions in TEC 2007 for frame members bounding the unretrofitted masonry infills is necessary to accurately estimate the level of damage.

With regards to the performance of masonry infill panels in both frames, the AAC masonry infill panels perform considerably better than the expected performance level in accordance with both codes, although TEC 2007 does not provide specific criteria for unretrofitted masonry infills. The observed performance and damage state at code specified limiting drifts were significantly better than that predicted by codes.

REFERENCES

Al-Chaar, G., Issa, M., Sweeney, S., "Behaviour of masonry- infilled non-ductile reinforced concrete frames", *Journal of Structural Engineering (ASCE):* 2002, Vol. 128, No. 8, pp. 1055-1063.

Alexandre, A. C., Andrea, P., Guido, M., "Seismic performance of Autoclave Aerated Concrete (AAC) masonry: From experimental testing of the in-plane capacity of walls to building response simulation", *Journal of Earthquake Engineering:*2011, 15: pp. 1-31.

American Concrete Institute, "Building Code Requirements for Structural Concrete and Commentary" ,*ACI 318-08*: 2008, Farmington Hills, Mich., 465 pp.

American Society of Civil Engineers, "Seismic Rehabilitation of Existing Buildings", *ASCE/SEI 41:*2006, Reston, Virginia.

American Society of Civil Engineers, "Seismic Rehabilitation of Existing Buildings: Supplement #1", *ASCE/SEI 41-06:* 2007, Reston, Virginia.

Bertero, V., Brokken, S., "Infills in seismic resistant building", *Journal of Structural Engineering (ASCE):* 1983, Vol. 109, No. 6, pp. 1337-1361.

Birely, A. C., Lowes, L. N., Lehman, D. E., "Linear Analysis of Concrete Frames Considering Joint Flexibility", *ACI Structural Journal*: 2012, Vol. 109, No. 3.

Buonopane, S.G., White, R.N., "Pseudo-dynamic testing of masonry infilled reinforced concrete frame," *Journal of Structural Engineering (ASCE):* 1999,Vol. 125, No. 6, pp. 578-589.

Canbay, E., Ersoy, U., Ozcebe, G., "Contribution of Reinforced Concrete Infills to Seismic Behaviour of Structural Systems", *ACI Structural Journal:* 2003, Vol. 100, No. 5, pp. 637-643.

Chopra, A.K., and Goel, R.K., "A Modal Pushover Analysis Procedure for Estimating Seismic Demands for Buildings", *Earthquake Engineering and Structural Dynamics:* 2002, Vol. 31, pp. 561-582.

Coleman, J. and Spacone, E., "Localization Issues in Force-Based Frame Elements", *Journal of Structural Engineering(ASCE):* 2001, Vol. 127, No. 11, pp. 1257-1265.

Crisafulli, F. J., Carr, A. J., Park, R., "Analytical modelling of infilled frame structures – A general review", *Bull. of the New Zealand Society for Earthquake Engineering:* 2000, Vol. 33, No. 1.

Dawe, J. L., Seah, C. K., "Analysis of concrete masonry infilled steel frames subjected to in-plane loads", *Proceeding of the 5th Canadian Masonry Symposium:* 1989, Vancouver, pp. 329–40

Dazio, A. and Yazgan, U., "Simulating Maximum and Residual Displacements of RC Structures", *Earthquake Spectra:* 2011, Vol. 27, No. 4, pp. 1182-1218.

Durrani, A. J., Luo, Y. H., "Seismic retrofit of flat-slab buildings with masonry infills", *Proceeding from the NCEER workshop on seismic response of masonry infills, Report NCEER-94-0004:* 1994, pp. 1/3–8.

EERI/PEER, “New Information on the Seismic Performance of Existing Concrete Buildings”, *Seminar Notes:* 2006, Earthquake Engineering Research Institute, Oakland, California.

Fardis, M. N., Panagiotakos, T. B., “Seismic design and response of bare and masonry-infilled reinforced concrete buildings, Part II: Infilled structures”, *Journal of Earthquake Engineering:* 1997, 1 _3_, pp. 475–503.

Federal Emergency Management Agency, “Guidelines for the Seismic Rehabilitation of Buildings”, *Report* No. FEMA-273, Oct. 1997.

Federal Emergency Management Agency, “Prestandard and Commentary for the Seismic Rehabilitation of Buildings”, *FEMA (Series) 356:* 2000, Washington, D.C.

Fiore, A., Netti, A., and Monaco, P., “The influence of masonry infill on the seismic behaviour of RC frame buildings”, *Engineering Structures:* 2012, 42, pp. 133-145.

Kadir, M. R. A.,“The structural behaviour of masonry infill panels in framed structures”, PhD Thesis: *University of Edinburgh;*1974. Print.

Karsan, I. D., and Jirsa, J. O., “Behaviour of Concrete under Compressive Loading”, *Journal of the Structural Division (ASCE):* 1969, Vol. 95, ST 12, pp. 2543-2563.

Kent, D. C., and Park R., “Flexural Members with Confined Concrete”, *Journal of the Structural Division (ASCE):* 1971, Vol. 97, ST 7, pp. 1969-1990.

Klingner, R.E., Bertero, V.V., “Infilled frames in earthquake-resistant construction” *Report EERC/76-3:* 1976, *Earthquake Engineering Research Center, University of California, Berkeley,* CA, USA.

Klingner, R.E., Bertero, V.V., “Earthquake resistance of infilled frames”, *Journal of the Structural Division (ASCE):*1978, Vol. 104, No. 6,pp. 973–989.

Kose, M. M., “Parameters affecting the fundamental period of RC buildings with infill walls”, *Engineering Structures:* 2009, 31, pp. 93-102.

Koutromanos, I., “Numerical Analysis of Masonry-Infilled Reinforced Concrete Frames Subjected to Seismic Loads and Experimental Evaluation of Retrofit Techniques”, PhD Thesis: *University of California, San Diego*, 2011. Print.

Lynn, A. C., Moehle, J. P., Mahin, S. A., and Holmes, W. T., “Seismic Evaluation of Existing Reinforced Concrete Building Columns”, *Earthquake Spectra*: 1996, Vol. 12, No. 4, pp. 715-739.

Mahin, S. A., Shing, P. B., “Pseudo-dynamic Method for Seismic Testing”, *Journal of Structural Engineering (ASCE)*:1985, Vol. 111, No. 7, pp. 1482-1503.

Mazzoni et al., “OpenSees Command Language Manual”, *Pacific Earthquake Engineering Research Center*, 2007.

Mehrabi, A.B., Shing, P.B., Schuller, M.P., Noland, J.L., “Experimental evaluation of masonry-infilled RC frames”,*Journal of Structural Engineering (ASCE)*:1996, Vol. 122, No. 3, pp. 228–237.

Middle East Technical University. “108G084 Tübitak Project Progress Report #1”. Aug. 5, 2010. Print.

Ministry of Public Works and Settlements, “Turkish code for buildings in seismic zones”, *Turkish Earthquake Code*: 2007, Ankara, Turkey, 159 pp.

Ministry of Public Works and Settlement, "Requirements for Design and Construction of Reinforced Concrete Structures", *Turkish Standards Institution*, *TS 500*: 2000, Ankara, Turkey.

Molina, F. J., Pegon, P., Verzeletti, G., "Time-domain identification from seismic pseudo-dynamic test results on civil engineering specimens", *2nd International Conference on Identification in Engineering Systems*: 1999, Cromwell Press, Wiltshire, UK.

Mosalam, K. M. A., "Experimental and computational strategies for the seismic behaviour evaluation of frames with infill walls", PhD Thesis: *Cornell University-NY,*1996.Print.

Mosalam, K.M.A., White, R.N., Ayala, G., "Response of infilled frames using pseudo-dynamic experimentation", *Earthquake Engineering and Structural Dynamics*: 1998,Vol. 27, No. 6,pp. 589-608.

Mutlu, M.B., "Numerical Simulations of Reinforced Concrete Frames Tested using Pseudo-Dynamic Method", *Graduate Thesis: Middle East Technical University*: 2012. Print.

Narayanan, N., Ramamurthy, K., "Structure and properties of aerated concrete – a review", *Cement and Concrete Composites*: 2000, Vol. 22, pp. 321-329.

Polyakov, S.V., "On the interaction between masonry filler walls and enclosing frame when loaded in the plane of the wall," *Earthquake Engineering, EERI*: 1960, San Francisco, pp. 36-42.

Pujol, S., Fich, D., "The test of a full-scale three-story RC structure with masonry infill walls," *Engineering Structures*: 1979,Vol. 32, No. 10, pp. 3112-3121.

Stafford Smith, B. "Behaviour of square infilled frames", *Journal of the Structural Division (ASCE)*:1966, Vol. 92, No. 1, pp. 381–403.

Stafford Smith, B., and Carter, C., "A method of analysis for Infilled Frames", *Institution of Civil Engineers*: 1969, Vol. 44.

Stafford Smith, B., "Methods of predicting the lateral stiffness and strength of Multi-storey Infilled frames", *Building Science*: 1967, Vol. 2, pp 247-257.

Sucuoğlu, H., Yazgan, U., Yakut, A., "A Screening Procedure for Seismic Risk Assessment in Urban Building Stocks," *Earthquake* Spectra: 2007, Vol. 23, No. 2, pp. 441-458.

Takanashi, K., Udagawa, K., Seki, M., Okada, T., and Tanaka H. "Nonlinear earthquake response analysis of structures by a computer-actuator on-line system" *Bulletin of Earthquake Resistant Structure Research Center 8*: 1975, *Institute of Industrial Science*, University of Tokyo, Japan.

Uva, G., Raffaele, D., Porco, F., Fiore, A., "On the role of equivalent strut models in the seismic assessment of infilled RC buildings", *Engineering Structures*: 2012, 42, pp. 83-94.